KANSAS STATE UNIVERSITY
TRIGA MARK II NUCLEAR REACTOR FACILITY
LICENSE NO. R-88
DOCKET NO. 50-188

MINOR REVISION
SAFETY ANALYSIS REPORT (CH 4, 6, 7, 13)
DATED 6 JULY 2005

REDACTED VERSION*
IN ACCORDANCE WITH
10 CFR 2.390(d)(1)

*Redacted text and figures blacked out or denoted by brackets

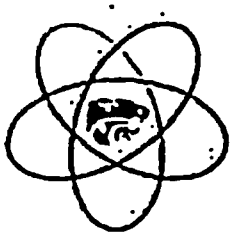

Kansas State University

Minor Revision

SAR (Ch 4, 6, 7, 13)

Kansas State University

TRIGA Mark II Nuclear Reactor Facility

License R-88

Docket 50-188

6 July 2005

Department of Mechanical and Nuclear Engineering
Kansas State University
302 Rathbone Hall
Manhattan, KS 66506

K-State Nuclear Reactor Facility
110 Ward Hall
Manhattan, KS 66506

Minor and editorial changes to SAR

- Chapter 4

  Changes:

  Label added in *Table 4.3, Summary of Reactor SCRAMs* linking trip information to the footnote that period and fuel temperature trips are not required

  Missing constant incorporated in equation 8

  Temperature and CHF information associated with the new power level incorporated in section 4.8.3

- Chapter 6

  Changes: 500 kW changed to 1,250 kW

- Chapter 7

  Changes: Editorial ("continuous energized" changed to "continuously energized")

- Chapter 13

  Changes:

  Table 13.4, 1,259 kW changed to 1,250 kW

  Section 13.2.2.a, 500 kW changed to 1,250 kW

4. Reactor Description

4.1 Summary Description

The Kansas State University (KSU) Nuclear Reactor Facility, operated by the Department of Mechanical and Nuclear Engineering, is located in Ward Hall on the campus in Manhattan, Kansas. The Department is also the home of the Tate Neutron Activation Analysis Laboratory. The TRIGA reactor was obtained through a 1958 grant from the United States Atomic Energy Commission and is operated under Nuclear Regulatory Commission License R-88 and the regulations of Chapter 1, Title 10, Code of Federal Regulations. Chartered functions of the Nuclear Reactor Facility are to serve as: 1) an educational facility for all students at KSU and nearby universities and colleges, 2) an irradiation facility for researchers at KSU and for others in the central United States, 3) a facility for training nuclear reactor operators, and 4) a demonstration facility to increase public understanding of nuclear energy and nuclear reactor systems.

The KSU TRIGA reactor is a water-moderated, water-cooled thermal reactor operated in an open pool and fueled with heterogeneous elements consisting of nominally [redacted] percent enriched uranium in a zirconium hydride matrix and clad with stainless steel. Principal experimental features of the KSU TRIGA Reactor Facility are:

- Central thimble
- Rotary specimen rack
- Thermalizing column with bulk shielding tank
- Thermal column with removable door
- Beam ports
  - Radial (2)
  - Piercing (fast neutron) (1)
  - Tangential (thermal neutron) (1)

The reactor was licensed in 1962 to operate at a steady-state thermal power of 100 kilowatts (kW). The reactor has been licensed since 1968 to operate at a steady-state thermal power of 250 kW and a pulsing maximum thermal power of 250 MW. Application is made concurrently with license renewal to operate at a maximum of 1,250 kW, with fuel loading to support 500 kW steady state thermal power with pulsing to $3.00 reactivity insertion. All cooling is by natural convection. The 250-kW core consists of 81 fuel elements typically (at least [redacted] planned for the 1,250-kW core), each containing as much as [redacted] grams of ^{235}U. The reactor core is in the form of a right circular cylinder about 23 cm (approximately 9 in.) radius and 38 cm (14.96 in.) depth, positioned with axis vertical near the base of a cylindrical water tank 1.98 m (6.5 ft.) diameter and 6.25 m (20.5 ft.) depth. Criticality is controlled and shutdown margin assured by three control rods in the form of aluminum or stainless-steel clad boron carbide or borated graphite. A fourth control rod would be used for 1,250-kW operation. A biological shield of reinforced concrete at least 2.5 m (8.2 ft) thick provides radiation shielding at the side and at the base the reactor tank. The tank and shield are in a 4078-m^3 (144,000 $ft.^3$) confinement building made of reinforced

concrete and structural steel, with composite sheathing and aluminum siding. Sectional views of the reactor are shown in Figures 4.1 and 4.2.

Criticality was first achieved on October 16, 1962 at 8:25 p.m. In 1968 pulsing capability was added and the maximum steady-state operating power was increased from 100 kW to 250 kW. The original aluminum-clad fuel elements were replaced with stainless-steel clad elements in 1973. Coolant system was replaced (and upgraded in 2000), the reactor operating console was replaced, and the control room was enlarged and modernized in 1993, with support from the U.S. Department of Energy. All neutronic instrumentation was replaced in 1994.

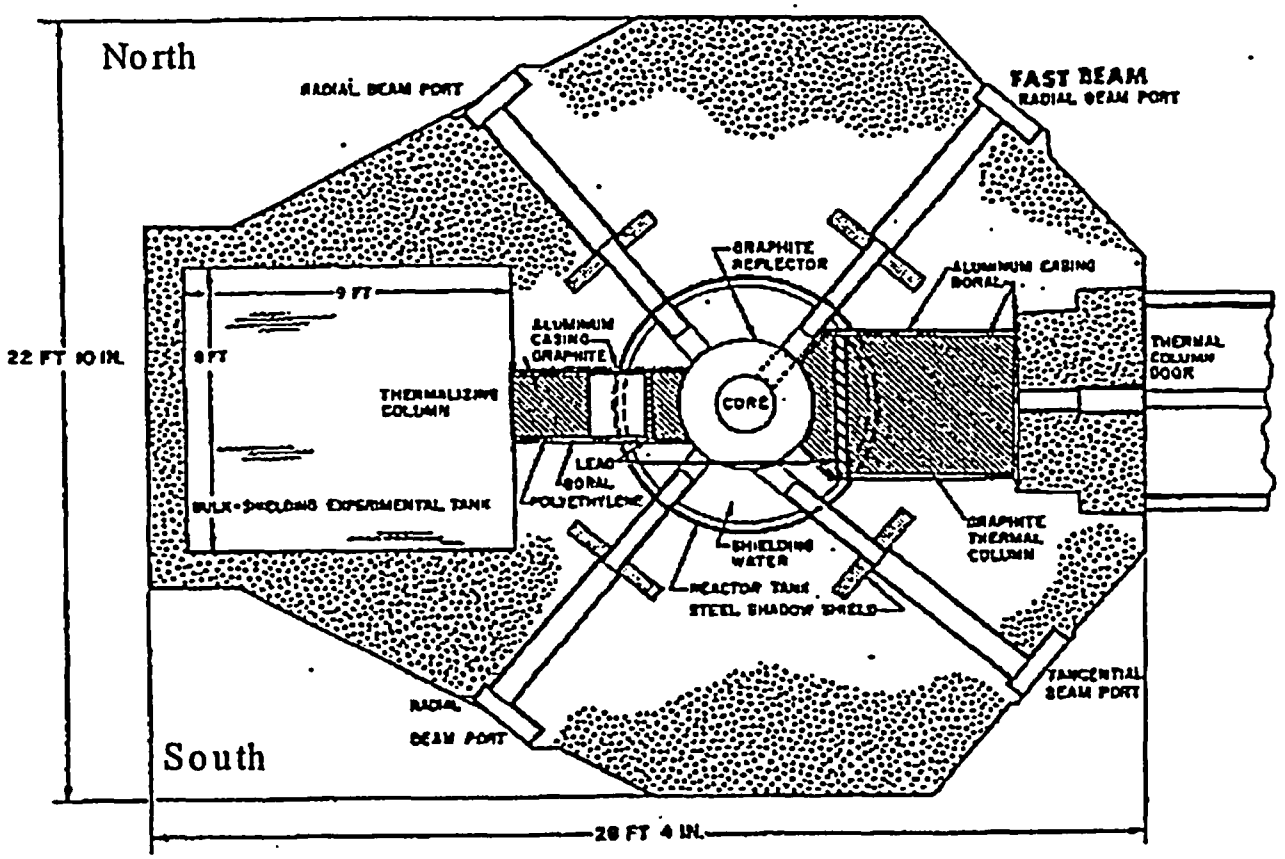

Figure 4. 1, Vertical Section Through the KSU TRIGA Reactor.

4.2 Reactor Core

The General Atomics TRIGA reactor design began in 1956. The original design goal was a completely and inherently safe reactor. Complete safety means that all the available excess reactivity of the reactor can be instantaneously introduced without causing an accident. Inherent safety means that an increase in the temperature of the fuel immediately and automatically results in decreased reactivity through a prompt negative temperature coefficient. These features were accomplished by using enriched uranium fuel in a zirconium hydride matrix.

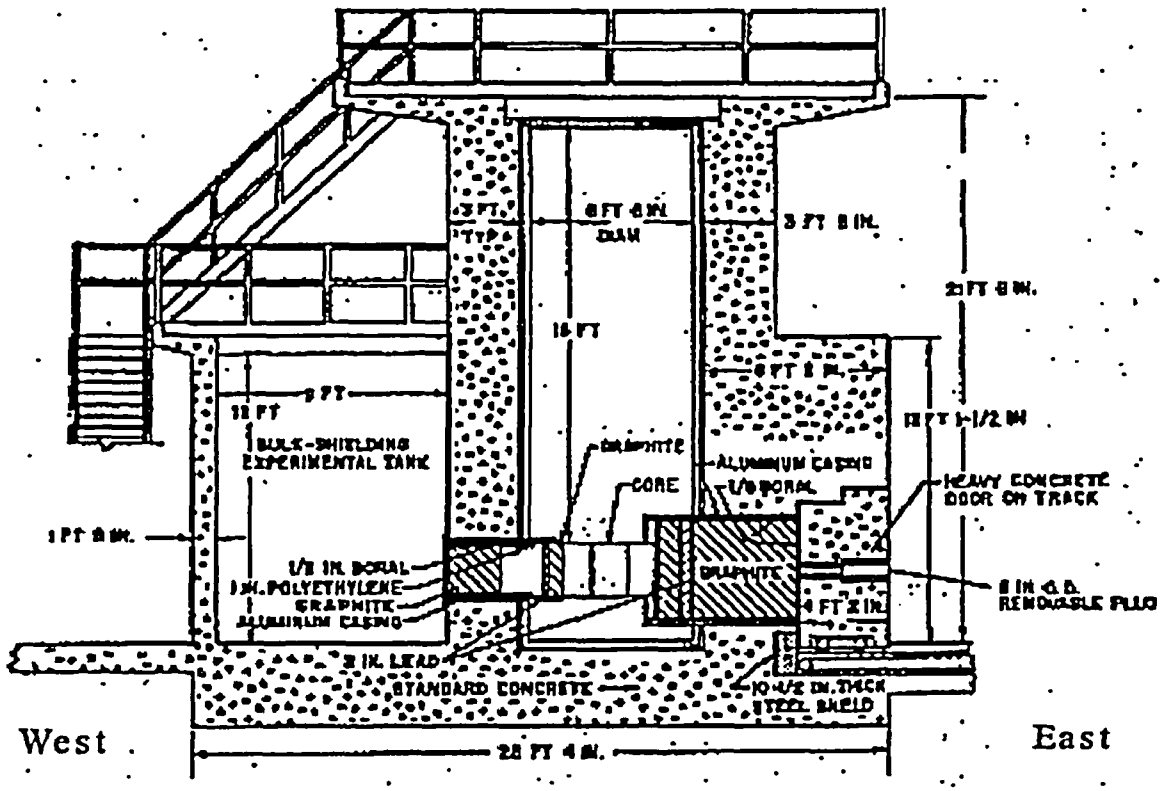

Figure 4.2, Horizontal Section Through the KSU TRIGA Reactor.

The basic parameter providing the TRIGA system with a large safety factor in steady state and transient operations is a prompt negative temperature coefficient, relatively constant with temperature (-0.01% $\Delta k/k°C$). This coefficient is a function of the fuel composition and core geometry. As power and temperature increase, matrix changes cause a shift in the neutron energy spectrum in the fuel to higher energies. The uranium exhibits lower fission cross sections for the higher energy neutrons, thus countering the power increase. Therefore, fuel and clad temperature automatically limit operation of the reactor.

It is more convenient to set a power level limit that is based on temperature. The design bases analysis indicates that operation at up to 1900 kW (with an 83 element core and 120°F inlet water temperature) with natural convective flow will not allow film boiling, and therefore high fuel and clad temperatures which could cause loss of clad integrity could not occur. An 85-element core distributes the power over a larger volume of heat generating elements, and therefore results in a more favorable, more conservative, thermal hydraulic response.

4.2.1 Reactor Fuel[1]

TRIGA fuel was developed around the concept of inherent safety. A core composition was sought which had a large prompt negative temperature coefficient of reactivity such that if all the available excess reactivity were suddenly inserted into the core, the resulting fuel temperature would automatically cause the power excursion to terminate before any core damage resulted. Zirconium hydride was found to possess a basic mechanism to produce the desired characteristic. Additional advantages were that ZrH has a high heat capacity, results in relatively small core sizes and high flux values due to the high hydrogen content, and could be used effectively in a rugged fuel element size.

TRIGA fuel is designed to assure that fuel and cladding can withstand all credible environmental and radiation conditions during its lifetime at the reactor site. As described in 3.5.1 (Fuel System) and NUREG 1282, fuel temperature limits both steady-state and pulse-mode operation. The fuel temperature limit stems from potential hydrogen outgassing from the fuel and the subsequent stress produced in the fuel element clad material. The maximum temperature limits of 1150°C (with clad < 500°C) and 950°C (with clad > 500°C) for U-ZrH ($H/Zr_{1.65}$) have been set to limit internal fuel cladding stresses that might challenge clad integrity (NUREG 1282). These limits are the principal design bases for the safety analysis.

a. Dimensions and Physical Properties.

The KSU TRIGA reactor is fueled by stainless steel clad Mark III fuel-elements. Three instrumented aluminum-clad Mark II elements are still available for use in the core. General properties of TRIGA fuel are listed in Table 4.1. The Mark III elements are illustrated in Figure 4.3. To facilitate hydriding in the Mk III elements, a zirconium rod is inserted through a 0.635 cm. (1/4-in.) hole drilled through the center of the active fuel section.

Instrumented elements have three chromel-alumel thermocouples embedded to about 0.762 cm (0.3 in.) from the centerline of the fuel, one at the axial center plane, and one each at 2.54 cm. (1 in.) above and below the center plane. Thermocouple leadout wires pass through a seal in the upper end fixture, and a leadout tube provides a watertight conduit carrying the leadout wires above the water surface in the reactor tank.

[1]Unless otherwise indicated, fuel properties are taken from the General Atomics report of Simnad [1980] and from authorities cited by Simnad.

Graphite dummy elements may be used to fill grid positions in the core. The dummy elements are of the same general dimensions and construction as the fuel-moderator elements. They are clad in aluminum and have a graphite length of 55.88 cm (22 in.).

Table 4.1, Nominal Properties of Mark II and Mark III TRIGA Fuel Elements in use at the KSU Nuclear Reactor Facility.

Property	Mark II	Mark III
Dimensions		
Outside diameter, $D_o = 2r_o$	1.47 in. (3.7338 cm)	1.47 in. (3.7338 cm)
Inside diameter, $D_i = 2r_i$	1.41 in (3.6322 cm)	1.43 in. (3.6322 cm)
Overall length	28.4 in. (72.136 cm)	28.4 in. (72.136 cm)
Length of fuel zone, L	14 in. (35.56 cm)	15 in. (38.10 cm)
Length of graphite axial reflectors	4 in. (10.16 cm)	3.44 in (8.738 cm)
End fixtures and cladding	aluminum	304 stainless steel
Cladding thickness	0.030 in. (0.0762 cm)	0.020 in. (0.0508 cm)
Burnable poisons	Sm wafers	None
Uranium content		
Weight percent U	[redacted]	[redacted]
^{235}U enrichment percent	[redacted]	[redacted]
^{235}U content	[redacted]	[redacted]
Physical properties of fuel excluding cladding		
H/Zr atomic ratio	1.0	1.6
Thermal conductivity (W cm^{-1} K^{-1})	0.18	0.18
Heat capacity [T ≥0°C] (J cm^{-3} K^{-1})		2.04 + 0.00417T
Mechanical properties of delta phase U-ZrH[a]		
Elastic modulus at 20°C		9.1 × 10^6 psi
Elastic modulus at 650°C		6.0 × 10^6 psi
Ultimate tensile strength (to 650°C)		24,000 psi
Compressive strength (20°C)		60,000 psi
Compressive yield (20°C)		35,000 psi

[a]Source: Texas SAR [1991].

b. Composition and Phase Properties

The Mark III TRIGA fuel element in use at Kansas State University contains nominally [redacted]% by weight of uranium, enriched to [redacted]% ^{235}U, as a fine metallic dispersion in a zirconium hydride matrix. The H/Zr ratio is nominally 1.6 (in the face-centered cubic delta phase). The equilibrium hydrogen dissociation pressure is governed by the composition and temperature. For $ZrH_{1.6}$, the equilibrium hydrogen pressure is one atmosphere at about 760°C. The single-phase, high-hydride composition eliminates the problems of density changes associated with phase changes and with thermal diffusion of the hydrogen. Over 25,000 pulses have been performed with the TRIGA fuel elements at General Atomic, with fuel temperatures reaching peaks of about 1150°C.

The zirconium-hydrogen system, whose phase diagram is illustrated in Chapter 3, is essentially a simple eutectoid, with at least four separate hydride phases. The delta and epsilon phases are respectively face-centered cubic and face-centered tetragonal hydride phases. The two phase delta + epsilon region exists between $ZrH_{1.64}$ and $ZrH_{1.74}$ at room temperature, and closes at $ZrH_{1.7}$ at 455°C. From 455°C to about 1050°C, the delta phase is supported by a broadening range of H/Zr ratios.

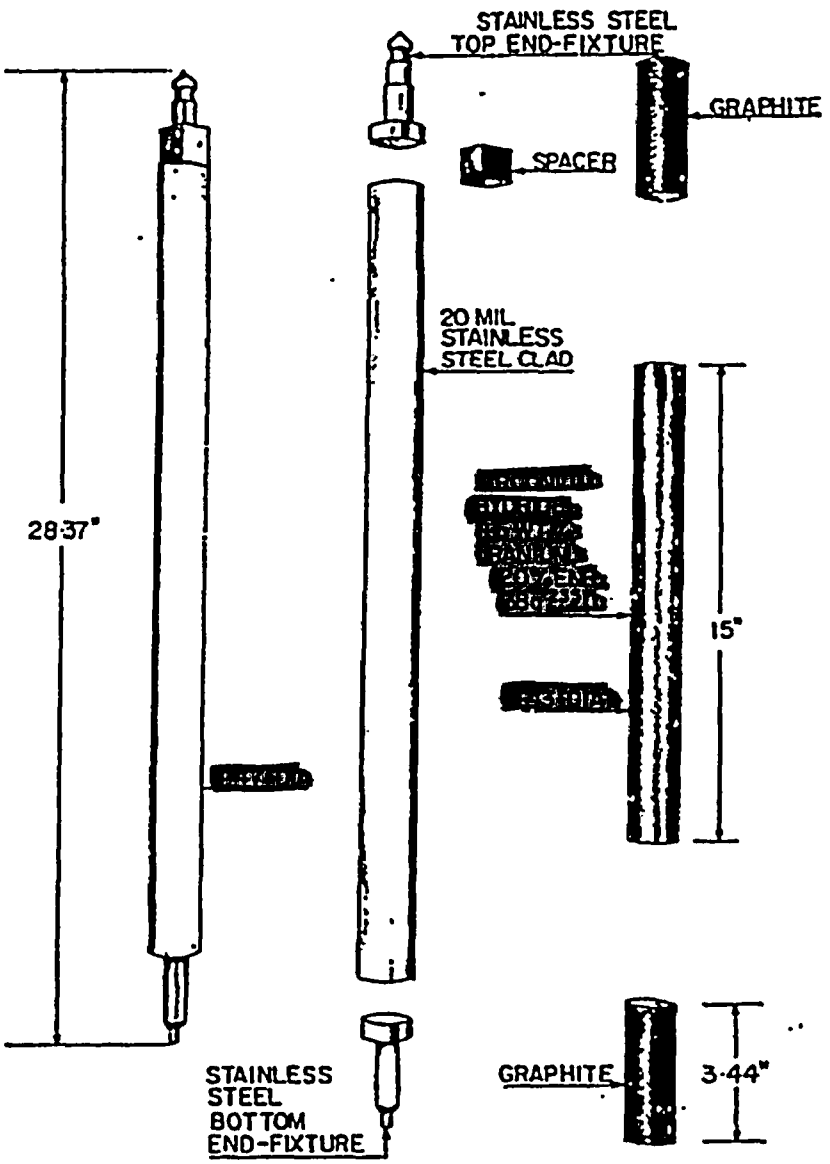

Figure 4.3, TRIGA Fuel Element.

c. Core Layout

A typical layout for a KSU TRIGA II 250-kW core (Core II-18) is illustrated in Figure 4.4. The layout for the 1,250-kW core is expected to be similar, except that the graphite elements will be replaced by fuel elements, one additional control rod will be added, and control rod positions will be adjusted..

[

]

The additional fuel elements are required to compensate for higher operating temperatures from the higher maximum steady state power level. The additional control rod is required to meet reactivity control requirements at higher core reactivity associated with the additional fuel. The control rod positions will be different to allow a higher worth pulse rod (the 250 kW pulse rod reactivity worth is $2.00, the 1,250 kW core pulse rod reactivity worth is $3.00), balancing the remaining control rod's worth to meet minimum shutdown margin requirements, and meeting physical constraints imposed by the dimensions of the pool bridge

4.2.2 Control Rods

The pulse rod is 3.175 cm. (1.25 in.) diameter. Other rods are 2.225 cm (7/8 in.) diameter. Control rods are 50.8 cm. (20 in.) long boron carbide or borated graphite, clad with a 0.0762 cm. (30-mil) aluminium sheath.

The control rod drives are connected to the control rod clutches through three extension shafts. The clutch and upper extension shaft for standard rods extend through an assembly designed with slots that provides a hydraulic cushion (or buffer) for the rod during a scram, and also limits the bottom position of the control rods so that they do not impact the bottom of the control rod guide tube (in the core). The buffers for two standard rods are shown in the left hand picture below (slotted tubes on the right hand side) along with the top section of the pulse/transient rod extension. The pulse rod drive clutch connects to a solid extension shaft through a pneumatic cylinder; the dimensions of the cylinder limits bottom travel.

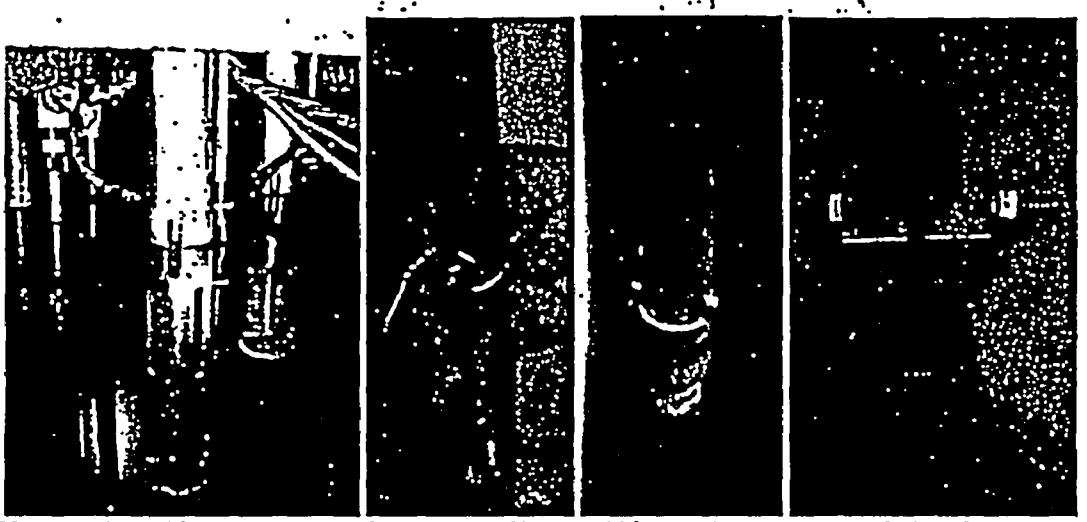

Figure 4.5, Control Rod Upper Extension Assemblies

The bottom of the pulse rod is shown on the left hand side of Figure 4.5. The upper extension shaft is a hollow tube, the middle extension is solid. The upper extension shaft is connected to the middle extension shaft with lock wire or a pin and lock wire for standard rods, with a bolted collar for the pulse rod (the mechanical shock during a pulse requires a more sturdy fastener). Securing the upper control rod extension to the middle extension at one of several holes drilled in the upper part of the middle extension (Figure 4.6) provides adjustment for the control rods necessary to ensure the control rod full in position is above the bottom of the guide tube.

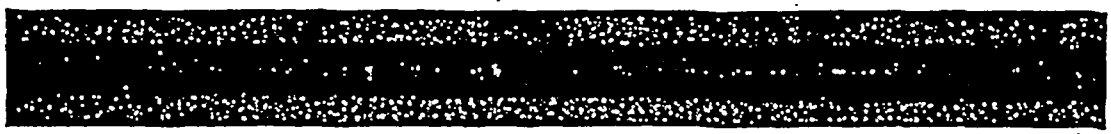

Figure 4.6, Middle Extension Rod Alignment Holes

The middle solid extension is similarly connected to the lower extension. The lower extension is hollow, the middle extension fits into the lower extension and a hole drilled in the overlap secures the lower extension to the middle extension. Typically the lower extension has a tighter fit than the upper extension because the lower and middle extension are not separated for inspections and because the interface with upper extension is used to set the bottom position of the control rod. Pictures of the lower connector for the pulse rod and one standard rod are shown at the left in Figure 4.7..

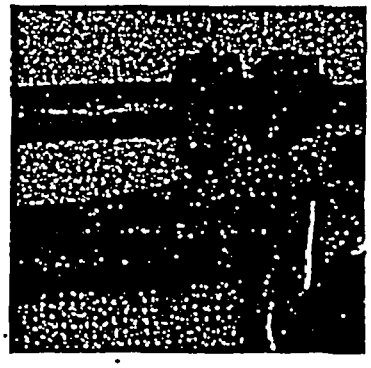

Figure 4.7, Standard & Pulse Rod Lower Coupling

The bottom of the lower extension attaches directly to the control rod. Pictures of the control rods taken during the 2003 control rod inspection are in Figure 4.8. The rods move within control rod guide tubes, shown in Figure 4.9. The guide tubes have perforated walls. The guide tubes have a small metal wire in the tip that fits into the lower grid plate; a setscrew inside the bottom of the guide tube pushes the wire against the lower grid plate to secure the guide tube.

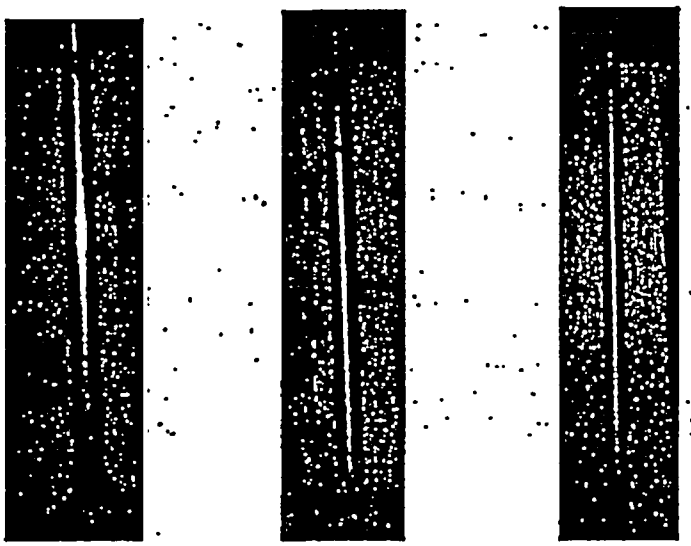

Pulse Rod Shim Rod Reg Rod

Figure 4.8, Control Rods During 2003 Inspection

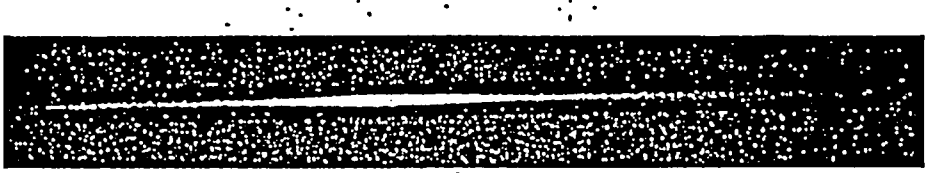

Full Guide Tube

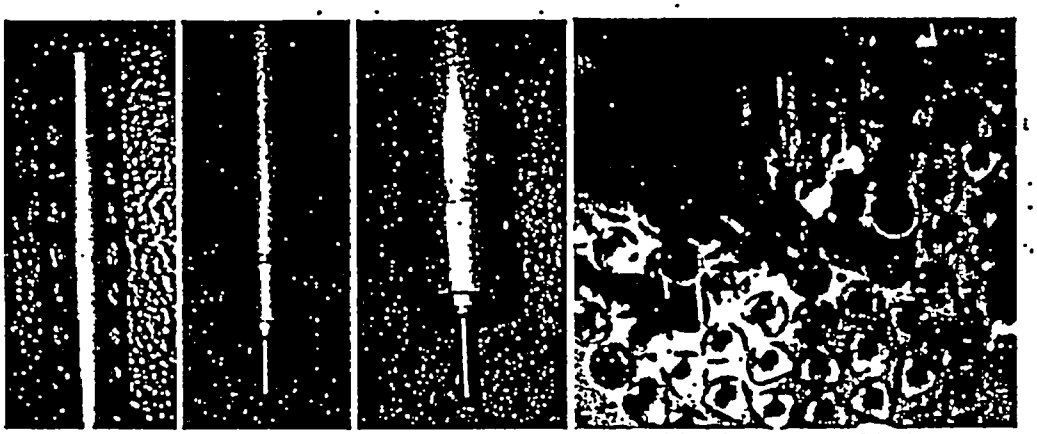

Upper Lower Lower Detail Position in Upper Grid Plate

Figure 4.9, Control Rod Guide Tubes

a. Control Function

While three control rods were adequate to meet Technical Specification requirements for reactivity control with the 100 kW and 250 kW cores, reactivity limits for operation at a maximum power level of 1,250 kW requires four control rods (three standard and one transient/pulsing control rod). The control-rod drives are mounted on a bridge at the top of the reactor tank. The control rod drives are coupled to the control rod through a connecting rod assembly that includes a clutch. The standard rod clutch is an electromagnet; the transient rod clutch is an air-operated shuttle. Scrams cause the clutch to release by de-energizing the magnetic clutch and venting air from the transient rod clutch; gravity causes the rod to fall back into the core. Interlocks ensure operation of the control rods remains within analyzed conditions for reactivity control, while scrams operation at limiting safety system settings. A detailed description of the control-rod system is provided in Chapter 7; a summary of interlocks and scrams is provided below in Table 4.2 and 4.3. Note that (1) the high fuel temperature and period scrams are not required, (2) the fuel temperature scram limiting setpoint depends on core location for the sensor, and (3) the period scram can be prevented by an installed bypass switch.

Table 4.2, Summary of Control Rod Interlocks

INTERLOCK	SETPOINT	FUNCTION/PURPOSE
Source Interlock	2 cps	Inhibit standard rod motion if nuclear instrument startup channel reading is less than instrument sensitivity/ensure nuclear instrument startup channel is operating
Pulse Rod Interlock	Pulse rod inserted	Prevent applying power to pulse rod unless rod inserted/prevent inadvertent pulse
Multiple Rod Withdrawal	Withdraw signal, more than 1 rod	Prevent withdrawal of more than 1 rod/Limit maximum reactivity addition rate
Pulse Mode Interlock	Mode switch in Hi Pulse	Prevent withdrawing standard control rods in pulse mode
Pulse-Power Interlock	10 kW	Prevent pulsing if power level is greater than 10 kW

NOTE: Pulse-Power Interlock normally set at 1 kW

b. Evaluation of Control Rod System

The reactivity worth and speed of travel for the control rods are adequate to allow complete control of the reactor system during operation from a shutdown condition to full power. The TRIGA system does not rely on speed of control as significant for safety of the reactor; scram times for the rods are measured periodically to monitor potential degradation of the control rod system. The inherent shutdown mechanism (temperature feedback) of the TRIGA prevents unsafe excursions and the control system is used only for the planned shutdown of the reactor and to control the power level in steady state operation.

Table 4.3, Summary of Reactor SCRAMs

Measuring Channel	Limiting/Trip Setpoint		Actual Setpoint
	Steady State	Pulse	
Linear Channel High Power	110%	N/A	104%
Power Channel High power	110%	N/A	104%
Detector High Voltage	90%	90%	90%
High Fuel Temperature[1]	600°C B Ring element		450°C
	555°C C Ring element		
	480°C D Ring element		
	380°C E Ring element		350°C
Period [1]	N/A	N/A	3 sec

NOTE [1]: Period trip and temperature trip are not required

The reactivity worth of the control system can be varied by the placement of the control rods in the core. The control system may be configured to provide for the excess reactivity needed for 1,250 kW operations for eight hours per day (including xenon override) and will assure a shutdown margin of at least $0.50.

Nominal speed of the standard control rods is about 12 in. (30.5 cm) per minute (with the stepper motor specifically adjusted to this value), of the transient rod is about 24 in. (61 cm) per minute, with a total travel about 15 in. (38.1 cm). Maximum rate of reactivity change for standard control rods is specified in Technical Specifications.

4.2.3 Neutron Moderator and Reflector

Hydrogen in the Zr-H fuel serves as a neutron moderator. Demineralized light water in the reactor pool also provides neutron moderation (serving also to remove heat from operation of the reactor and as a radiation shield). Water occupies approximately 35% of the core volume. A graphite reflector surrounds the core, except for a cutout containing the rotary specimen rack (described in Chapter 10). Each fuel element contains graphite plugs above and below fuel approximately 3.4 in. in length, acting as top and bottom reflectors.

The radial reflector is a ring-shaped, aluminum-clad, block of graphite surrounding the core radially. The reflector is 0.457-m (18.7 in.) inside diameter, 1.066-m (42 in.) outside diameter, and 0.559-m (20 in.) height. Embedded as a circular well in the reflector is an aluminum housing for a rotary specimen rack, with 40 evenly spaced tubular containers, 3.18-cm (1.25 in.) inside diameter and 27.4-cm (10.8 in.) height. The rotary specimen rack housing is a watertight assembly located in a re-entrant well in the reflector.

The radial reflector assembly rests on an aluminum platform at the bottom of the reactor tank. Four lugs are provided for lifting the assembly. A radial void about 6 inches (15.24 cm) in diameter is located in the reflector such that it aligns with the radial piercing beam port (NE beam port). The reflector supports the core grid plates, with grid plate positions set by alignment fixtures. Graphite inserts within the fuel cladding provide additional reflection. Inserts are placed at both ends of the fuel meat, providing top and bottom reflection.

4.2.4 Neutron Startup Source

A 2-curie americium-beryllium startup source (approximately 2×10^6 n s^{-1}) is used for reactor startup. The source material is encapsulated in stainless steel and is housed in an aluminum-cylinder source holder of approximately the same dimensions as a fuel element. The source holder may be positioned in any one of the fuel positions defined by the upper and lower grid plates. A stainless-steel wire may be threaded through the upper end fixture of the holder for use in relocating the source manually from the 22-ft level (bridge level) of the reactor.

4.2.5 Core Support Structure

The fuel elements are spaced and supported by two 0.75-in. (1.9 cm) thick aluminum grid plates. The grid plates have a total of 91 spaces, up to [redacted] of which are filled with fuel-moderator elements and dummy elements, and the remaining spaces with control rods, the central thimble, the pneumatic transfer tube, the neutron source holder, and one or more voids. The bottom grid plate, which supports the weight of the fuel elements, has holes for receiving the lower end fixtures. Space is provided for the passage of cooling water around the sides of the bottom grid plate and through 36 special holes in it. The 1.5-in. (3.8 cm) diameter holes in the upper grid plate serve to space the fuel elements and to allow withdrawal of the elements from the core. Triangular-shaped spacers on the upper end fixtures allow the cooling water to pass through the upper grid plate when the fuel elements are in position. The reflector assembly supports both grid plates.

4.3 Reactor Tank

The KSU TRIGA reactor core support structure rests on the base of a continuous, cylindrical aluminum tank surrounded by a reinforced, standard concrete structure (with a minimum thickness of approximately 249 cm. or 8 ft 2 in), as illustrated in Figures 4.1 and 4.2. The tank is a welded aluminum structure with 0.635 cm. (1/4-in.) thick walls. The tank is approximately 198 cm (6.5-ft) in diameter and approximately 625 cm (20.5-ft) in depth. The exterior of the tank was coated with bituminous material prior to pouring concrete to retard corrosion. Each experiment facility penetration in the tank wall (described below) has a water collection plenum at the penetration. All collection plenums are connected to a leak-off volume through individual lines with isolation valves, with the leak-off volumes monitored by a pressure gauge. The bulk shield tank wall is known to have a small leak into the concrete at the thermalizing column plenum, therefore a separate individual leak-off volume (and pressure gauge) is installed for the bulk shield tank; all other plenums drain to a common volume. In the event of a leak from the pool

through an experiment facility, pressure in the volume will increase; isolating individual lines allows identification of the specific facility with the leak.

A bridge of steel plates mounted on two rails of structural steel provides support for control rod drives, central thimble, the rotary specimen rack, and instrumentation. The bridge is mounted directly over the core area, and spans the tank. Aluminum grating with clear plastic attached to the bottom is installed that can be lowered over the pool. The grating can be lowered when activities could cause objects or material to fall into the reactor pool. The grating normally remains up to reduce humidity at electro-mechanical components of the control rod drive system and to prevent the buildup of radioactive gasses at the pool surface during operations.

Four beam tubes run from the reactor wall to the outside of the concrete biological shield in the outward direction. Tubes welded to the inside of the wall run toward the reactor core. Three of the tubes (NW, SW, and SE) end at the radial reflector. The NE beam tube penetrates the radial reflector, extending to the outside of the core. Two penetrations in the tank allow neutron extraction into a thermal column and a thermalizing column (described in Chapter 10).

4.4 Biological Shield

The reactor tank is surrounded on all sides by a monolithic reinforced concrete biological shield. The shielding configuration is similar to those at other TRIGA facilities operating at power levels up to 1 MW. Above ground level, the thickness varies from approximately 249 cm. (8 ft 2 in.) at core level to approximately 91 cm. (3 ft.) at the top of the tank.

The massive concrete bulk shield structure provides additional radiation shielding for personnel working in and around the reactor laboratory and provides protection to the reactor core from potentially damaging natural phenomena.

4.5 Nuclear Design

The strong negative temperature coefficient is the principal method for controlling the maximum power (and consequently the maximum fuel temperature) for TRIGA reactors. This coefficient is a function of the fuel composition, core geometry, and temperature. For fuels with [redacted] U, [redacted] enrichment, the value is nearly constant at 0.01% Δk/k per °C, and varies only weakly dependent on geometry and temperature.

Fuel and clad temperature define the safety limit. A power level limit is calculated that ensures that the fuel and clad temperature limits will not be exceeded. The design bases analysis indicates that operation at 1,250 kW thermal power with an [redacted] element across a broad range of core and coolant inlet temperatures with natural convective flow will not allow film boiling that could lead to high fuel and clad temperatures that could cause loss of clad integrity.

Increase in maximum thermal power from 250 to 1,250 kW does not affect fundamental aspects of TRIGA fuel and core design, including reactivity feedback coefficients, temperature safety

limits; and fission-product release rates. Thermal hydraulic performance is addressed in Section 4.6.

4.5.1 Design Criteria - Reference Core

The limiting core configuration for this analysis is a compact core defined by the TRIGA Mk II grid plates (Section 4.2.5). The grid plates have a total of [redacted] spaces, up to [redacted] of which are filled with fuel-moderator elements and graphite dummy elements, and the remaining spaces with control rods, the central thimble, the pneumatic transfer tube, the neutron source holder, and one or more voids in the E or F (outermost two rings) as required to support experiment operations or limit excess reactivity. The bottom grid plate, which supports the weight of the fuel elements, has holes for receiving the lower end fixtures.

4.5.2 Reactor Core Physics Parameters

The limiting core configuration differs from the configuration prior to upgrade only in the addition of a fourth control rod, taking the place of a graphite dummy element or void experimental position. For this reason, core physics is not affected by the upgrade except for linear scaling with power of neutron fluxes and gamma-ray dose rates.

For comparison purposes, a tabulation of total rod worth for each control element from the K-State reactor from a recent rod worth measurement is provided with the values from the Cornell University TRIGA reactor as listed in NUREG 0984 (Safety Evaluation Report Related to the Renewal of the Operating license for the Cornell University TRIGA Research Reactor).

Table 4.4, 250 kW Core Parameters.	
β (effective delayed neutron fraction)	0.007
ℓ (effective neutron lifetime)	43 :S
α_{Tf} (prompt temperature coefficient)	-$0.017 EC^{-1} @ 250kW ~275EC
α_v (void coefficient)	-0.003 1%$^{-1}$ void
α_p (power temperature coefficient – weighted ave)	-$0.006 kW^{-1} to – $0.01 kW^{-1}

Table 4.5, Comparison of Control Rod Worths.			
KSU TRIGA-II (250 kW)		Cornell University (500 kW)	
C-3, Shim	$2.88	D-16, Shim	$2.20
D-16, Regulating	$1.58	D-4, Safety	$1.99
D-10, Pulse	$1.96	D-10, Transient	$1.88
-- TBD	TBD	E-1, Regulating	$0.58

The pulse rod is similar to a standard control rod, and the worth of the pulse rod compares well with the comparable standard control rods in similar ring positions. A maximum pulse is analyzed for thermal hydraulic response and maximum fuel temperature.

4.5.3 Fuel and Clad Temperatures

This section analyzes expected fuel and cladding temperatures with realistic modeling of the fuel-cladding gap. Analysis of steady state conditions reveals maximum heat fluxes well below the critical heat flux associated with departure from nucleate boiling. Analysis of pulsed-mode behavior reveals that film boiling is not expected, even during or after pulsing leading to maximum adiabatic fuel temperatures.

Chapter 4, Appendix A of this chapter reproduces a commonly cited analysis of TRIGA fuel and cladding temperatures associated with pulsing operations. The analysis addresses the case of a fuel element at an average temperature of 1000°C immediately following a pulse and estimates the cladding temperature and surface heat flux as a function of time after the pulse. The analysis predicts that, if there is no gap resistance between cladding and fuel, film boiling can occur very shortly after a pulse, with cladding temperature reaching 470°C, but with stresses to the cladding well below the ultimate tensile strength of the stainless steel. However, through comparisons with experimental results, the analysis concludes that an effective gap resistance of 450 Btu hr^{-1} ft^{-2} $°F^{-1}$ (2550 W m^{-2} K^{-1}) is representative of standard TRIGA fuel and, with that gap resistance, film boiling is not expected. This section provides an independent assessment of the expected fuel and cladding thermal conditions associated with both steady-state and pulse-mode operations.

a. Heat Transfer Models

The overall heat transfer coefficient relating heat flux at the surface of the cladding to the difference between the maximum fuel (centerline) temperature and the coolant temperature can be calculated as the sum of the temperature changes through each element from the centerline of the fuel rod to the water coolant, where the subscripts for each of the ΔT's represent changes between bulk water temperature and cladding outer surface, (br_0), changes between cladding outer surface and cladding inner surface (r_0r_i), cladding inner surface and fuel outer surface – gap (g), and the fuel outer surface to centerline (r_icl):

$$T_{cl} = T_b + \Delta T_{br_0} + \Delta T_{r_0r_i} + \Delta T_g + \Delta T_{r_icl} \qquad (1)$$

A standard heat resistance model for this system is:

$$T_o = T_b + q''\left[\frac{1}{h} + \frac{r_o \ln\left(r_o/r_i\right)}{k_c} + \frac{r_o}{r_i h_g} + \frac{r_o}{2k_f}\right] \quad (2)$$

and heat flux is calculated directly as:

$$q'' = U\Delta T = \frac{T_{max} - T_b}{\frac{1}{h} + \frac{r_o \ln(r_o/r_i)}{k_c} + \frac{r_o}{r_i h_g} + \frac{r_o}{2k_f}}, \quad (3)$$

in which r_o and r_i are cladding inner and outer radii, h_g is the gap conductivity, h is the convective heat transfer coefficient, and k_f is the fuel thermal conductivity. The gap conductivity of 2840 W m^{-2} K^{-1} (500 Btu h^{-1} ft^{-2} $°F^{-1}$) is taken from Appendix A. The convective heat transfer coefficient is mode dependent and is determined in context. Parameters are cross-referenced to source in Table 4.6.

Table 4.6: Thermodynamic Values

Parameter	Symbol	Value	Units	Reference
Fuel conductivity	k_f	18	W m^{-1} K^{-1}	Table 13.3
Clad conductivity	k_g	14.9	W m^{-1} K^{-1} (300 K)	Table 13.3
		16.6	W m^{-1} K^{-1} (400 K)	Table 13.3
		19.8	W m^{-1} K^{-1} (600 K)	Table 13.3
Gap resistance	h_g	2840	W m^{-2} K^{-1}	Appendix A
Clad outer radius	r_0	0.018161	M	Table 13.1
Fuel outer radius	r_i	0.018669	M	Table 13.1
Active fuel length	L_f	0.381	M	Table 13.1
No. fuel elements	N	[redacted]	N/A	Chap 13
Axial peaking factor	APF	$\pi/2$	N/A	Table 13.4

General Atomics reports that fuel conductivity over the range of interest has little temperature dependence, so that:

$$\frac{r_o}{2k_f} = 5.1858\text{E-}04\,\frac{m^2 K}{W} \quad (4)$$

Gap resistance has been experimentally determined as indicated, so that:

$$\frac{r_o}{r_i h_g} = 3.6196\text{E-}04\,\frac{m^2 K}{W} \quad (5)$$

Temperature change across the cladding is temperature dependent, with values quoted at 300 K, 400 K and 600 K. Under expected conditions, the value for 127°C applies so that:

$$\frac{r_o \ln \frac{r_o}{r_i}}{k_o} = 3.103e-5 \frac{m^2 K}{W} \tag{6}$$

Table 4.7, Cladding Heat Transfer Coefficient

Temp (°K)	Temp (°C)	$m^2 K w^{-1}$
300	27	3.457e-5
400	127	3.103e-5
600	327	2.601e-5

It should be noted that, since these values are less than 10% of the resistance to heat flow attributed to the other components, any errors attributed to calculating this factor are small.

The convection heat transfer coefficient was calculated at various steady state power levels. A graph of the calculated values results in a nearly linear response function.

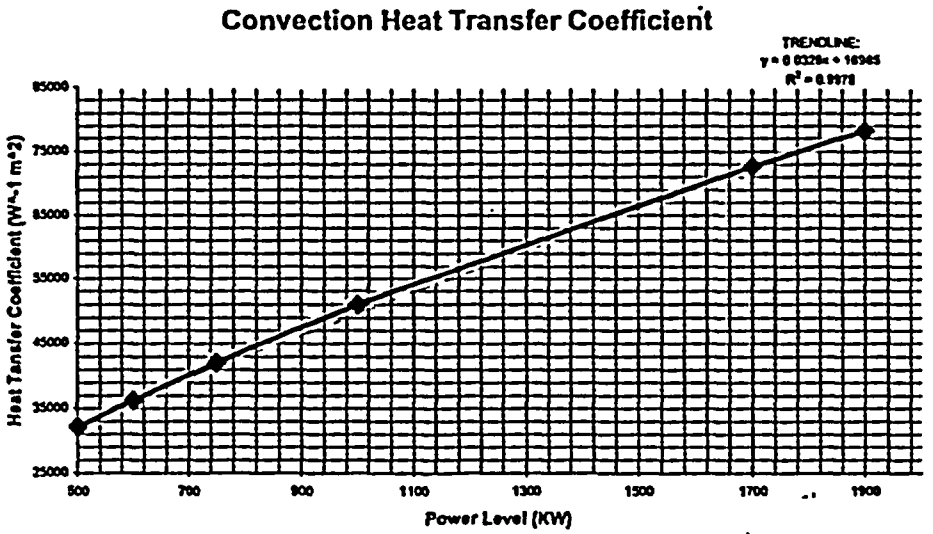

Figure 4.10, Convection Hear Transfer Coefficient versus Power Level

$$\frac{1}{h} = \frac{1}{0.0326P(watts) + 16985} \tag{7}$$

The reference core contains [redacted] fuel elements; temperature calculations using the reference core are conservative because at least [redacted] elements are required for steady state 500 kW operations, while analysis assumes 1.25 MW operation. Actual heat production will be less than heat calculated in analysis, so temperatures will be lower. More than [redacted] elements will distribute heat production across a larger number of fuel elements so that heat flux and temperatures will be lower than calculations based on the reference core. Average heat flux per fuel rod is therefore:

$$q_{ave}" = \frac{power}{area} = \frac{P}{83 * 2\pi r_0 L_f} \tag{8}$$

With the maximum heat flux of:

$$q_{max}" = q_{ave}" * APF = \frac{P}{83 * 2\pi r_0 L_f} * \frac{\pi}{2} = \frac{P}{332 r_0 L_f} = 0.423 m^{-1} P \tag{9}$$

Therefore, core centerline temperature for the fuel rod producing the maximum heat as a function of power can be calculated as:

$$T_{cl} = T_s + 0.423\, P\left[\frac{1}{0.0326 \cdot P + 16985} + 3.103\, e-5 + 3.620\, e-4 + 5.186\, e-4\right] \tag{10}$$

For the purposes of calculation, the two extremes of cladding thermal conductivity were assumed (300 K value and 600 K value) to determine expected centerline temperature as a function of power level. Calculations using both vales are provided graphically, and shows the effect of thermal conductivity changes are minimal. The graph also shows that fuel temperature remains below about 750 °C at power levels up to 1900 kW with pool temperature at 27 °C (300 K), and 1700 kW with pool temperatures at 100 °C.

Table 4.8, Calculated Temperature Data for 1,250 kW Operation

Fuel Centerline °C	Fuel/Gap Interface °C	Gap/Clad Interface °C	Clad/Water Interface °C	Bulk Water °C
503.2	229.0	37.7	21.2	20.0
582.0	307.8	116.4	100.0	100.0

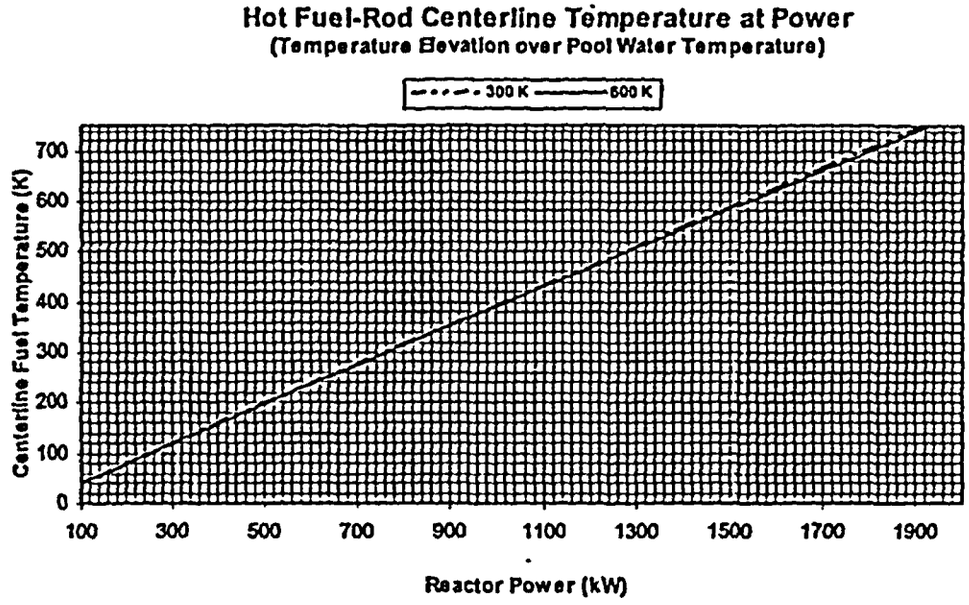

Figure 4.11, *Hot Fuel-Rod Centerline Temperature*

Finally, temperature calculations for the hottest location in the core were made assuming 1.25 MW steady state power at 20°C and 100°C with the following results:

For subcooled boiling, with water at ambient temperature T_b, the critical heat flux is calculated by (Ivey and Morris 1978)

$$(q''_{chf})_{sub} = (q''_{chf}) * \left[1 + 0.1 * \left(\frac{\rho_f}{\rho_g} \right)^{\frac{3}{4}} \frac{c_f (T_{SAT} - T_b)}{\lambda} \right], \qquad (11)$$

in which c_f is the heat capacity of the coolant. At the depth of the reactor core in the KSU TRIGA, static pressure is 0.153 MPa and coolant ambient temperature is taken to be 27°C. Thermodynamic and physical properties of water under these conditions are tabulated in *Chapter 4 Appendix B*.

b. Spatial Power Distribution

The following conservative approximations are made in characterizing the spatial distribution of the power during steady-state operations.

- The hottest fuel element delivers twice the power of the average.

Classically, the radial hot-channel factor for a cylindrical reactor (using R as the physical radius and R_e as the physical radius and the extrapolation distance) is given[2] by:

$$F_R'' = \frac{1.202 * \left(R/R_e\right)}{J_1\left[2.4048 * \left(R/R_e\right)\right]} \qquad (12)$$

with a radial peaking factor of 1.93 for the KSU TRIGA II geometry,. However, TRIGA fuel elements are on the order of a mean free path of thermal neutrons, and there is a significant change in thermal neutron flux across a fuel element. Calculated thermal neutron flux data[3] indicates that the ratio of peak to average neutron flux (peaking factor) for TRIGA cores under a range of conditions (temperature, fuel type, water and graphite reflection) has a small range of 1.36 to 1.40.

Actual power produced in the most limiting actual case is 14% less than power calculated using the assumption; therefore using a peaking factor of 2.0 to determine calculated temperatures and will bound actual temperatures by a large margin, and is extremely conservative.

- The axial distribution of power in the hottest fuel element is sinusoidal, with the peak power a factor of $\pi/2$ times the average, and heat conduction radial only.

The axial factor for power produced within a fuel element is given by:

$$g(z) = 1.514 * \cos\left(\frac{\pi}{2} * \frac{z}{2 * \ell + \ell_{ext}}\right), \qquad (13)$$

in which $\ell = L/2$ and ℓ_{ext} is the extrapolation length in graphite, namely, 0.0275 m. The value used to calculate power in the limiting location within the fuel element is therefore 4% higher a power calculated with the actual peaking factor. Actual power produced in the most limiting actual case is 4% less than power calculated using the assumption; therefore calculated temperatures will bound actual temperatures.

- At full power, the thermal power of $P_{max} = 1{,}250$ kW is distributed over [redacted] fuel elements, with a maximum heat flux given by:

[2] Elements of Nuclear Reactor Design, 2nd Edition (1983), J. Weisman, Section 6.3
[3] GA-4361, Calculated Fluxes and Cross Sections for TRIGA Reactors (8/14/1963), G. B. West

$$q''_{-} = \frac{\pi * P_{-}}{[\quad] * \pi * D_{\bullet} * L} = [\quad] W m^{-2} \tag{14}$$

- The radial and axial distribution of the power within a fuel element is given by

$$q'''(r,z) = q'''_{max} f(r) g(z), \tag{15}$$

in which r is measured from the vertical axis of the fuel element and z is measured along the axis, from the center of the fuel element. The axial peaking factor follows from the previous assumption of the core axial peaking factor, but (since there is a significant flux depression across a TRIGA fuel element) distribution of power produced across the radius of the fuel the radial peaking factor requires a different approach than the previous radial peaking factor for the core.

- The radial factor is given by:

$$f(r) = \frac{a + cr + er^2}{1 + br + dr^2}, \tag{16}$$

in which the parameters of the rational polynomial approximation are derived from flux-depression calculations for the TRIGA fuel (Ahrens 1999a). Values are: a = 0.82446, b = -0.26315, c = -0.21869, d = -0.01726, and e = +0.04679. The fit is illustrated in Figure 4.11.

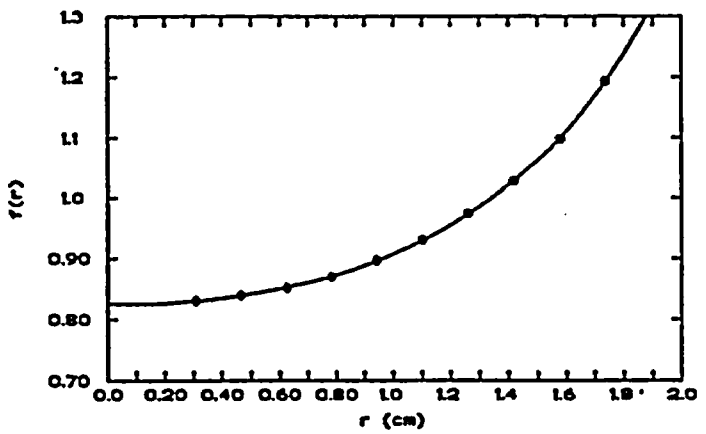

Figure 4.12, Radial Variation of Power Within a TRGIA Fuel Rod. (Data Points from Monte Carlo Calculations [Ahrens 1999a])

c. Steady-State Mode of Operation

Table 4.9 tabulates critical heat flux, Eqs. (3) and (4), as a function of coolant temperature from the assumed inlet temperature to the saturation temperature. Also shown in the table is the CHFR, i.e., the ratio of the critical heat flux and the maximum heat flux at full power.

Table 4.9: Critical Heat Flux and CHFR for 1.25 MW Operation at Selected Coolant Temperatures.

T_b (°C)	T_{sat}-T_b (°C)	q''_{cr} (MW m^{-2})	CHFR
27	84.9	6.02	5.8
30	81.9	5.86	5.6
40	71.9	5.33	5.1
60	51.9	4.26	4.1
100	11.9	2.13	2.0
111.9	0.0	1.49	1.4

It is clear from the table that there is a very wide margin between the operating heat flux and the critical heat flux even to unrealistically high pool water temperature, so that film boiling and excessive cladding temperature is not a consideration in steady-state operation. A parametric variation of this calculation for various power levels shows margin to DNBR up to 100°C pool temperature for power levels greater than 1.9 MW.

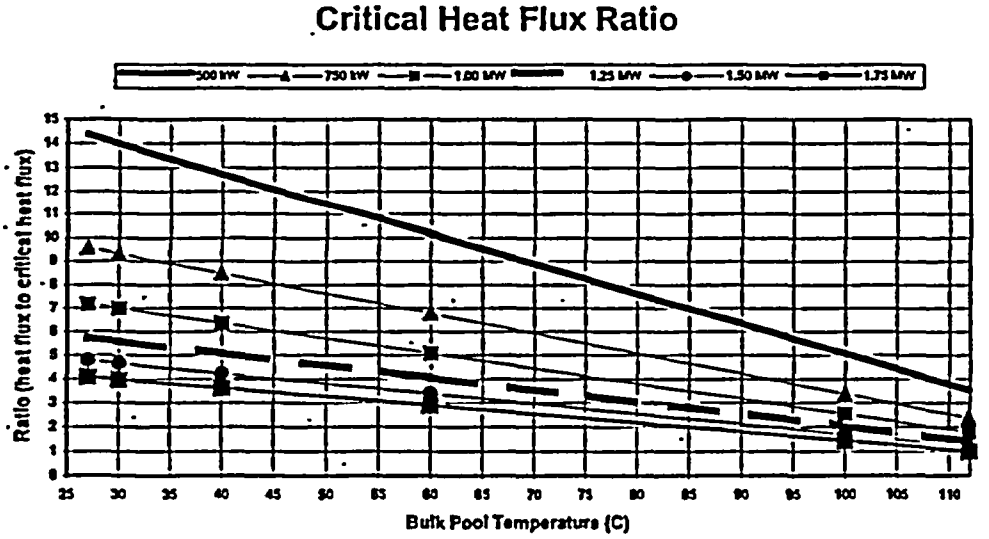

Figure 4.13, Ratio of Departure from Nucleate Boiling to Critical Heat Flux at Various Power Levels

d. Pulsed Mode of Operation

Transient calculations have been performed using a custom computer code TASCOT for transient and steady state two-dimensional conduction calculations (Ahrens 1999). For these calculations, the initial axial and radial temperature distribution of fuel temperature was based on Eqs. (6) and (7), with the peak fuel temperature set to 746 °C, i.e., a temperature rise of 719 °C above 27 °C ambient temperature. The temperature rise is computed in Chapter 13, Section 13.2.3 for a 2.1% ($3.00) pulse from zero power and a 0.7% ($1.00) pulse from power operation. In the TASCOT calculations, thermal conductivity was set to 0.18 W cm^{-1} K^{-1} (Table 4.1) and the overall heat transfer coefficient U was set to 0.21 W cm^{-1} K^{-1}. The convective heat transfer coefficient was based on the boiling heat transfer coefficient computed using the formulation (Chen 1963, Collier and Thome 1994)

$$q'' = h_b(T_w - T_{sat}) = h(T_w - T_b). \tag{17}$$

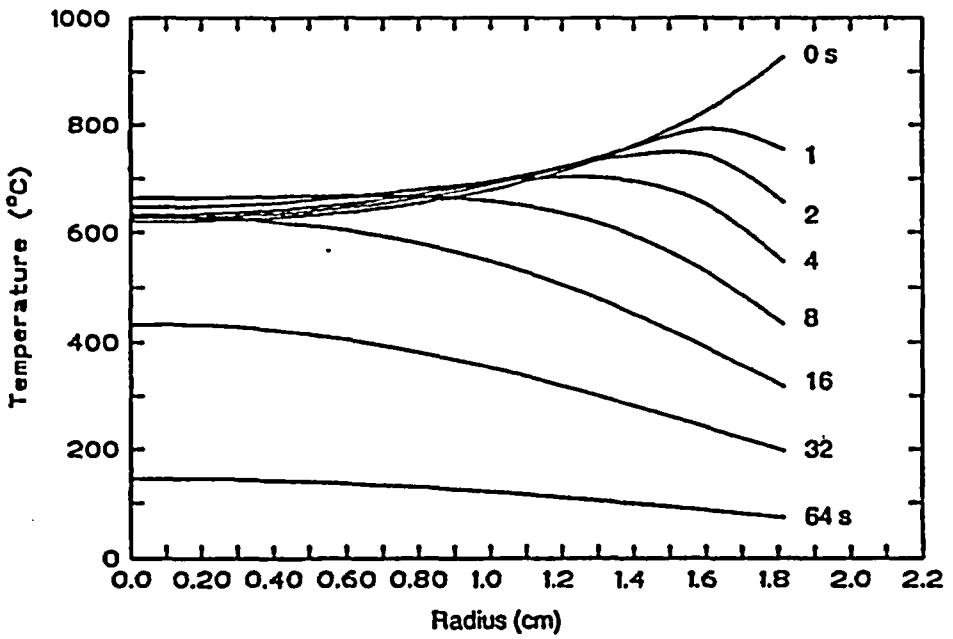

Figure 4. 14, Midplane Radial Variation of Temperature Within the Fuel Subsequent to a $3.00 Pulse.

The boiling heat transfer coefficient is given by the correlation (Forster & Zuber 1955)

$$h_b = 0.00122 * \left[\frac{k_f^{0.79} * c_{pf}^{0.45} * \lambda^{0.51}}{\sigma^{0.5} * \mu_f^{0.29} * \rho_g^{0.24} * \left(\nu_g - \nu_v\right)^{0.75} * T_{sat}^{0.75}} \right] * \left(T_w - T_{sat}\right)^{0.99}, \qquad (18)$$

in which T_w is the cladding outside temperature, T_{sat} the saturation temperature (111.9 °C), and T_b the coolant ambient temperature (27°C). Fluid-property symbols and values are given in Appendix B. Subscripts f and g refer respectively to liquid and vapor phases. The overall heat transfer coefficient U varies negligibly for ambient temperatures from 20 to 60 °C, and has the value 0.21 W cm^{-1} K^{-1} at $T_b = 27$ °C.

Figure 4.14 illustrates the radial variation of temperature within the fuel, at the midplane of the core, as a function of time after the pulse. Table 4.8 lists temperatures and heat fluxes as function of time after a 2.1% ($3.00) reactivity insertion in a reactor initially at zero power. The CHFR is based on the critical heat flux of 1.49 MW m^{-1} from Eqs. (3) and (4) and from Table 4.2 for saturated boiling. Figure 4A.3 of Appendix A, using the Ellion data, indicates a Leidenfrost temperature in excess of 500°C. Thus transition boiling, but not fully developed film boiling might be expected for a short time after the end of a pulse.

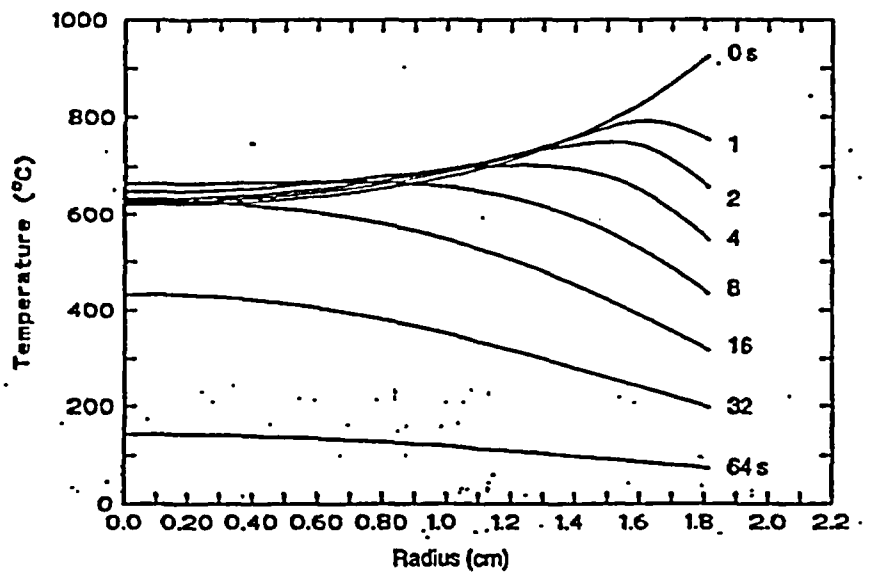

Table 4.10, Heat Flux and Fuel Temperatures Following a $3.00 Pulse from Zero Power, with 27(°C) Coolant Ambient Temperature.

Time (s)	$\dot{Q}''$ (W m^{-2})	CHFR	Fuel outside Temp. (°C)	Clad surface Temp. (°C)
0	-	-	953	-
1	3.57×10^5	4.2	781	224
2	7.34×10^5	2.0	683	432
4	8.52×10^5	1.7	574	498
8	7.54×10^5	2.0	461	443
16	5.71×10^5	2.6	344	342
32	3.46×10^5	4.3	224	218
64	1.04×10^5	14.4	100	84

4.6 Thermal Hydraulic Design and Analysis

A balance between the buoyancy driven pressure gain and the frictional and acceleration pressure losses accrued by the coolant in its passage through the core determines the coolant mass flow rate through the core, and the corresponding coolant temperature rise. The buoyancy pressure gain is given by

$$\Delta p_g = \rho_o \beta_o \Delta T g L, \tag{19}$$

in which ρ_o and β_o are the density and volumetric expansion coefficient at core inlet conditions (27°C, 0.15285 Mpa), g is the acceleration of gravity, 9.8 cm^2 s^{-1}, ΔT is the temperature rise through the core, and L is the height of the core (between gridplates), namely, 0.556 m. The frictional pressure loss is given by

$$\Delta p_f = \frac{\dot{m}^2 f L}{2A^2 D_h \rho_o}, \tag{20}$$

in which $\dot{m}$ is the coolant mass flow rate (kg s^{-1}) in a unit cell approximated as the equivalent annulus surrounding a single fuel element, A is the flow area, namely, 0.00062 m^2, and D_h is the hydraulic diameter, namely, 0.02127 m. The friction factor f for laminar flow through the annular area is given by 100 Re^{-1} (Shah & London 1978), in which the Reynolds number is given by $D_h \dot{m} / A\mu_o$ in which μ_o is the dynamic viscosity at core inlet conditions.

Entrance of coolant into the core is from the side, above the lower grid plate (see Section 4.2.5), and the entrance pressure loss would be expected to be negligible. The exit contraction loss is given by

$$\Delta p_e = \frac{\dot{m}^2 K}{2\rho_o A^2}. \tag{21}$$

The coefficient K is calculated from geometry of an equilateral-triangle spacer in a circular opening, for which

$$K \cong \left[\frac{A_t}{A_c}\right]^2 = \left[\frac{3 * R^2 \sin 60^\circ \cos 60^\circ}{\pi * R^2}\right] = 0.171, \qquad (22)$$

where R is the radius of the opening in the upper grid plate. Equations (11) through (13), solved simultaneously yield the mass flow rates per fuel element, and coolant temperature rises through the core listed in Table 4.9.

Table 4.11, Coolant Flow Rate and Temperature Rise for Natural-Convection Cooling the TRIGA Reactor During Steady-State Operations.

P (kWt)	$\dot{m}$ (kg s^{-1})	ΔT (°C)
50	0.047	3.1
100	0.061	4.7
200	0.077	7.5
300	0.090	9.6
400	0.100	11.5
500	0.108	13.3
750	0.125	17.2
1000	0.139	20.6
1250	0.150	23.8

4.7 Safety Limit

As described in 3.5.1 (Fuel System) and NUREG 1282, fuel temperature limits both steady-state and pulse-mode operation. The fuel temperature limit stems from potential hydrogen outgassing from the fuel and the subsequent stress produced in the fuel element clad material by heated hydrogen gas. Yield strength of cladding material decreases at a temperature of 500°C; consequently, limits on fuel temperature change for cladding temperatures greater than 500°C. A maximum temperature of 1150°C (with clad < 500°C) and 950°C (with clad > 500°C) for U-ZrH ($H/Zr_{1.65}$) will limit internal fuel cladding stresses that might lead to clad integrity (NUREG 1282) challenges.

4.8 Operating Limits

4.8.1 Operating Parameters

The main safety consideration is to maintain the fuel temperature below the value that would result in fuel damage. Setting limits on other operating parameters, that is, limiting safety system settings, controls the fuel temperature. The operating parameters established for the KSU TRIGA reactor are:

- Steady-state power level
- Fuel temperature measured by thermocouple during pulsing operations
- Maximum step reactivity insertion of transient rod

4.8.2 Limiting Safety System Settings

Heat transfer characteristics (from the fuel to the pool) controls fuel temperature during normal operations. As long as thermal hydraulic conditions do not cause critical heat flux to be exceeded, fuel temperature remains well below any limiting value. Figure 4.13 illustrates that critical heat flux is not reached over a wide range of pool temperatures and power levels. As indicated in Table 4.9, the ratio of actual to critical heat flux is at least 2.0 for temperatures less than 100°C bulk pool water temperature for 1.25 MW operation. Operation at less than 1.25 MW ensures fuel temperature limits are not exceeded by a wide margin.

Limits on the maximum excess reactivity assure that operations during pulsing do not produce a power level (and generate the amount of energy) that would cause fuel-cladding temperature to exceed these limits; no other safety limit is required for pulsed operation.

4.8.3 Safety Margins

For 1,250 kW steady-state operations, the critical heat flux ratio indicated in Table 4.9 ranges from 5.8 for pool water at room temperature (27°C) to 4.1 at 60 °C (pool temperatures are controlled to less than 48°C for operational concerns). Even at pool water temperatures approaching boiling, the margin remains above 2. Therefore, margins to conditions that could cause excessive temperatures during steady state operations while cladding temperatures is below 500°C are extremely large.

Normal pulsed operations initiated from power levels below 10 kW with a $3.00 reactivity insertion result in maximum hot spot temperatures of 746°C, a 34% margin to the fuel temperature limit. As indicated in Chapter 13, pulsed reactivity insertions of $3.00 from initial conditions of power operation can result in a maximum hot spot temperature of 869°C. Although administratively controlled and limited by an interlock, this pulse would still result in a 15% margin to the fuel temperature safety limit for cladding temperatures below 500°C.

Analysis shows that cladding temperatures will remain below 500°C when fuel is in water except following large pulses. However, mechanisms that can cause cladding temperature to achieve 500°C (invoking a 950°C fuel temperature limit) automatically limit fuel temperature as heat is transferred from the fuel to the cladding.

Immediately following a maximum pulsed reactivity additions, heat transfer driven by fuel temperature can cause cladding temperature to rise above 500°C, but the heat transfer simultaneously cools the fuel to much less than 950°C.

If fuel rods are placed in an air environment immediately following long-term, high power operation, cladding temperature can essentially equilibrate with fuel temperature. In worst-case air-cooling scenarios, cladding temperature can exceed 500°C, but fuel temperature is significantly lower than the temperature limit for cladding temperatures greater than 500°C.

4.9 Bibliography

"TASCOT: A 2-D, Transient and Steady State Conduction Code for Analyhsis of a TRIGA Fuel Element," Report KSUNE-99-02, Department of Mechanical and Nuclear Engineering, Kansas State University, Manhattan, Kansas, 1999. Ahrens, C.,

"Investigation of the Radial Variation of the Fission-Heat Source in a TRIGA Mark III Fuel Element Using MCNP," Report KSUNE-99-01, Department of Mechanical and Nuclear Engineering, Kansas State University, Manhattan, Kansas, 1999a. Ahrens, C.,

"A Correlation for Boiling Heat Transfer to Saturated Fluids in Convective Flow," ASME Preprint 63-HT-34, 6th National Heat Transfer Conference, Boston, 1963. Chen, J.C.,

Kansas State University TRIGA MkII Reactor Hazards Summary Report," License R-88, Docket 50-188, 1961. Clack, R.W., J.R. Fagan, W.R. Kimel, and S.Z. Mikhail

Convective Boiling and Condensation, 3rd ed., Oxford Press, New York, 1994.Collier, J.G., and J.R. Thome,

"Bubble Dynamics and Boiling Heat Transfer," AIChE Journal 1, 532 (1955). Forster, H.K., and N. Zuber,

Theory and Design of Modern Pressure Vessels, 2d. ed., Van Nostrand Reinhold, New York, 1974. p. 32. Harvey, J.F.,

"On the Relevance of the Vapour-Liquid Exchange Mechanism for Sub-Cooled Boiling Heat Transfer at High Pressure." Report AEEW-R-137, United Kingdom Atomic Energy Authority, Winfrith, 1978. Ivey, H. J. and D. J. Morris

"On the prediction of the Minimum pool boiling heat flux," J. Heat Transfer, Trans. ASME, 102, 457-460 (1980). Lienhard, J. H. and V. K. Dhir,

Thermal Migration of Hydrogen in Uranium-Zirconium Alloys, General Dynamics, General Atomic Division Report GA-3618, November 1962. Merten, U., et al.,

MNRC, McClellan Nuclear Radiation Center Facility Safety Analysis Report, Rev. 2, April 1998.

NUREG-1282, "Safety Evaluation Report on High-Uranium Content, Low-Enriched Uranium-Zirconium Hydride Fuels for TRIGA Reactors," U.S. Nuclear Regulatory Commission, 1987.

"Laminar Forced Convection in Ducts," p. 357, Academic Press, New York, 1978. Shah, R.K., and A.L. London,

"The U-Zr-Hx Alloy: Its Properties and Use in TRIGA Fuel," Report E-117-833, General Atomics Corp., 1980. Simnad, M.T.

"Safety Analysis Report, TRIGA Reactor Facility, Nuclear Engineering Teaching Laboratory, University of Texas at Austin, Revision 1.01, Docket 50-602, May, 1991.

Appendix 4-A
Post-Pulse Fuel and Cladding Temperature

This discussion is reproduced from Safety Analysis Reports for the University of Texas Reactor Facility (UTA 1991) and the McClellan Nuclear Radiation Center (MNRC 1998).

The following discussion relates the element clad temperature and the maximum fuel temperature during a short time after a pulse. The radial temperature distribution in the fuel element immediately following a pulse is very similar to the power distribution shown in Figure 4A.1. This initial steep thermal gradient at the fuel surface results in some heat transfer during the time of the pulse so that the true peak temperature does not quite reach the adiabatic peak temperature. A large temperature gradient is also impressed upon the clad which can result in a high heat flux from the clad into the water. If the heat flux is sufficiently high, film boiling may occur and form an insulating jacket of steam around the fuel elements permitting the clad temperature to tend to approach the fuel temperature. Evidence has been obtained experimentally which shows that film boiling has occurred occasionally for some fuel elements in the Advanced TRIGA Prototype Reactor located at GA Technologies [Coffer 1964]. The consequence of this film boiling was discoloration of the clad surface.

Thermal transient calculations were made using the RAT computer code. RAT is a 2-D transient heat transport code developed to account for fluid flow and temperature dependent material properties. Calculations show that if film boiling occurs after a pulse it may take place either at the time of maximum heat flux from the clad, before the bulk temperature of the coolant has changed appreciably, or it may take place at a much later time when the bulk temperature of the coolant has approached the saturation temperature, resulting in a markedly reduced threshold for film boiling. Data obtained by Johnson et al. [1961] for transient heating of ribbons in 100°F water, showed burnout fluxes of 0.9 to 2.0 Mbtu ft^{-2} hr^{-1} for e-folding periods from 5 to 90 milliseconds. On the other hand, sufficient bulk heating of the coolant channel between fuel elements can take place in several tenths of a second to lower the departure from nucleate boiling (DNB) point to approximately 0.4 Mbtu ft^{-2} hr^{-1}. It is shown, on the basis of the following analysis, that the second mode is the most likely; i.e., when film boiling occurs it takes place under essentially steady-state conditions at local water temperatures near saturation.

A value for the temperature that may be reached by the clad if film boiling occurs was obtained in the following manner. A transient thermal calculation was performed using the radial and axial power distributions in Figures 4A.1and 4A.2, respectively, under the assumption that the thermal resistance at the fuel-clad interface was nonexistent. A boiling heat transfer model, as shown in Figure 4A.3, was used in order to obtain an upper limit for the clad temperature rise. The model used the data of McAdams [1954] for subcooled boiling and the work of Sparrow and Cess [1962] for the film boiling regime. A conservative estimate was obtained for the minimum heat flux in film boiling by using the correlations of Speigler et al. [1963], Zuber [1959], and Rohsenow and Choi [1961] to find the minimum temperature point at which film boiling could occur. This calculation gave an upper limit of 760°C clad temperature for a peak initial fuel temperature of 1000°C, as shown in Figure. 4A.4. Fuel temperature distributions for this case are shown in Figure 4A.5 and the heat flux into the water from the clad is shown in Figure 4A.6. In this limiting case, DNB occurred only 13 milliseconds after the pulse, conservatively calculated

assuming a steady-state DNB correlation. Subsequently, experimental transition and film boiling data were found to have been reported by Ellion [9] for water conditions similar to those for the TRIGA system. The Ellion data show the minimum heat flux, used in the limiting calculation described above, was conservative by a factor of 5. An appropriate correction was made which resulted in a more realistic estimate of 470°C as the maximum clad temperature expected if film boiling occurs. This result is in agreement with experimental evidence obtained for clad temperatures of 400°C to 500°C for TRIGA Mark F fuel elements which have been operated under film boiling conditions [Coffer et al. 1965].

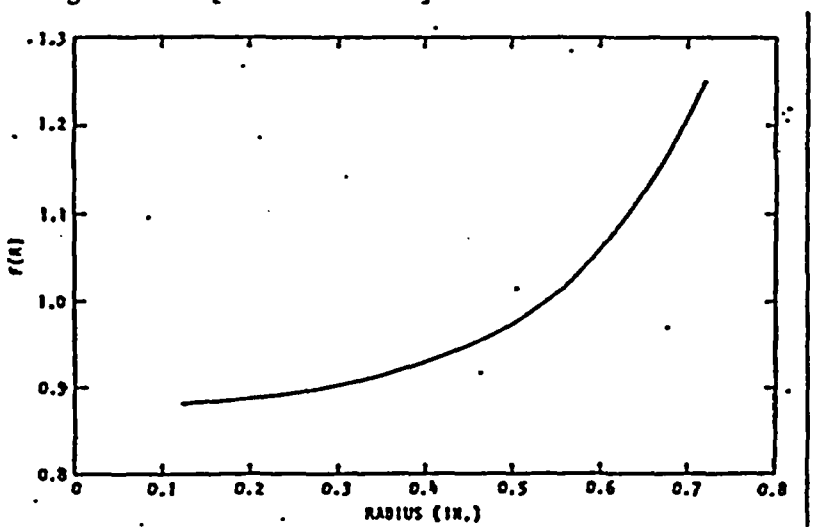

Figure 4A.1. Representative Radial Variation of Power Within the TRIGA Fuel Rod

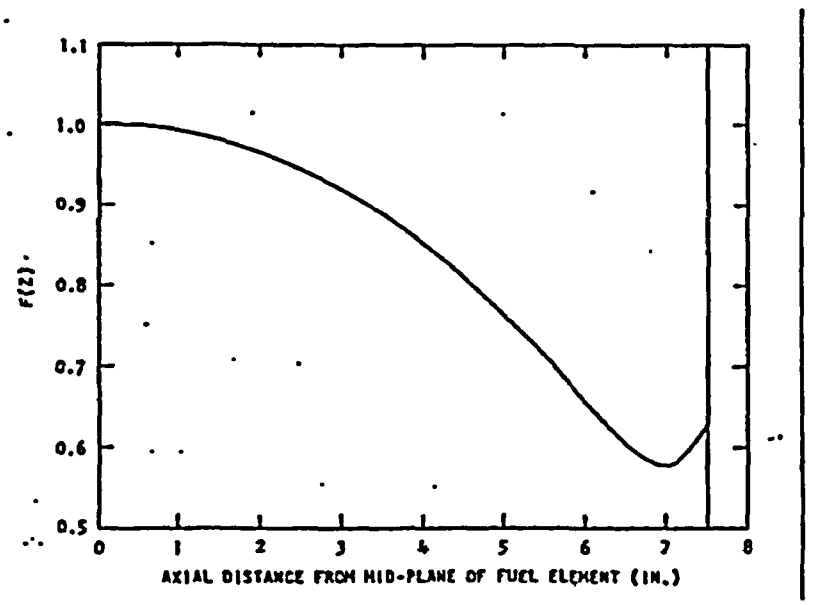

Figure 4A.2, Representative Axial Variation of Power Within the TRIGA Fuel Rod.

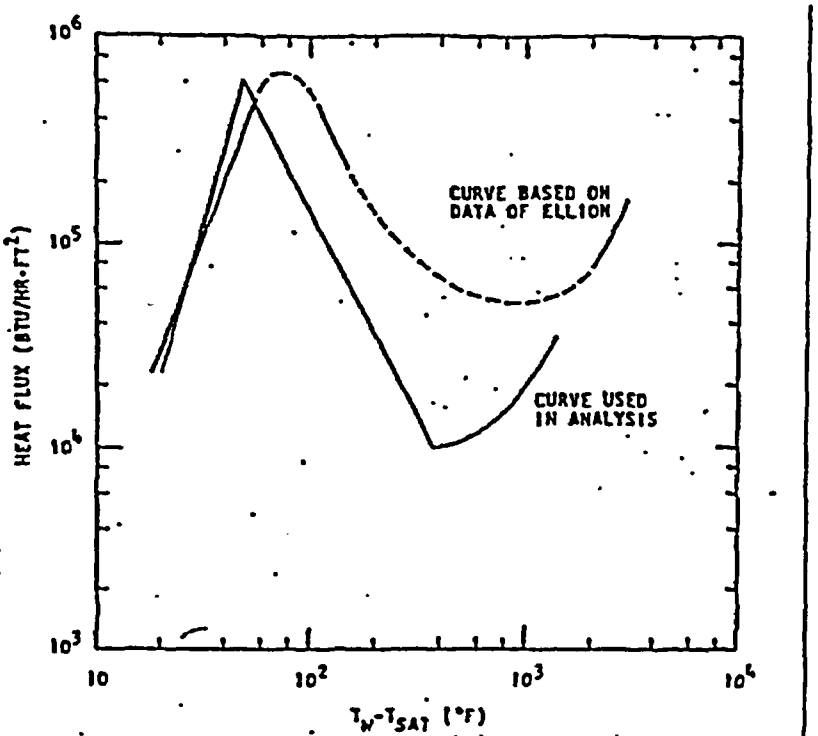

Figure 4A.3, Subcooled Boiling Heat Transfer for Water.

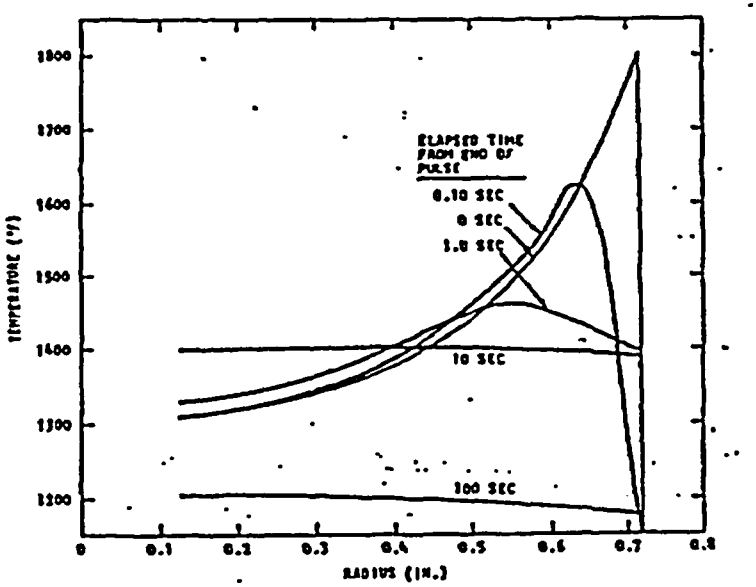

Figure 4A.4, Fuel Body Temperature at the Midplane of a Well-Bonded Fuel Element After Pulse.

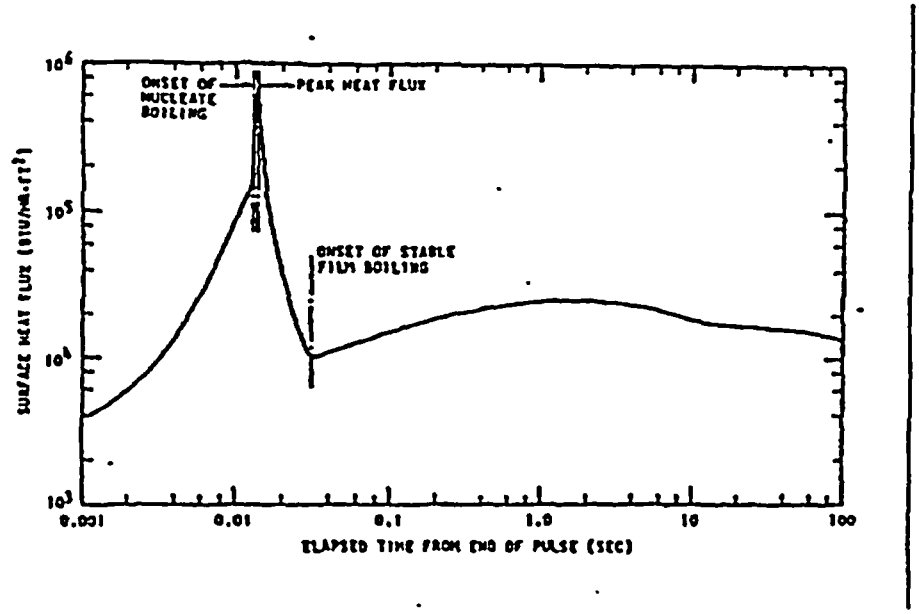

Figure 4A.5, Surface Heat Flux at the Midplane of a Well Bonded Fuel Element After a Pulse.

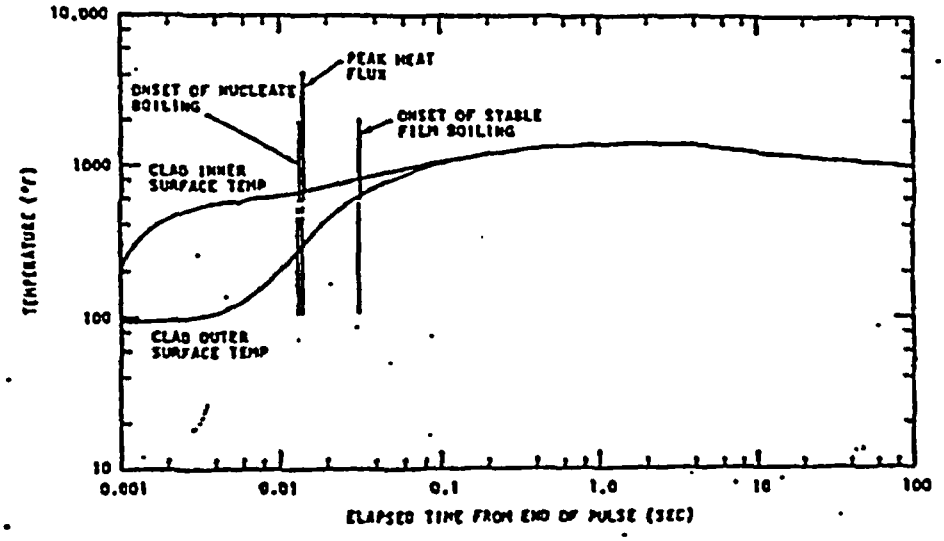

Figure 4A.6, Clad Temperature at Midpoint of Well-Bonded Fuel Element.

The preceding analysis assessing the maximum clad temperatures associated with film boiling assumed no thermal resistance at fuel-clad interface. Measurements of fuel temperatures as a function of steady-state power level provide evidence that after operating at high fuel temperatures, a permanent gap is produced between the fuel body and the clad by fuel expansion. This gap exists at all temperatures below the maximum operating temperature. (See, for example, Figure 16 in the Coffer report [1965].) The gap thickness varies with fuel temperature and clad temperature so that cooling of the fuel or overheating of the clad tends to widen the gap and decrease the heat transfer rate. Additional thermal resistance due to oxide and other films on the fuel and clad surfaces is expected. Experimental and theoretical studies of thermal contact resistance have been reported [Fenech and Rohsenow 1959, Graff 1960, Fenech and Henry 1962] which provide insight into the mechanisms involved. They do not, however, permit quantitative prediction of this application because the basic data required for input are presently not fully known. Instead, several transient thermal computations were made using the RAT code. Each of these was made with an assumed value for the effective gap conductance, in order to determine the effective gap coefficient for which departure from nucleate boiling is incipient. These results were then compared with the incipient film boiling conditions of the 1000°C peak fuel temperature case.

For convenience, the calculations were made using the same initial temperature distribution as was used for the preceding calculation. The calculations assumed a coolant flow velocity of 1 ft per second, which is within the range of flow velocities computed for natural convection under various steady-state conditions for these reactors. The calculations did not use a complete boiling curve heat transfer model, but instead, included a convection cooled region (no boiling) and a subcooled nucleate boiling region without employing an upper DNB limit. The results were analyzed by inspection using the extended steady-state correlation of Bernath [1960] which has been reported by Spano [1964] to give agreement with SPERT II burnout results within the experimental uncertainties in flow rate.

The transient thermal calculations were performed using effective gap conductances of 500, 375, and 250 Btu ft^{-2} hr^{-1} $°F^{-1}$. The resulting wall temperature distributions were inspected to determine the axial wall position and time after the pulse which gave the closest approach between the local computed surface heat flux and the DNB heat flux according to Bernath. The axial distribution of the computed and critical heat fluxes for each of the three cases at the time of closest approach is given in Figures 4A.7 through 4A.9. If the minimum approach to DNB is corrected to TRIGA Mark F conditions and cross-plotted, an estimate of the effective gap conductance of 450 Btu ft^{-2} hr^{-1} $°F^{-1}$ is obtained for incipient burnout so that the case using 500 is thought to be representative of standard TRIGA fuel.

The surface heat flux at the midplane of the element is shown in Figure 4A.10 with gap conductance as a parameter. It may be observed that the maximum heat flux is approximately proportional to the heat transfer coefficient of the gap, and the time lag after the pulse for which the peak occurs is also increased by about the same factor. The closest approach to DNB in these calculations did not necessarily occur at these times and places, however, as indicated on the curves of Figures 4A.7 through 4A.9. The initial DNB point occurred near the core outlet for a local heat flux of about 340 kBtu ft^{-2} hr^{-1} $°F^{-1}$ according to the more conservative Bernath correlation at a local water temperature approaching saturation.

This analysis indicates that after operation of the reactor at steady-state power levels of 1 MW(t), or after pulsing to equivalent fuel temperatures, the heat flux through the clad is reduced and therefore reduces the likelihood of reaching a regime where there is a departure from nucleate boiling. From the foregoing analysis, a maximum temperature for the clad during a pulse which gives a peak adiabatic fuel temperature of 1000°C is conservatively estimated to be 470°C.

As can be seen from Figure 4.7, the ultimate strength of the clad at a temperature of 470°C is 59,000 psi. If the stress produced by the hydrogen over pressure in the can is less than 59,000 psi, the fuel element will not undergo loss of containment. Referring to Figure 4.8, and considering U-ZrH fuel with a peak temperature of 1000°C, one finds the stress on the clad to be 12,600 psi. Further studies show that the hydrogen pressure that would result from a transient for which the peak fuel temperature is 1150°C would not produce a stress in the clad in excess of its ultimate strength. TRIGA fuel with a hydrogen to zirconium ratio of at least 1.65 has been pulsed to temperatures of about 1150°C without damage to the clad [Dee et al. 1966].

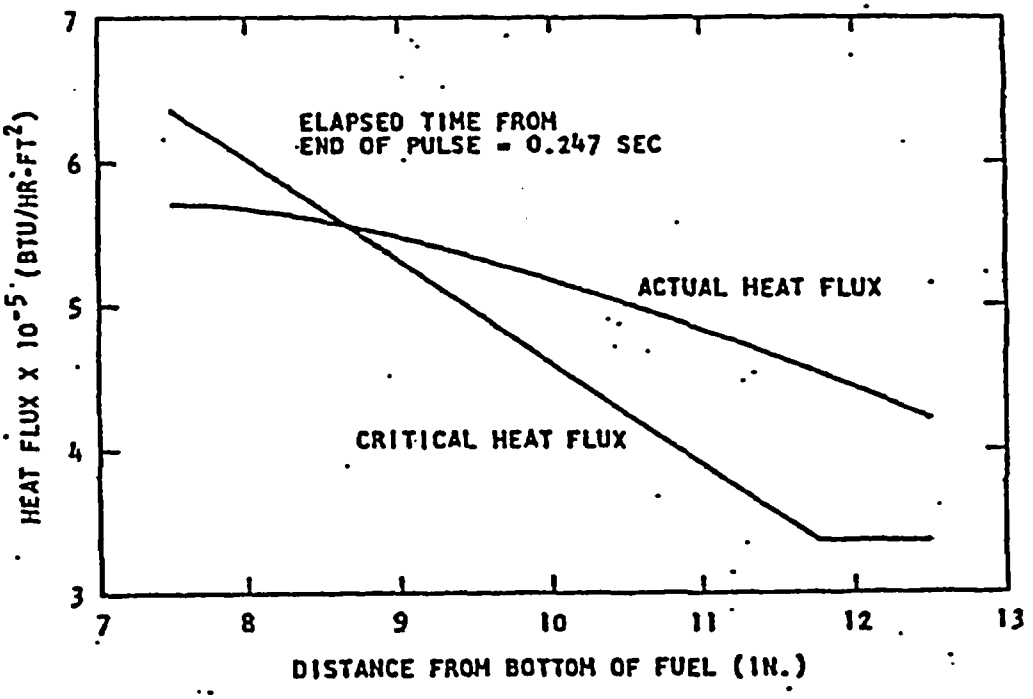

Figure 4A.7, Surface Heat Flux Distribution for Standard Non-Gapped (h_{gap} = 500 Btu/h ft^2 °F) Fuel Element After a Pulse.

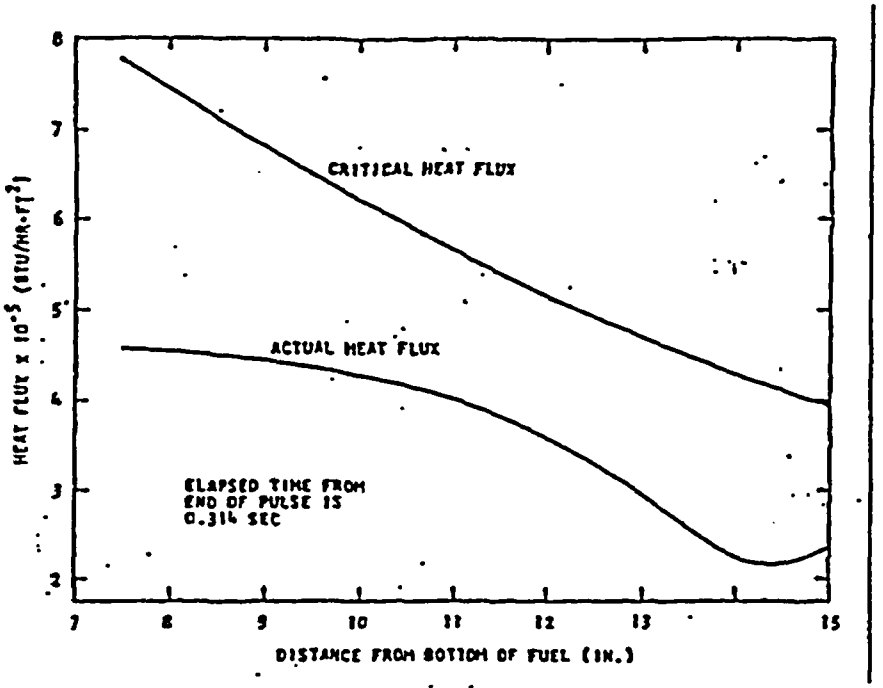

Figure 4A.8, Surface Heat-Flux Distribution for Standard Non-Gapped Fuel Element (h_{gap} = 375 Btu/h ft^2 °F) After a Pulse.

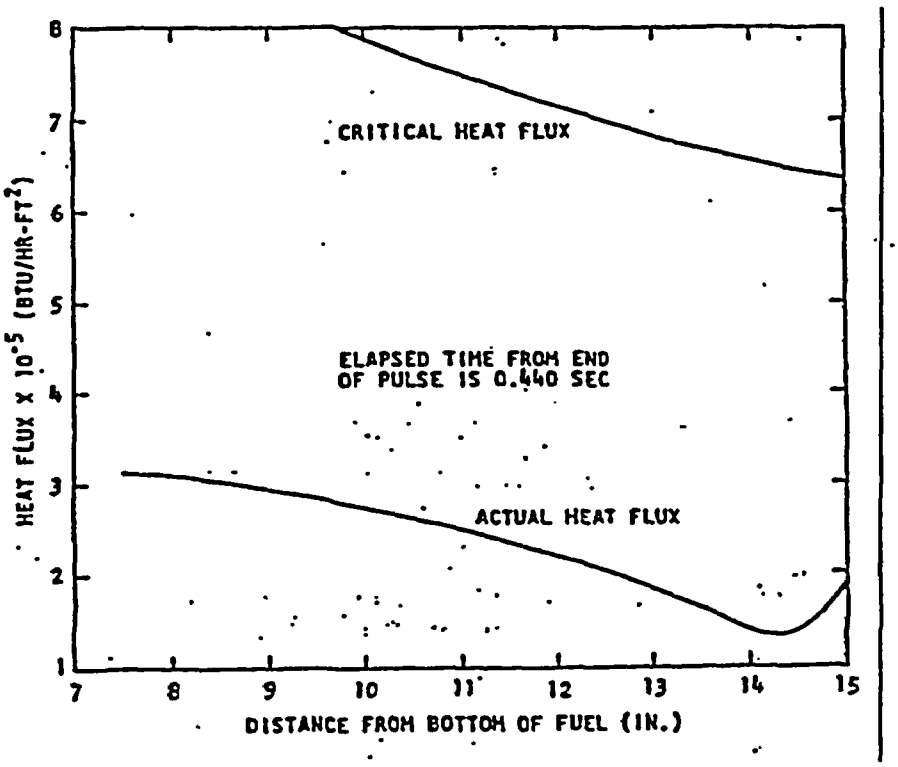

Figure 4A.9, Surface Heat-Flux Distribution for Standard Non-Gapped Fuel Element (h_{gap} = 250 Btu/h ft^2 °F) After a Pulse.

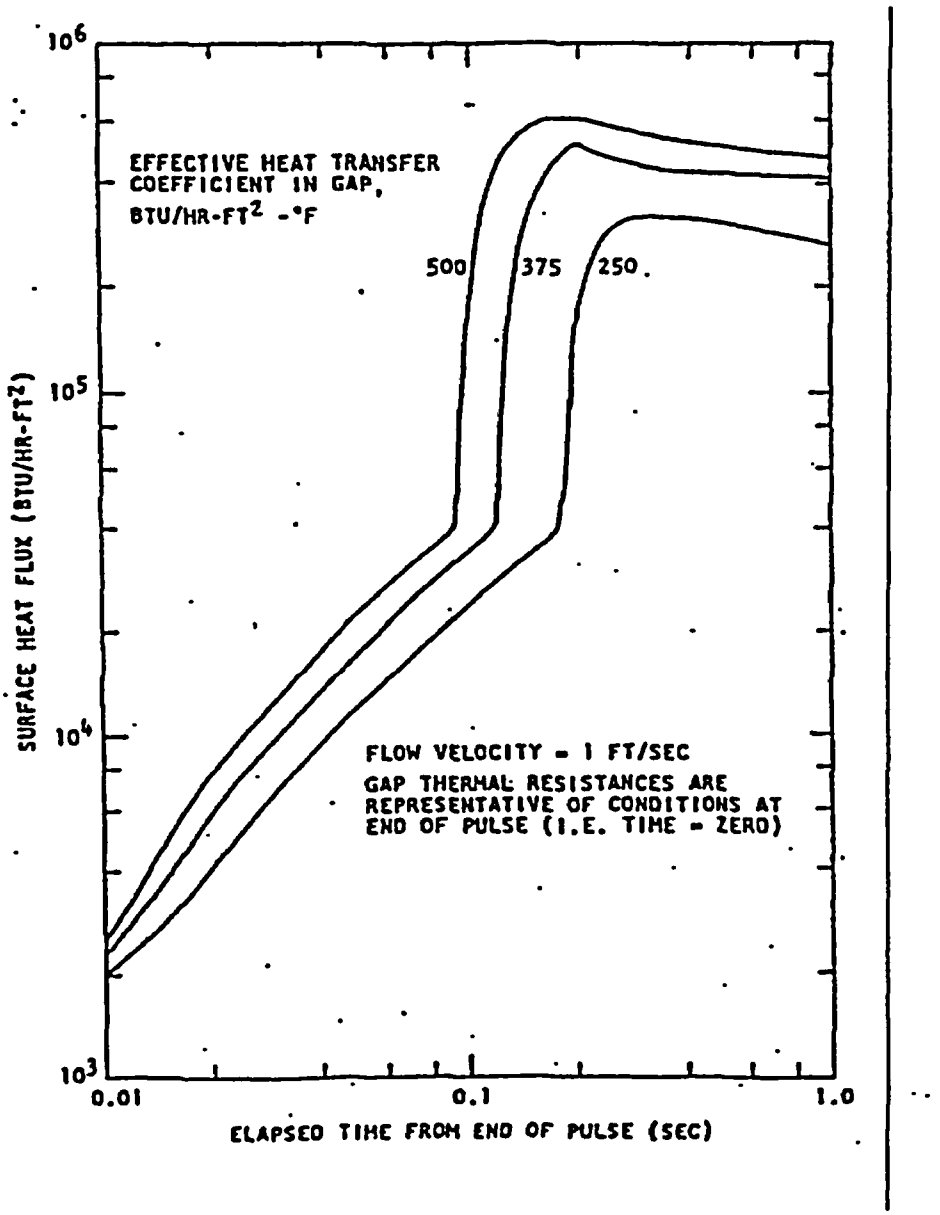

Figure 4A.10, Surface Heat Flux at Midpoint vs. Time for Standard Non-Gapped Fuel Element After a Pulse.

Bibliography

"A Theory of Local Boiling Burnout and Its Application to Existing Data," Heat Transfer - Chemical Engineering Progress Symposium Series, Storrs, Connecticut, 1960, v. 56, No. 20.Bernath, L.,

Research in Improved TRIGA Reactor Performance, Final Report, General Dynamics, General Atomic Division Report GA-5786, October 20, 1964. Coffer, C.O., et al.,

Characteristics of Large Reactivity Insertions in a High Performance TRIGA U-ZrH Core, General Dynamics, General Atomic Division Report GA-6216, April 12, 1965.Coffer, C. O., et al.

Annular Core Pulse Reactor, General Dynamic, General Atomic Division Report GACD 6977, Supplement 2, 1966.Dee, J. B., T. B. Pearson, J. R. Shoptaugh, Jr., M. T. Simnad,

Temperature Variation, Heat Transfer, and Void Volume Development in the Transient Atmosphere Boiling of Water, Report SAN-1001, U. Cal., Berkeley, January, 1961. Johnson, H.A., and V.E. Schrock, et al.,

A Study of the Mechanism of Boiling Heat Transfer, JPL Memorandum No. 20-88, March 1, 1954.Ellion, M.E.,

Thermal Conductance of Metallic Surfaces in Contact, USAEC NYO-2130, May, 1959.Fenech, H., and W. Rohsenow,

An Analysis of a Thermal Contact Resistance, Trans. ANS 5, p. 476, 1962.Fenech, H., and J.J. Henry,

"Thermal Conductance Across Metal Joints," Machine Design, Sept. 15, 1960, pp 166-172. Graff, W.J.

Heat Transmission, 3rd Ed., McGraw-Hill, 1954McAdams, -W.H ..

MNRC, McClellan Nuclear Radiation Center Facility Safety Analysis Report, Rev. 2, April 1998.

Heat, Mass and Momentum Transfer, Prentice-Hall, 1961, pp 231-232.Rohsenow, W., and H. Choi,

"Quarterly Technical Report SPERT Project, April, May, June, 1964," ISO 17030. Spano, A. H.,

"The Effect of Subcooled Liquid on Film Boiling," Heat Transfer 84, 149-156, (1962).Sparrow, E.M. and R.D. Cess,

"Onset of Stable Film Boiling and the Foam Limit," **Int. J. Heat and Mass Transfer 6, 987-989, (1963). Speigler, P., et al.,**

UTA, University of Texas at Austin TRIGA Reactor Facility Safety Analysis Report, Docket 50-602, Rev. 1.01, May 1991.

"Hydrodynamic Aspects of Boiling Heat Transfer," AEC Report AECV-4439, TIS, ORNL, 1959. Zuber, W.

Appendix B
Water Properties at Nominal Operating Conditions

The following data are from the NBS/NRC Steam Tables, by L. Haar, J.S. Gallagher, and G.S. Kell, Hemisphere 1984.

Saturated Water at 0.153 MPa		
TEMPERATURE, T	111.9	°C
PRESSURE, P	0.153	MPa
HEAT OF VAPORIZATION, λ	2.22E+03	kJ kg^{-1}
SURFACE TENSION, σ	5.66E-02	J m^{-2}
ρ, density (kg m^{-3})	9.50E+02	8.78E-01
C_v, heat capacity (kJ kg^{-1} K^{-1})	3.71E+00	1.55E+00
C_p, heat capacity (kJ kg^{-1} K^{-1})	4.24E+00	2.09E+00
s, entropy (kJ kg^{-1} K^{-1})	1.44E+00	7.22E+00
i, enthalpy (kJ kg^{-1})	4.70E+02	2.69E+03
u, internal energy (kJ kg^{-1})	4.69E+02	2.52E+03
sonic speed (m s^{-1})	1.53E+03	4.79E+02
k, thermal conductivity (W m^{-1} K^{-1})	6.82E-01	2.65E-02
μ, dynamic viscosity (kg m^{-1} s^{-1})	2.50E-04	1.27E-05
ν, kinematic viscosity (m^2 s^{-1})	2.64E-07	1.45E-05
α, thermal diffusivity (m^2 s^{-1})	1.70E-07	1.44E-05
Pr, Prandtl Number	1.55E+00	1.00E+00
β, volumetric expansion coefficient	8.14E-04	2.86E-03

Subcooled Water at 27°C, 0.153 MPa

TEMPERATURE	(T)	27 °C
PRESSURE	(P)	0.153 MPa
DENSITY	(ρ)	9.97E+02 kg m^{-3}

C_v, heat capacity (kJ kg^{-1} K^{-1})	[redacted]
C_p, heat capacity (kJ kg^{-1} K^{-1})	
s, entropy (kJ kg^{-1} K^{-1})	
i, enthalpy (kJ kg^{-1})	
u, internal energy (kJ kg^{-1})	
sonic speed (m s^{-1})	
k, thermal conductivity (W m^{-1} K^{-1})	
μ, dynamic viscosity (kg m^{-1} s^{-1})	
ν, kinematic viscosity (m^2 s^{-1})	
α, thermal diffusivity (m^2 s^{-1})	
Pr, Prandtl Number	
β, volumetric expansion coefficient	

6. Engineered Safety Features

As discussed in Chapter 13, from previous analysis, and from experience at other TRIGA reactors, emergency core cooling is not required for operations at steady state thermal powers below 1900 kW. No engineered safety features are required for the KSU reactor because the steady state power limit is 1,250 kW.

6.1 Bibliography

Kansas State University TRIGA Mark II Reactor Hazards Summary Report, by R.W. Clack, J.R. Fagan, W.R. Kimel, and S.Z. Mikhail, License R-88, Docket 50-188, 1961.

Analysis of Certain Hazards Associated with Operation of the Kansas State University TRIGA Mark II Reactor at 250 kW Steady State and with Pulsed Operation to $2.00, by R.W. Clack, et al., and the Safety Evaluation by the U.S. Atomic Energy Commission Division of Reactor Licensing, License R-88, Docket 50-188, 1968.

NUREG-1282, "Safety Evaluation Report on High-Uranium Content, Low-Enriched Uranium-Zirconium Hydride Fuels for TRIGA Reactors," U.S. Nuclear Regulatory Commission, 1987.

7. INSTRUMENTATION AND CONTROL SYSTEMS

Much of the reactor's original instrumentation and control (I&C) systems were replaced during the control room modifications in 1993 and 1994. The original console and vacuum-tube instruments were replaced by a surplus solid-state console obtained from U.S. Geological Survey's TRIGA Mark-I reactor. This console was then outfitted with new N-1000 series neutronic channels from General Atomics. These channels have optically isolated outputs, allowing other devices to utilize the neutronic data.

7.1 Summary Description

The bulk of the reactor I&C systems are hard-wired analog systems primarily manufactured by General Atomics and widely used at various NRC-licensed facilities. The general layout of these systems is shown in Figure 7.1.

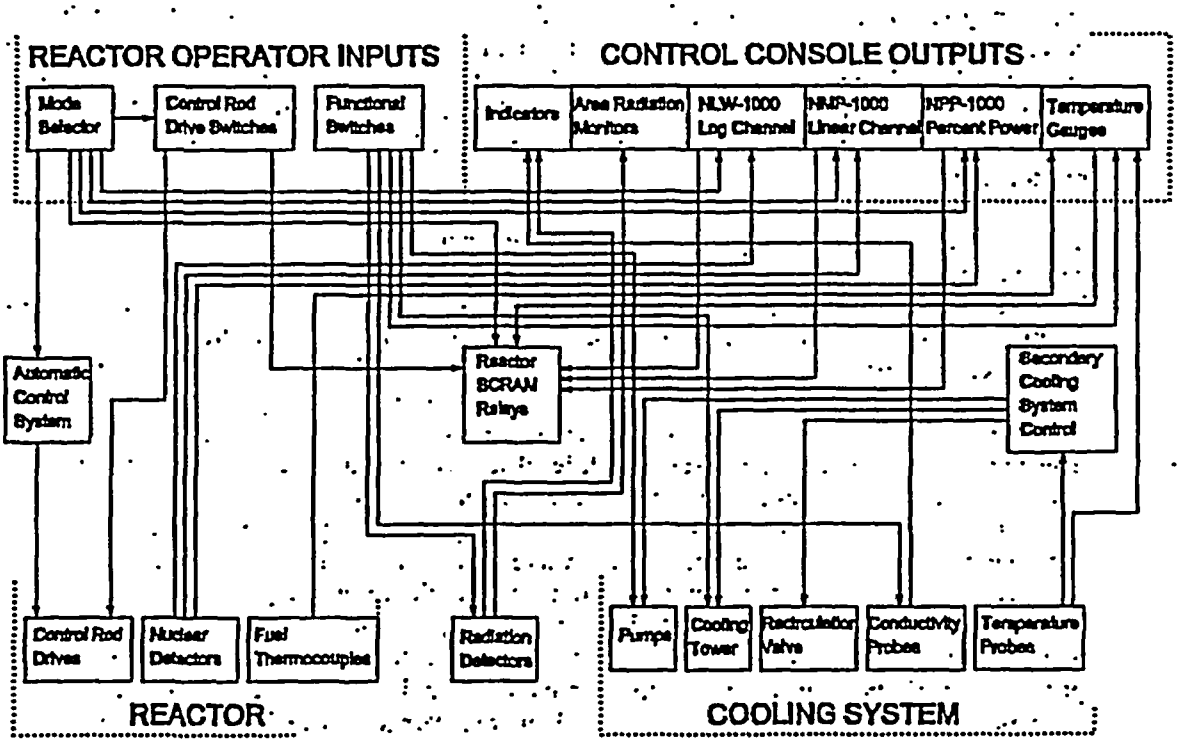

Figure 7.1, Inter-connectivity Diagram.

The reactor control system (RCS) consists of the instrumentation channels, the control rod drive circuitry and interlocks, and an automatic flux controller. The RCS measures several key reactor parameters including power, fuel temperature, water temperature, and water conductivity. Three neutronic instruments measure reactor power separately: a wide-range logarithmic channel, a multi-range linear channel, and a percent power channel. These provide at least two indications

of reactor power from source range to power range. Additionally, if a reactor pulse is performed another channel is added to the central thimble to record pulse data. Fuel temperatures can be monitored on both the console and on an auxiliary panel. Primary water temperature is displayed on the console and measured by an RTD in the water box. Titanium electrodes at the entrance and exit of the cleanup loop measure water conductivity.

The control rod drives and their associated circuitry are simple in design. A rotary switch configures the primary mode of operation, namely automatic, steady-state, or pulse mode. Numerical indicators give drive position, with illuminated switches to manipulate the rods and to indicate rod and drive status. Several interlocks are incorporated to prevent unintentional rapid insertions of reactivity, except in pulse mode. An automatic control system links the RCS with the neutronic channels providing regulation of the power level.

The reactor protection system (RPS) is a component of the RCS instruments. The RPS will initiate a reactor scram if any of several measured parameters in the RCS are outside of their limited safety system settings. The reactor scram effectively places the reactor in a subcritical configuration by releasing the control rods from their respective drives. Since the rods are no longer physically attached to the drive, they fall into the reactor core by gravity. High reactor power, high fuel temperature, loss of detector high voltage, loss of building power, and short reactor period will automatically cause all of the control rods to be dropped into the reactor core. A bar above the control rod drive switches allows this system to be actuated manually. Since the core is cooled by natural convection, no other engineered safety features are necessary for safe reactor shutdown.

The control console and display instruments are primarily housed in a control console, with auxiliary instruments located in a rack next to the console. At the console, the reactor operator has direct control over mode of operation, control rod drive positions, cooling system operation, opening of reactor bay doors, and manual scram of the reactor. Display instruments located in the control console provide measurements of reactor power, control rod positions, primary water temperature, and fuel temperature. Indicators in the console display scram information, low air pressure, low primary water level, high reactor sump water level, sump high water level, sump overflow water level, secondary surge tank level low, source interlock status, reactor bay upper door open, reactor bay lower door open, thermal column door open, person on stairway, and rod drive status. Secondary surge tank makeup is controlled with a backlit pushbutton that indicates surge tank low level and surge tank makeup valve operation. An intercom system on the console provides communication to numerous locations around the reactor bay and staff offices. In the auxiliary rack, the operator can control pneumatic transfer system operation, actuate timers, and add water to the secondary cooling system. Display instruments located in this rack include, primary water conductivity, water activity, remote area radiation monitors, fuel temperature, and a strip-chart output of reactor power. Several audible alarms indicate high radiation levels in the primary coolant and at various locations throughout the reactor bay. A breaker-box in the control room provides control over electrical devices in the reactor facility, including ventilation systems.

Radiation protection instruments are distributed throughout the reactor bay. :All instruments have visual indication of radiation level, visible alarm conditions, and audible alarms. Radiation area monitors (RAM) strategically cover potential radiation areas throughout the reactor bay. A combined pool surface and primary water monitor indicated water activity. A 5 $R \cdot h^{-1}$ evacuation

alarm is located on the 22-foot level. A continuous air monitor (CAM) is energized during reactor operation.

The human-machine interface principles incorporated into control room design allow the reactor to be operated by a single individual. All monitoring instruments are visible to the reactor operator at the console. The instruments and controls necessary for reactor operation are within reach of the operator, including an intercom and telephone. Surveillance instruments are located next to the console, with visual and audible alarms to signal the operator to abnormal conditions.

7.2 Design of Instrumentation and Control System

7.2.1 Design Criteria

Reliability of essential equipment is ensured through redundancy. Multiple instruments and safety systems perform similar functions for all modes of reactor operation. The construction and installation of instruments was performed according to applicable regulations at the time of introduction. However, all crucial instruments are checked daily for calibration and operability. Testing and calibration procedures exist for repair and general service. The majority of these I&C systems were manufactured by General Atomics, or other industrial manufacturers of nuclear equipment. Crucial systems to be considered include neutronic instruments, control rod drives, radiation monitors, and control systems.

Redundancy is designed into each of these systems. During steady state operation, a minimum of two neutronic channels provide reactor power level indication, two of which provide high power level RPS actuation (scram). These neutronic instruments are tested prior to reactor operation for demonstration of scram capability. Two are also tested for operability by internal calibration tests. There are two fuel temperature indications. The control rod drives drop their rods into the reactor core upon loss of power or RPS actuation, providing sufficient shutdown margin with even the most reactive rod stuck out. Multiple remote area radiation monitors cover important areas, including two directly above the reactor core and two monitoring primary coolant activity.

The maximum steady state power level for KSU TRIGA Mark II reactor is proposed to be 500 kW. Similar reactors operate up to 2 MW with 2 GW pulses. Therefore, the limited safety systems settings associated with reactor are extremely conservative when compared to the safety limits of the reactor. Thus the reactor has a considerable safety margin.

7.2.2 Design-Basis Requirements

The primary function of the RCS is to govern the manner in which reactivity is varied in the reactor core. The RCS system should prevent the reactor operator from unintentionally inserting large amounts of reactivity, through various interlock systems. The operator should only be able to remove one rod at a time from the reactor core, preventing large insertion rates. The pulse rod must not be able to be rapidly ejected from the core while in steady-state operation. Furthermore, the pulse rod should be the only rod that can be withdrawn in pulse mode, preventing supercritical pulses. There should also be an interlock to prevent startup without a power level signal above the minimum instrument sensitivity, preventing unmonitored or unanticipated

criticality. Rod position indicators should show the rod position to 0.2% or total travel for accurate reactivity calculations.

Another primary function of the RCS is to provide the reactor operator with reactor status information. Reactor power, a crucial parameter, requires at least two instruments to provide confirmation of reactor power from shutdown to operating levels. Three instruments are used to cover this range: a wide-range logarithmic channel, a multi-range linear channel, and a percent power channel. Accuracy of measurement at full rated power increases accordingly with the refinement of scale. The log channel provides gross reactor power indication and is accurate to 20% of scale, the linear channel is accurate to 5% of scale, and the percent power channel is accurate to 3% of scale. The percent power channel will also display pulse parameters for large pulses. These instruments are calibrated annually and checked for operability at the start of each operating day. An additional channel is installed and calibrated in the central thimble to record pulse data. Fuel temperature must be monitored during pulsing operation.

The primary function of the RPS is to automatically insert the control rods into the reactor core when certain parameters deviate from limited safety system settings. Several scrams involve the neutronic channels in the RCS. If 110% rated power level is exceeded in steady state mode, one of two trip-points will scram the reactor. Failure of the high voltage power supplies for operating neutronic channels will also cause a scram. Manual scram will be available in all modes of reactor operation. Rod drop times for the standard rods will be measured regularly to ensure proper RPS function. No other ESF features are required in this design.

The primary function of the radiation monitoring instruments is for personnel protection measures and emergency assessment actions. The area monitors provide the reactor operator with information regarding the actual radiation environment inside the reactor bay. With this knowledge, reactor users can be informed of possible hazards. A 5 $R \cdot h^{-1}$ monitor on the 22-foot level signals personnel to evacuate the reactor bay. A number of survey instruments (ion chambers, rem balls, G-M counters) are also available to personnel. Other instruments such as the constant air monitor, pool surface monitor, and water box monitor indicate the presence of dispersible radioactive materials, an indication of possible fuel cladding failures.

The control room is designed so a single operator can manipulate all significant controls without leaving the room. The reactor operator should be able to de-energize all equipment and experiments in the reactor bay. The control room should provide sufficient ventilation to provide cooling of the reactor instruments.

7.2.3 System Description

The overall system layout is depicted in Figure 7.2. The majority of the RCS is housed in a General Atomics (GA) console originally manufactured for the USGS reactor, which is shown with modifications in Figure 7.2. A detailed description of this figure is provided in Table 7.1. Figure 7.3 shows a representative layout of the auxiliary instrumentation rack. Since the instrument racks are general use equipment, configuration may be changed to allow better utilization of space, installation of new equipment, support specific equipment modifications, etc. without affecting function. The functions of each piece of equipment in this configuration are discussed in following sections with additional figures showing location and layout.

7.2.4 System Performance Analysis

The system performance of the current I&C systems surpasses the original equipment. Reliability has been high, with few unanticipated reactor shutdowns. Since daily checkouts are performed, any discrepancies would be observed and corrected in a prompt manner. The opto-isolated outputs of the neutronic channels allow the data to be utilized by other devices without concern over those devices affecting the channels. A line conditioner provides regulated power to the instruments, protecting the equipment from electrical disruptions.

7.2.5 Conclusion

The current I&C systems outperform the original equipment supplied with the reactor, while meeting all of the necessary design bases for the facility. The human design factors used in control room development allow the reactor to be operated by a single individual. Checkout and testing procedures ensure that all equipment is maintained in operational status.

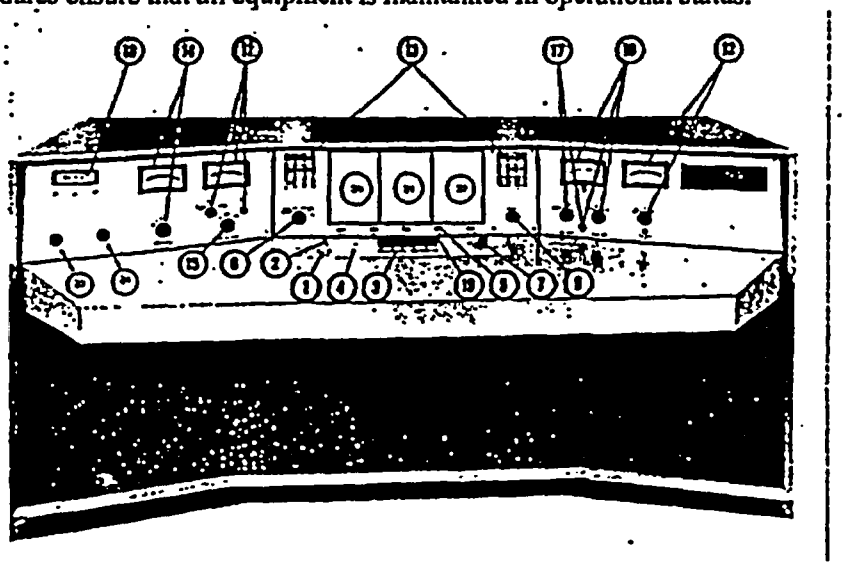

Figure 7.2, USGS TRIGA Console with Modifications.

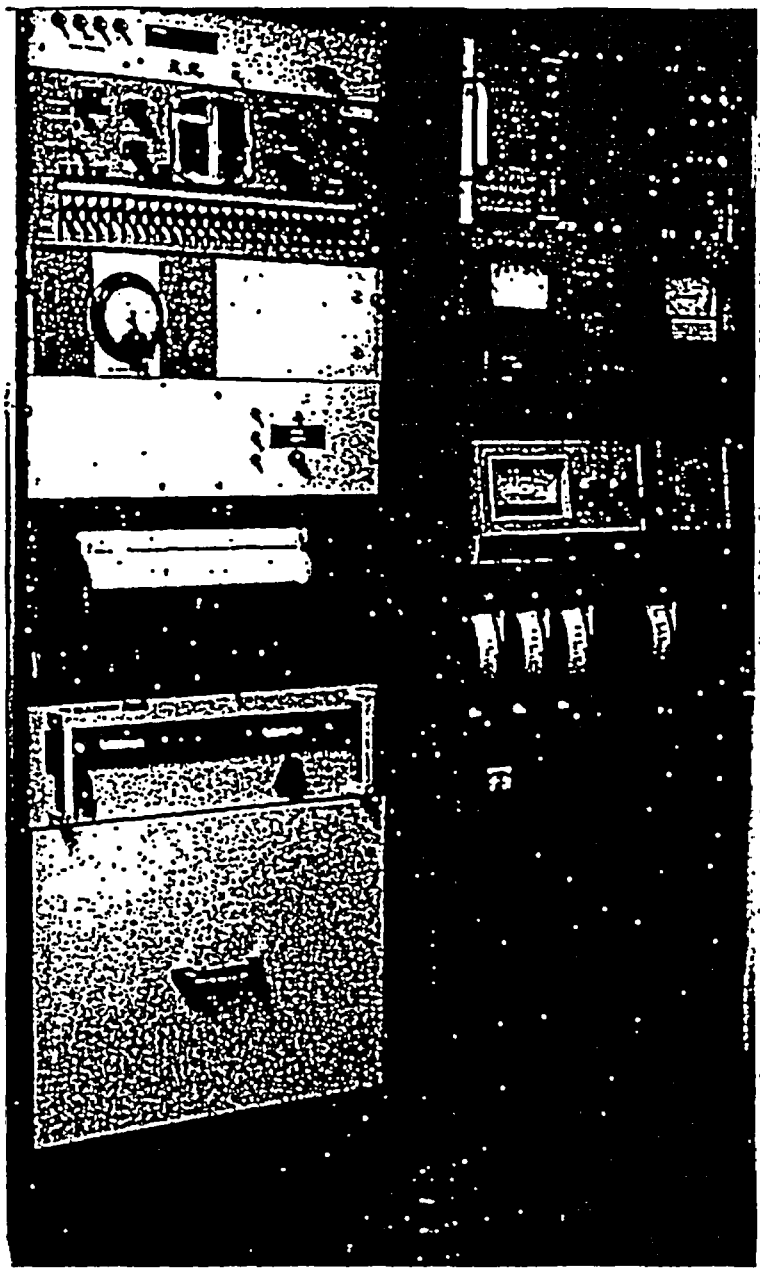

Figure 7.3, Instrumentation Rack.

Table 7.1, Description of Figure 7.2.

Number	Function	Description
1	Console Power	Push Button Switch
2	Magnet Power / Scram Reset	Key Switch
3	Control Rod Drive Position	Push Button Switches
4	Apply Air to Pulse Rod	Push Button Switch
5	Rod Position Indicators	LED Displays
6	Mode Selector	Rotary Switch
7	Removed	Backup Range Switch
9	Automatic Power Demand Control	10 Turn Potentiometer
10	Manual Scram Bar	Bar Covering Scram Switches
11	(not used)	Backup Period Channel
12	Fuel #2 & Water Temperature	Display and Selector Switch
13	Scram Status, Source Interlock, Low Air Pressure, Hi & Hi-Hi sump level, surge tank level & makeup, Upper & Lower Doors, and Cooling System Power	Indicators and Control Switches
14	(not used)	Backup Count Rate Channel
15	(not used)	Backup Log Channel
16-17	(not used)	Backup Percent Power Channel
18	(not used)	N/A
20	Wide Range Log Power Channel	GA NLW-1000 Channel
21	Multi-Range Linear Power Channel	GA NMP-1000 Channel
22	Percent Power and Pulsing Channel	GA NPP-1000 Channel
23	Source Interlock Override	Key Switch
24	Period Scram Override	Key Switch

7.3 Reactor Control System

The bulk of the reactor control system (RCS) is housed in the USGS console shown in Figure 7.2. The remainder is contained in the auxiliary rack-mount panel next to the console, shown in Figure 7.3. The RCS consists of the instrumentation channels, the control rod drive circuitry and interlocks, and an automatic flux controller. These are shown in Figure 7.4. The RCS measures several key reactor parameters including power, fuel temperature, water temperature, and water conductivity.

7.3.1 Neutronic Instruments (Reactor Power)

Three neutronic instruments measure reactor power separately: a wide-range logarithmic channel, a multi-range linear channel, and a percent power channel, as shown in Figure 7.5. Wiring diagrams and calibration procedures are found in the instrument maintenance manuals listed in the bibliography.

The wide-range log channel uses a fission counter for detecting thermal neutrons in the range of 1.4 to 1.4 x 10^5 nv, and provides approximately 0.7 counts·nv^{-1}. The detector has an aluminum case, an aluminum electrode, a U_3O_8 [(redacted)% enriched in ^{235}U) coating as the neutron sensitive material, and an argon-nitrogen mixture for a fill gas. A preamplifier is used to minimize noise and signal loss from the detector to the console, and it is located on the 12-foot level.

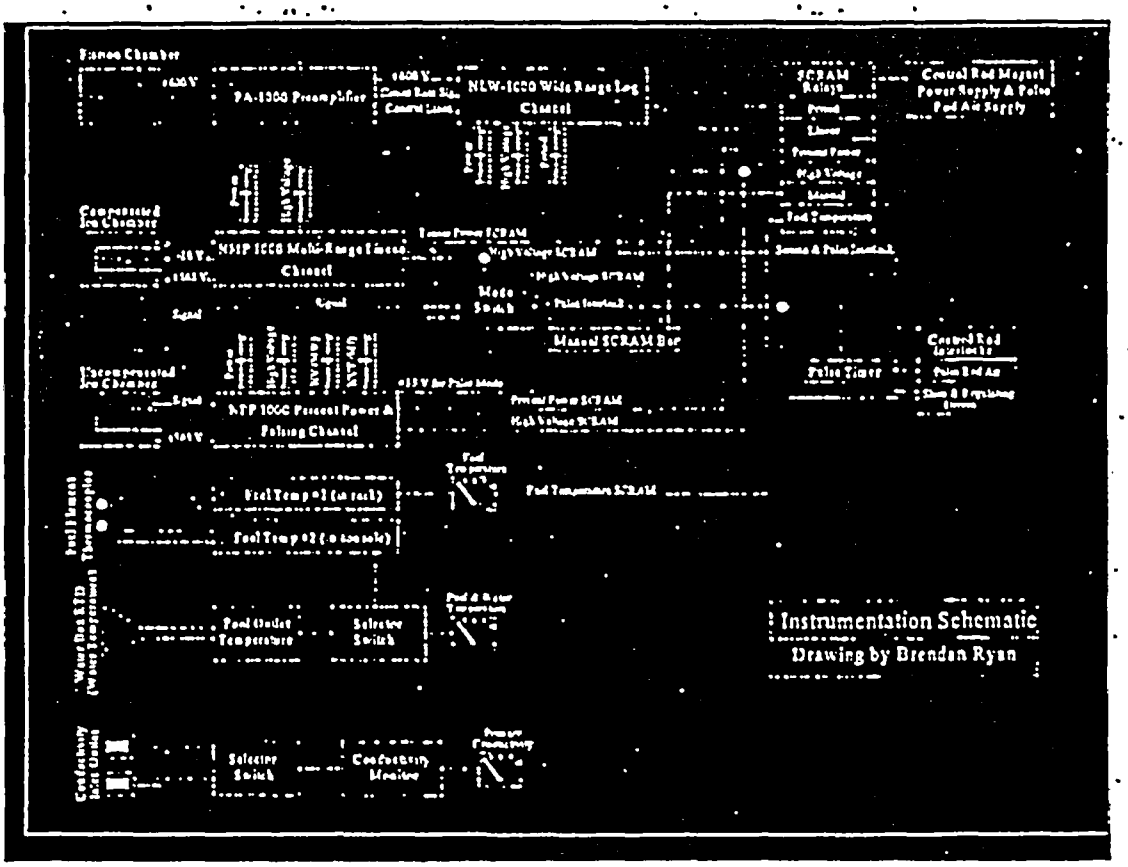

Figure 7.4, Instrumentation Diagram.

The remainder of the channel circuitry is located in the NLW-1000 unit in the central console. The NLW-1000 unit supplies the high voltage for the detector and power for the preamplifier. The instrument switches from pulse mode operation to current mode as reactor power increases out of the source range, allowing the instrument to measure reactor power in the upper ranges. Three displays indicate reactor power, high voltage, and reactor period. The power signal is permanently recorded via an opto-isolated output to a strip-chart recorder located in the instrumentation rack. The period meter has a scram at 3 sec and there is a high voltage scram, both of which are bypassed in pulse mode. This channel also provides a protective interlock which prevents rod withdrawal when indicated neutron flux is < 2 cps, which is also activated in pulse mode to prevent removal of the shim, safety and regulating rods. Another interlock prevents pulsing when reactor power is above 10 kW (normally set at 1 kW). The unit has two

calibration checks in pulse mode, two in current mode, and checks for the period and high voltage scrams.

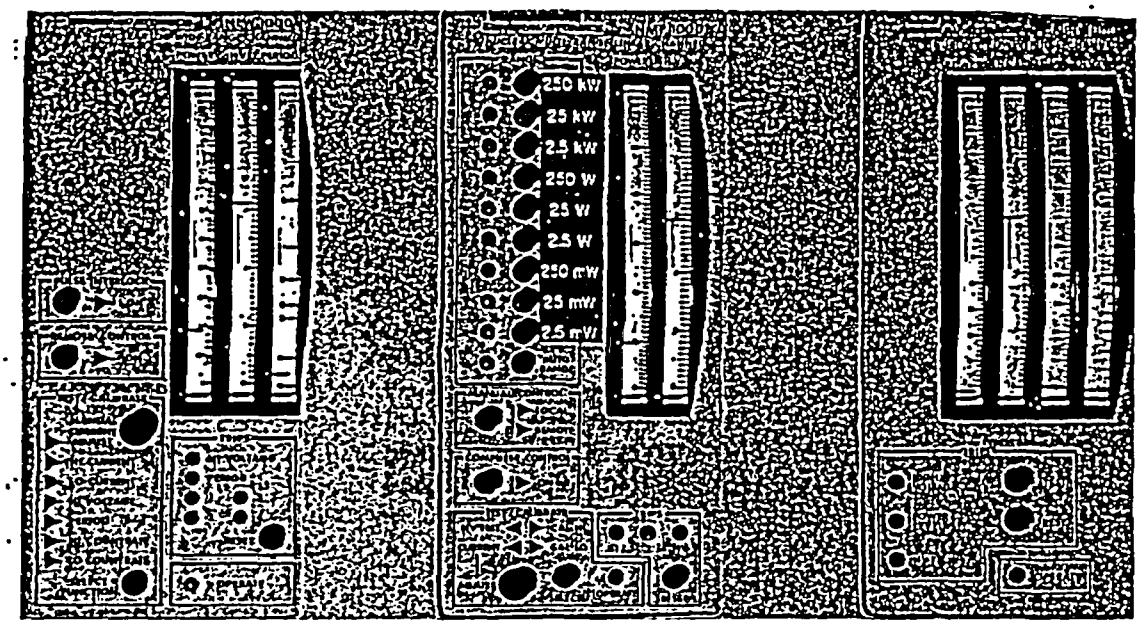

Figure 7.5, N-1000 Series Instruments.

The second channel provides multi-range linear power indication. This channel uses a compensated ion chamber for detection of thermal neutrons. The linear channel detector signal goes directly to the NMP-1000 unit in the center console, which in turn supplies high and compensation voltages. This unit features automatic or manual ranging to select the appropriate decade of power displayed. The instrument provides two indicators, power and high voltage. The power signal is permanently recorded via an opto-isolated output to a strip-chart recorder located in the instrumentation rack. In addition there is also a high power level scram (normally set for 104% nominal rated power) and a high voltage scram. The signal from the detector and the high voltage scram are bypassed in the pulsing mode. The unit has two calibration checks, an auto-ranging test feature, and checks for high power level and high voltage scrams.

Power range indication of neutron flux is provided by an uncompensated ion chamber signal, which indicates percentage of power in the upper two decades of the power range. The uncompensated ion chamber is virtually identical in construction to the compensated ion chamber, but no gamma compensation is provided in the circuitry. The detector sends its signal to the NPP-1000 instrument in the center console, which provides a visual indication of reactor power, high voltage, nv, and nvt measurements. The NPP-1000 supplies the high voltage for the detector. There is a high power scram (normally set for 104% of full power) and a high voltage scram. In pulse mode, the channel is designed to read off the maximum power and integral output of a reactor pulse. However, the pulse output readings are measured in reference to the 250 MW maximum. Hence an additional channel is added to the central thimble to permit recovery of data from pulses of various magnitudes. The unit has checks for high power and high voltage scrams.

An added pulsing channel consists of a small BF_3 chamber, which can be inserted into the central thimble of the reactor core. A separate high voltage supply powers the instrument and a multi-range picoammeter reads the detector current. A reference voltage output of the picoammeter is sent to a computer in the control room, which collects the pulse data. This channel is calibrated prior to pulsing operations and range selected in advance based upon the anticipated peak power.

7.3.2 Temperature

Temperature indications for the primary water and specific B-Ring fuel elements are provided on the front section of the control panel and in the instrumentation rack. The instrumented fuel elements have three chromel-alumel thermocouples in the fuel element that are used for temperature indication on the console or in the instrumentation rack. The thermocouples are located 0.76 cm (0.3-in) below the fuel surface, spaced at the midpoint of the element and at ±, 2.5 (1 in.) cm from the midpoint; an averaged value from all three thermocouples is typically used for instrument readings. The temperature in the primary cleanup loop is a nickel alloy thermistor, and is displayed on a console meter, which is shared with fuel temperature via a rotary switch. Another indication of fuel temperature is located in the instrumentation rack with the capability of initiating reactor scram if the measured fuel temperature exceeds a preset value (normally 400 °C).

Several other temperature measurements can be obtained from the computer in the control room. The computer can read two additional fuel thermocouples from other fuel elements in various positions in the reactor core. Additionally AD590 temperature transducers are located on the inlet and exit of both the primary and secondary sides of the heat exchanger to evaluate performance. Two other transducers are located in the reactor tank for bulk pool temperature measurement and high temperature alarm.

7.3.3 Water Conductivity

Primary water conductivity is measured at the inlet and outlet of the purification loop by titanium electrode cells that send signals to a bridge circuit in the instrumentation rack. The bridge circuit is automatically temperature compensated and nulled to provide good conductivity measurements over all reactor conditions. The inlet and outlet conductivities provide a good indication of the overall purity of the primary water and the effectiveness of the ion exchanger.

7.3.4 Control Rod Drives

Four control rods are required for reactor operations at 1,250 kW to meet reactivity control requirements: a shim rod, a regulating rod, a transient rod, and a safety rod. The shim, regulating and safety rods share identical control circuitry (Figure 7.7) and provide coarse and fine power control. Two of the rod drives are original, analog systems. One of the rod drives uses a stepper motor. Drive position is determined by voltage drop across a potentiometer that is adjusted as the control rod drive is moved. The position indicator for the analog motors is attached to a shaft coupled to the drive motor shaft with a setscrew, while the stepper motor is connected to the

position indicator with a chain drive. The pulse rod is designed so that it can be rapidly ejected from the core to a preset height to initiate a reactor pulse. However, it still functions as a normal control rod in steady state mode. All rods can be individually scrammed without shutting down the reactor.

a. Standard Control Rod Drives

The rod drive mechanism (see Figure 7.6) is an electric motor actuated linear drive, equipped with a magnetic coupler. Its purpose is to adjust the reactor control rod position. In the analog drive motor, a 110-V, 60-cps, two phase motor drives a pinion gear and a 10-turn potentiometer. The potentiometer provides rod position indication. The pinion engages a rack attached to the magnet drawtube. An electromagnet mounted on the lower end of the drawtube engages an iron armature that screws into the end of a long connecting rod which terminates (at its lower end) in the control rod.

The magnet, armature, and upper portion of the connecting rod are housed in a tubular barrel that extends well below the reactor water line. Located part way down the connecting rod is a piston equipped with a stainless steel piston ring. Rotation of the motor shaft rotates the pinion, thus raising or lowering the magnet draw tube. If the magnet is energized, the armature and connecting rod will follow the draw tube so that the control rod is withdrawn from or inserted into the reactor core. In the event of a reactor scram, the magnet will be de-energized and release the armature. The connecting rod, piston, and control rod will then drop, thus reinserting the control rod into the reactor. Since the upper portion of the barrel is well ventilated, the piston will move freely through this range. However, when the connecting rod is within 2-in (5 cm). of the bottom of its travel, the piston is restrained by the dashpot action of the restricted ports in the lower end of the barrel. This restraint cushions bottoming impact. Control rod drop times are measured semi-annually and must be less than one second.

The analog rod drive motor is dynamically braked and held by an electrically locked motor. In the static condition, both windings are energized with the same phase (see Figure 7.7), electrically locking the motor. Clockwise (up) or counter-clockwise (down) rotation is enabled by shifting the phase between the windings with a 1-μF capacitor; motor control switches allow the appropriate phase shift. The stepper motor operates using phase switched direct current power. The motor shaft advances 200 steps per revolution (1.8 degrees per step). Since current is maintained on the motor winding when the motor is not being stepped, high holding torque is maintained. A translator module drives the stepping motor.

Three microswitches limit and control the travel of the magnet drawtube. Actuation of the magnet up limit microswitch (S901) applies line voltage to one winding therefore allowing only the phase shift, which gives counter-clockwise rotation.

Actuation of the magnet down limit microswitch (S902) applies line voltage to the other winding therefore allowing only the phase shift that gives clockwise rotation. Actuation of the rod down microswitch (S903A) causes the phase shift for counter-clockwise rotation. Therefore, if the control rod drops, the magnet drawtube drives down until the

magnet down limit microswitch locks the rotor. Since the rod down microswitch drives the magnet draw tube down, then the rod down microswitch must be open before the magnet down microswitch during coupled withdrawal of the control rod.

Three lights indicate that, 1) the magnet drawtube is full up, 2) the magnet drawtube is full down, and 3) the armature and magnet are coupled. When the magnet drawtube is full up, microswitch (S901) is actuated opening the short across the magnet up light (DS321). When the magnet draw tube is full down, microswitch (S902) is actuated opening the short across the magnet down light (DS324). When the control rod drops, the non-actuated magnet down microswitch (S902) and the actuated rod down microswitch (S903B) short the contact light (DS317) indicating separation of the magnet and the armature.

Other features of the circuit are an adjustable bias resistor (R902), a 220-ohm surge resistor, 50-ohm current limiting resistors. The adjustable bias resistor compensates for the torque applied by the weight of the control rod and the magnet drawtube. The 220-ohm surge resistor limits the capacitor current surge during switching. The 50-ohm current limiting resistors limit the currents in the 12-volt indicating circuits when the indicating lamps are shorted.

The unconventional circuit employed in the rod-drive system minimizes the number of switch contacts required. Therefore, relays with their attendant reliability problems are not required. It should be noted that the rod drive units are identical both mechanically and electrically (with the exception that one unit uses a stepper motor) and they are, therefore, interchangeable.

The rod position indicators are three digit, LED display indicators that receive a variable DC voltage input from 10-turn potentiometers that are driven by the respective rod drive motors. The digital display is simply a voltmeter, since the voltage across the potentiometer is directly related to the control rod position. The position indicators have their own variable power supplies and are therefore completely independent. The indicator systems are located in the control console except for the 10-turn potentiometers on the drive and the associated wiring.

Normal rod motion speed is about 12-in. per minute. Using rod speed, rod position indication at UP and DOWN limit switch positions, and respective rod worth curves, the operator can determine the reactivity insertion rate for a given interval of rod motion.

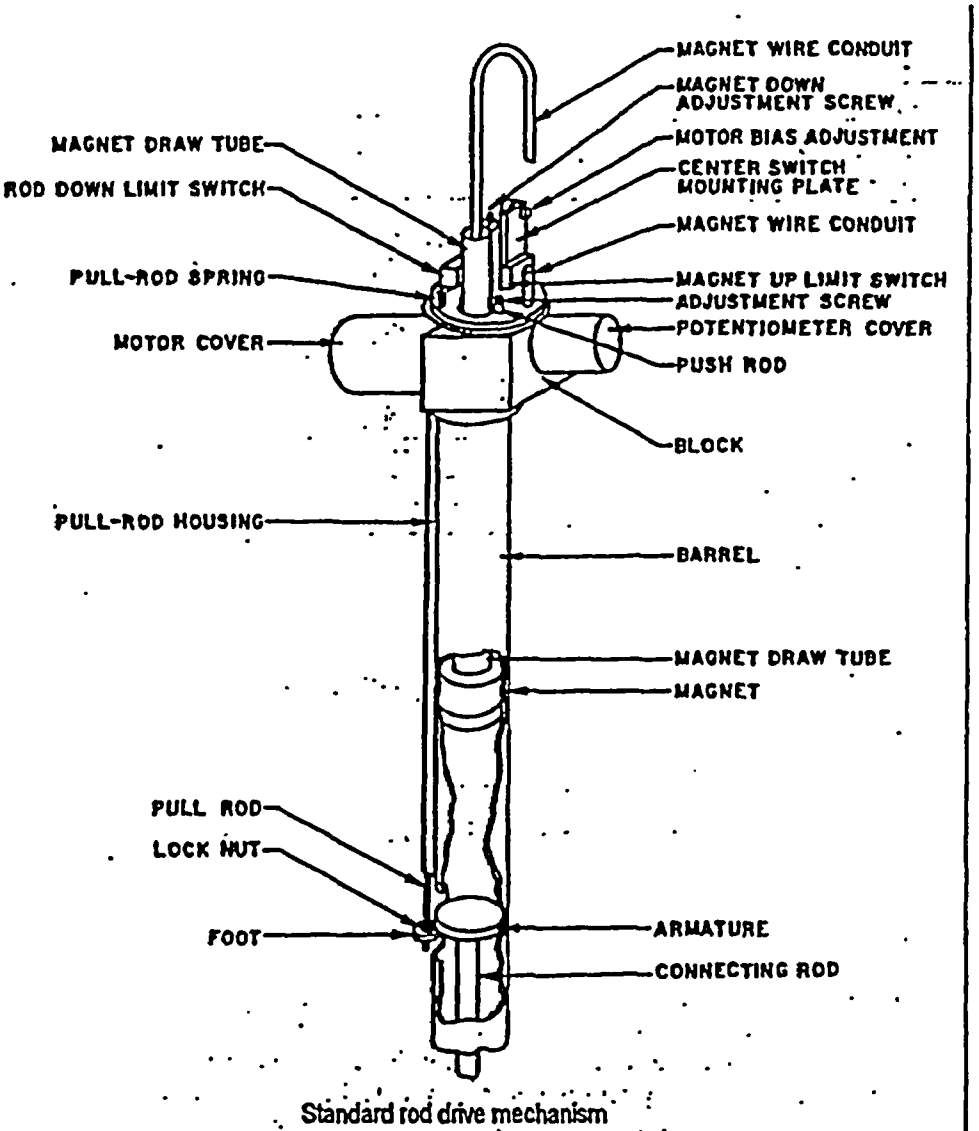

Figure 7.6, Regulating, Safety and Shim Rod Drive.

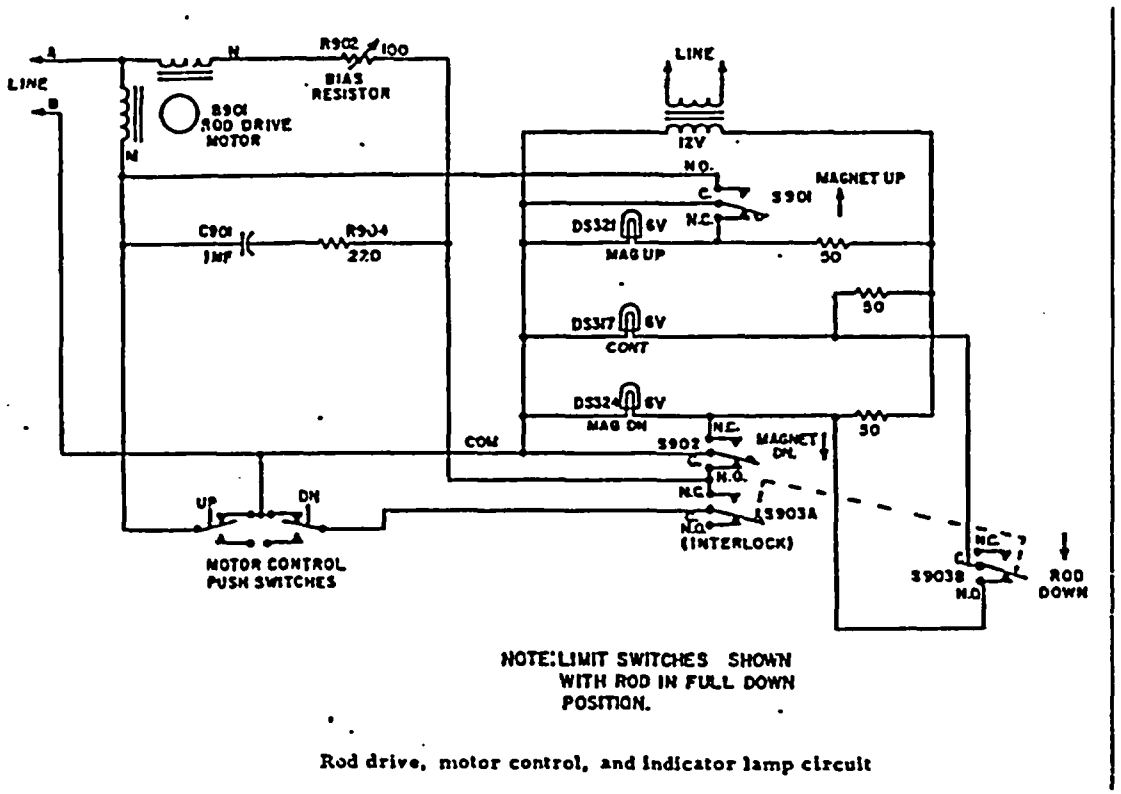

Rod drive, motor control, and indicator lamp circuit

Figure 7.7, Control Rod Drive Circuit.

b. Transient Rod Drive

The transient rod-drive (Figure 7.8) is an electrically controlled, pneumatically operated, mechanically limited system. The transient rod and aluminum extension rod are mechanically connected to a pneumatically driven piston inside a worm gear and ball-screw assembly. The system is housed on a steel support structure mounted above the reactor tank. A three-way solenoid valve mounted below the support controls air to the piston. The throw of the piston, and hence the amount of reactivity inserted into the core during pulsing operations, is regulated by adjusting the worm gear and ball-screw assembly. The adjustment is made from the central console by actuating a reversible motor drive, which is coupled to a worm gear and a 10-turn potentiometer for position indication. The operation of the position indicator is identical to that of the shim, safety and regulating control rods. The drive circuitry is identical to the shim, safety and regulating rods (Figure 7.7), except for that the motor is not continuously energized. Relays in the drive unit allow it act similarly to the electrically locked motors. Since air is used to support the rod, there is no compensation for rod weight. The remaining differences involve the pneumatic relay controls.

The solenoid valve is actuated by means of the console mounted transient rod fire and air release (scram) switches. When the rod fire switch is depressed, the solenoid valve opens, admitting air to the cylinder, coupling the piston and rod to the shock absorber. Depressing the air release switch de-energizes the solenoid valve, which removes air from the cylinder and vents air to the atmosphere. In the event of a reactor scram, the solenoid will be de-energized via the scram circuitry, which will allow the transient rod to drop into the core after the air is removed. Micro-switches are used to indicate the extreme positions, up or down, of the shock absorber. In steady state mode, an interlock prevents actuation of the rod fire switch if the drive is not in its fully down position.

In the pulse mode, a variable timer (usually six seconds) de-energizes the solenoid valve after the pulse is initiated. The shock absorber will remain in its preset position until the mode selector switch is taken to steady state. In the steady state mode of operation, the adjustable (normally six second) timer is disengaged and the cylinder remains pressurized. If the air supply for the pulse rod drive should drop below approximately 45 psig, an amber low air pressure warning light will be actuated on the control console. Loss of air pressure will cause the rod to fall into the core.

c. Interlocks

Several interlocks are built into the control system of the reactor to prevent improper operation. These interlocks are hard-wired into the control rod drive circuitry. They are stated below:

1. No control rod withdrawal (shim, regulating and safety rods only) is possible unless the count rate neutron channel is indicating > 2 cps. This interlock prevents the possibility of a startup without a functional power level startup channel.

   The low count rate interlock may be bypassed during fuel loading operations when core inventory is not high enough to multiply the source above 2 cps.

2. Air may not be applied to the pulse rod if the pulse rod shock absorber is above its full down position and the reactor is in the steady state mode. This interlock prevents the inadvertent pulsing of a reactor in the steady state mode.

3. There is no simultaneous withdrawal of two or more control rods when the reactor is in the steady state mode. This interlock prevents violation of the maximum reactivity insertion rate of the reactor.

4. The pulse rod is the only control rod that can be withdrawn when the reactor is in the PULSE mode (this does not prevent the scramming of any control rod). This interlock minimizes the possibility of pulsing a supercritical reactor. This interlock is provided by the source interlock, which is engaged when the log channel is placed in pulse mode.

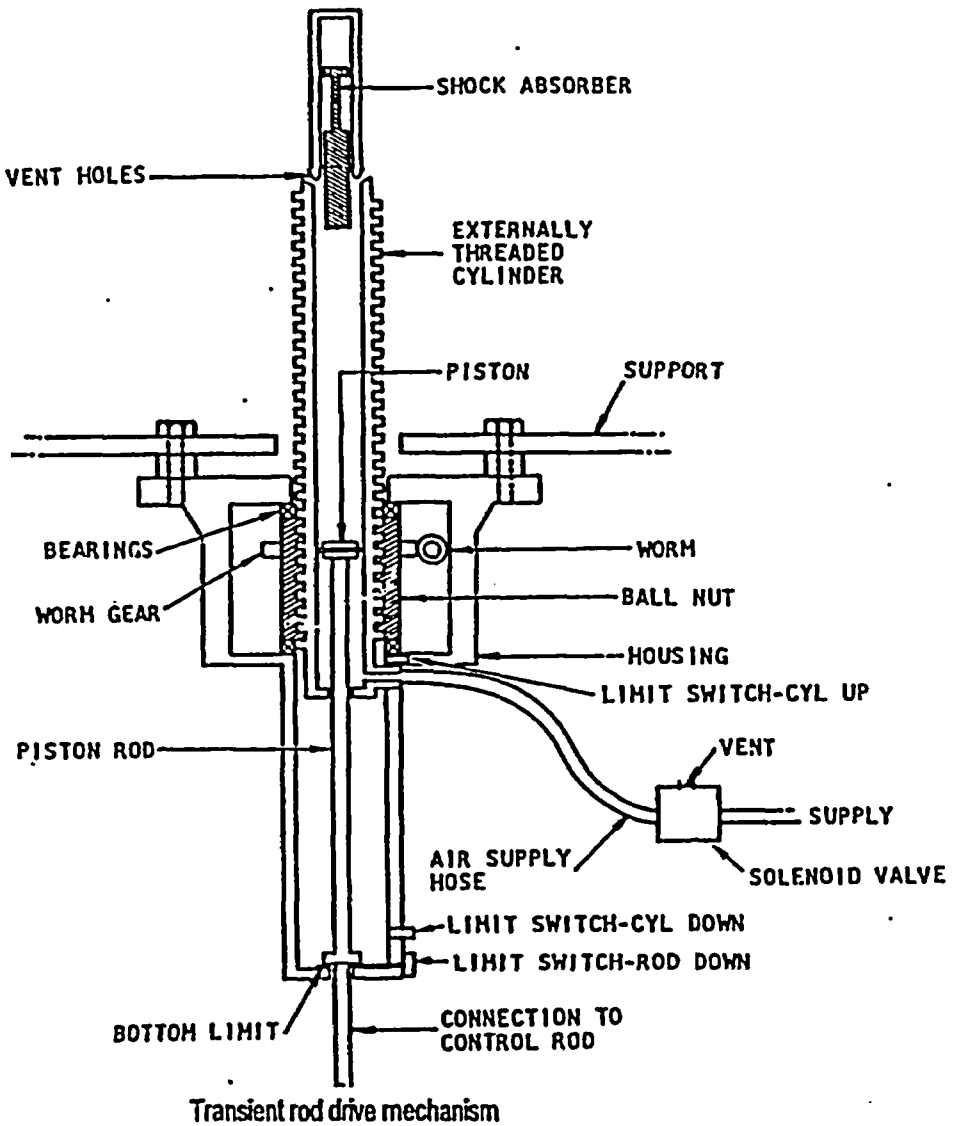

Figure 7.8, Transient Rod Drive.

Additionally, there is an interlock that prevents reactor pulses from being fired if the reactor power is above 10 kW (normally set at 1 kW). There is also a key switch for bypassing the source interlock during fuel loading operations to check for criticality.

7.4 Reactor Protection System

The reactor protection system (RPS) will initiate a reactor scram if any of several measured parameters are outside their limited safety system settings (LSSS). The reactor scram effectively shuts down the reactor by de-energizing portions of the shim, regulating, transient, and safety rod drives, causing the control rods to drop into the reactor core by gravity. The shim, safety and regulating rod drives utilize electromagnets to hold up their respective control rods. The pulse rod drive utilizes an electric solenoid to apply compressed air to the pulse rod. High reactor power, high fuel temperature, loss of detector high voltage, or short reactor period will automatically cause the control rods to be dropped into the reactor core. The reactor operator may manually scram the reactor as well by means of a scram bar on the console. If beam ports are in use in their open configuration, an additional reactor scram may be added to reduce radiation levels if personnel attempt to enter the beam area.

During steady state operation, the high reactor power scram, the high voltage power supply failure scrams for all neutronic channels, and the manual scram are required for operation. Although the period scram is normally in operation, it can be bypassed provided that the reactor operator calculate reactor period for each rod movement and that the calculated reactor period is greater than one second. The fuel temperature scram is active, but it is not necessary since the fuel temperature setpoint (usually set for 400°C) will normally not be reached during steady state mode.

In pulse mode, the mode selector switch is set to the HI PULSE position, interrupting detector signal to the linear channel. When the pulse interlock is activated (to initiate the source interlock) to prevent withdrawal of the shim, safety and regulating rods, the detector signal to the logarithmic wide range detector is interrupted. Consequently, the period scram and the linear high power scrams are disabled. High voltage scrams for the linear and log channels are also disconnected as large pulses produce detector currents that may temporarily overload the power supplies. The percent power channel increases its range to the pulse range (the percent power channel high voltage power supply scram remains active). The uncompensated ion chamber for the percent power channel is positioned further away from the reactor core, allowing for measurements of both steady state and pulsing power levels without excessive current from the high voltage supply.

7.5 Engineered Safety Features Actuation Systems

There are no engineered safety features actuation systems. Control rod insertion is provided by gravity and core cooling is provided by natural convection in water or air. Therefore, ESF systems are not required in this design.

7.6 Control Console and Display Instruments

The control console and display instruments are shown in Figures 7.2-7.5, 7.9, 7.10 and 7.12. Their layout (Figure 7.11) provides a single operator with all relevant reactor information. All push buttons required for general operation are located on the control console, within easy reach by a seated operator. All instruments on both the console and instrumentation rack are visible

from this seated position. In addition to the various analog displays, a computer display on top of console can also be used to show relevant reactor status information on a single screen.

There are several additional pieces of equipment in the control room. [redacted] to interrupt power to electrical devices in the control room and reactor bay (see Figure 7.13a). A halon fire extinguisher is located next to the breakers for use in fighting electrical fires. Current core and facility configuration is shown in a display cabinet (Figure 7.13.b). [redacted] A local radiation area monitor (including indicator and alarm) is located above the door in the control room to the reactor bay.

7.7 Radiation Monitoring Systems

Radiation monitoring systems are employed throughout the reactor facility: G-M detectors at the reactor pool surface and cleanup loop, 7 remote area monitor channels (3 general area or process monitors, 4 channels for beam ports – 11 beam port channels is currently instrumented, with the remainder scheduled for instrumentation near term), a 5 $R \cdot h^{-1}$ evacuation alarm, several air activity monitors, and numerous portable radiation monitors, including those for contamination monitoring. Additionally, an independent monitor with visual and audible alarms is located above the door to the reactor bay.

Figure 7.9, Control Room Overall View.

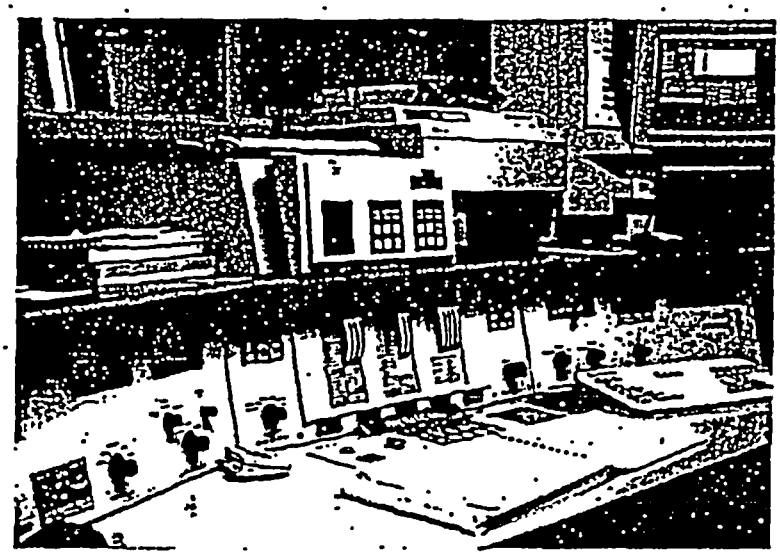

Figure 7.10, Control Console Operator's View.

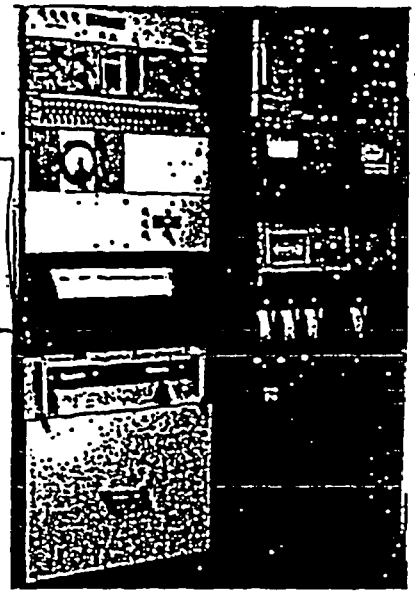

Figure 7.12, Instrumentation Rack Operator's View.

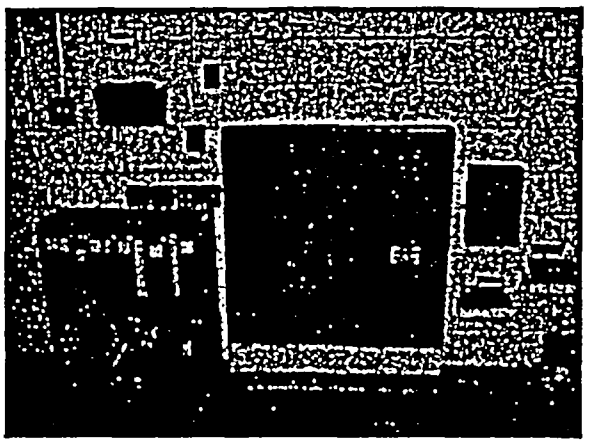

Figure 7.13a, Control Room Behind Operator.

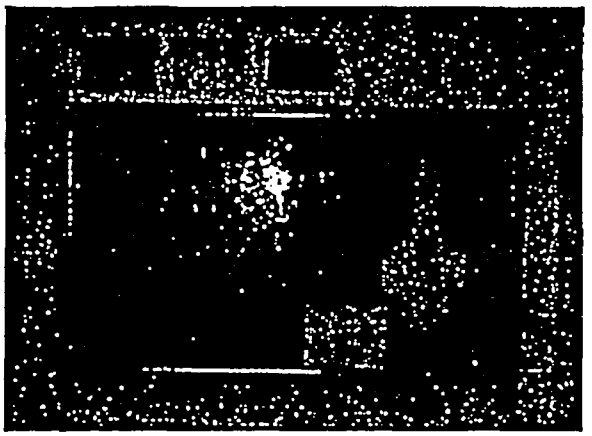

Figure 7.13b, Core Map.

The radiation monitor in the instrumentation rack provides an indication of radiation levels directly above the primary pool water surface. A meter on the right-hand section of the rack indicates a radiation dose rate of 100 $mR \cdot h^{-1}$ full scale, utilizing a GM tube detector measures coolant activity in the cleanup loop water box. The water box monitor has an audible alarm, with a reset button.

The remote area monitors utilize G-M detectors located throughout the reactor bay (typical unit illustrated in Figure 7.14). Permanent locations are: at the top of the reactor tank, above the bulk shield tank, and near the ion exchanger in the primary coolant system, and directly over the primary water tank. Each beam port has signal and power lines to support installing a beam port monitor. The detectors feature an analog readout in both the control room and locally with visual indicators for normal, alert, and alarm conditions. The control room alarm has an audible signal as well.

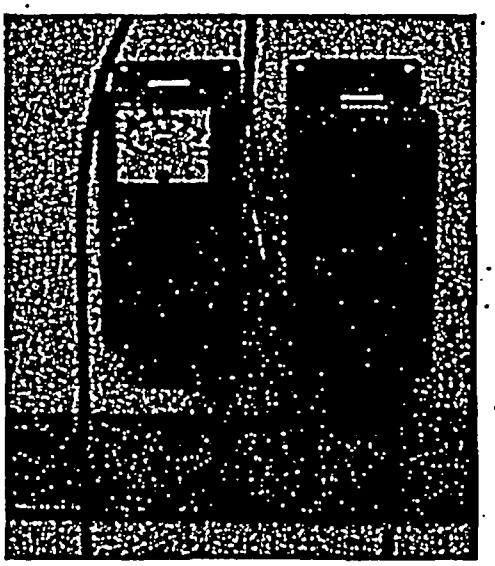

Figure 7.14, Typical Area Monitor Instillation.

A 5 $R \cdot h^{-1}$ monitor on the 22-foot level serves an evacuation alarm. The alarm signals a 100+ dB audible alarm in the reactor bay. Both the monitor and alarm are supplied by battery power in the event of a power failure.

There are numerous ion chamber and G-M portable survey instruments through the reactor bay and control room for gamma and beta surveys. These instruments are calibrated semi-annually. A rem-ball and a Bonner Sphere set are located in the reactor bay for neutron measurements. The rem-ball is calibrated annually. Low-level G-M counters in the reactor bay used for contamination monitoring. These are calibrated annually. Neutron and gamma sensitive pocket ion chambers are available in the control room for tours and personnel monitoring, and are calibrated semi-annually. Film and ring badges are issued to regular staff, which are read monthly and quarterly respectively.

An air monitoring system (Figure 7.15) samples air over the reactor pool. These monitors should sense any changes in radioactive discharge from the reactor pool to the environment. Channels are provided for monitoring particulate, noble gas and iodine activity.

An independent air monitoring system, a continuous air monitor (Figure 7.16), is stationed on the 12-foot level. This monitor should sense any changes in airborne contamination in the reactor bay. The continuous air monitor has active background discrimination. One channel monitors radioactive contamination on a filter exposed to airflow from the reactor bay. A second channel monitors background radiation levels for a background subtraction

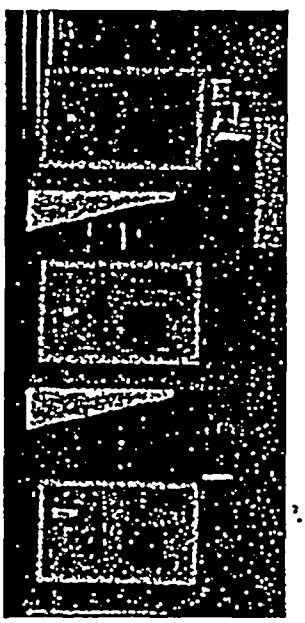

Figure 7.15: Air Monitoring System

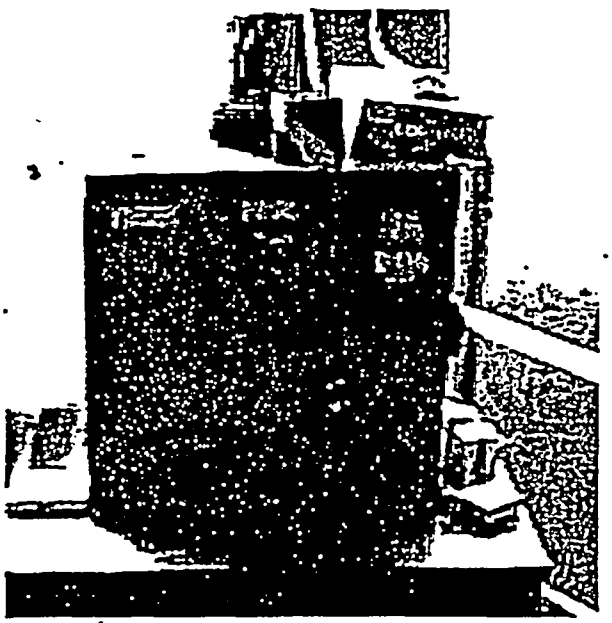

Figure 7.16: Continuous Air Monitor

7.8 Bibliography

250-kW TRIGA Mark II Pulsing Reactor Mechanical Maintenance and Operation Manual for KSU, General Atomics, GA-3399; 1 August 1962.

NMP-1000 Linear Power Channel: Operation and Maintenance Manual General Atomics, , E-117-1017, Rev. 1; 1991.

NLW-1000 Log Power Channel: Operation and Maintenance Manual, General Atomics, E117-1019; 1992.

NPP-1000 Percent Power Channel: Operation and Maintenance Manual, General Atomics, , E117-1010, Rev. 2; 1992.

TRIGA Mark I Reactor Instrumentation Manual for USGS, General Atomics, GA-9039; 1 November 1968. (For console acquired from USGS)

TRIGA Mark II Pulsing Reactor Instrumentation Maintenance Manual for KSU, General Atomics, GA-3114, no date.

13. ACCIDENT ANALYSIS

This chapter provides information and analysis to demonstrate that the health and safety of the public and workers are protected in the event of equipment malfunctions or other abnormalities in reactor behavior. The analysis demonstrates that facility design features, limiting safety system settings, and limiting conditions for operation ensure that no credible accident could lead to unacceptable radiological consequences to people or the environment.

13.1 Accident Initiating Events and Scenarios

This chapter deals with analysis of abnormal operating conditions and consequent effects on safety to the reactor, the public, and operations personnel. Three conditions to be analyzed are:

- Loss of coolant
- Insertion of excess reactivity
- Fuel encapsulation failure — the maximum hypothetical accident (MHA)

These are the three conditions considered in the initial licensing of the Reactor Facility in 1962 for 100-kW steady-state operation and in the 1968 upgrade of the license permitting 250-kW steady state operation and 250-MW pulsing operation. The analysis presented here treats the same conditions, but for steady-state operation at 1,250 kW and pulsing operation to a $3.00 reactivity insertion, estimated peak power of 1,340 MW.

The maximum hypothetical accident for a TRIGA reactor is the failure of the encapsulation of one fuel element, in air, resulting in the release of gaseous fission products to the atmosphere. Failure in air could result from a fuel-handling accident or, possibly, failure in the event of a loss of reactor coolant. Failure under water, leading ultimately to atmospheric release of fission products, could possibly result from insertion of excess reactivity or operation with damaged fuel. This chapter addresses the several scenarios potentially leading to fuel failure, and then the potential consequences, should failure occur in air.

13.2 Accident Analysis and Determination of Consequences

13.2.1 Notation and Fuel Properties

Tables 13.1-13.3 identify physical characteristics of the TRIGA Mark II fuel. Table 13.4 identifies the assumptions and design basis values used in the accident analyses.

Table 13.1, Dimensions of TRIGA MkII $ZrH_{1.6}$ Fuel Elements.

Property of Individual Element	Symbol	Value
Length of fuel zone	L_f	0.381 m
Fuel radius	r_i	0.018161 m
Clad outside radius	r_o	0.018669 m
Fuel volume	V_f	[redacted]
Clad volume	V_c	0.0000224 m^3
Fuel mass	M_f	[redacted]
Clad mass	M_c	0.1845 kg
Wt. Fraction U in fuel	x_u	[redacted]
Wt. Fraction $ZrH_{1.6}$ in fuel	x_m	[redacted]

Source: Training Manual, KSU TRIGA Nuclear Reactor Facility, 1998.

Table 13.2. Neutronic Properties of TRIGA MkII $ZrH_{1.6}$ Fuel Elements.

Property	Symbol	Value
Effective delayed neutron fractions	β	0.007
Effective neutron lifetime	ℓ	43 μsec
Temperature coefficient of reactivity	α	-0.000115 K^{-1}

Source: West et al. (1967).

Table 13.3, Thermal and Mechanical Properties of TRIGA MkII $ZrH_{1.6}$ Fuel Elements and Type 304 Stainless Steel Cladding.

Property	Symbol	Value	Temp.
Fuel			
Density	ρ_f	5996 kg m^{-1}	
Thermal conductivity	k_f	18 W m^{-1} K^{-1}	All
Heat capacity, $c_{pf} = 340.1 + 0.6952T(°C)$	c_{pf}	340.1 J kg^{-1} K^{-1}	0 °C
Cladding			
Density	ρ_c	7900 kg m^{-1}	300 K
Thermal conductivity	k_c	14.9 W m^{-1} K^{-1}	300 K
		16.6	400 K
		19.8	600 K
Heat capacity	c_{pc}	477 J kg^{-1} K^{-1}	300 K
		515	400 K
Yield strength		250 Mpa	400 °C
Tensile strength		455 Mpa	400 °C

Source: fuel properties from Simnad (1980); cladding properties from Incropera and DeWitt (1990) and from Metals Handbook (1961).

Table 13.4, KSU TRIGA Core-Conditions Basis for Calculations.

Steady state maximum power, P_o	1,250 kW
Fuel mass per element	2.367 kg
Heat capacity per element at T (°C)	$805.0 + 1.646T$ (J K^{-1})
Minimum number of fuel elements, N	[redacted]
Core radial peaking factor	2
Axial peaking factor	$\pi/2$
Excess reactivity	\$4.00 (2.8% Δk/k)
Maximum pulsing reactivity insertion	\$3.00 (2.1% Δk/k)
Excess reactivity at 500 kW maximum power[a]	\$1.16 (0.81% Δk/k)
Fuel average temperature at 500 kW maximum power[a]	285 °C

[a]Source: Data from GA Torrey Pines TRIGA reactor

13.2.2 Loss of Reactor Coolant

Although total loss of reactor pool water is considered to be an extremely improbable event, calculations have been made to determine the maximum fuel temperature rise that could be expected to result from such an event taking place after long-term operation at full power of 500 kW. Limiting design basis parameters and values are addressed by Simnad (1980) as follows:

> *Fuel-moderator temperature is the basic limit of TRIGA reactor operation. This limit stems from the out-gassing of hydrogen from the ZrH_x and the subsequent stress produced in the fuel element clad material. The strength of the clad as a function of temperature can set the upper limit on the fuel temperature. A fuel temperature safety limit of 1150°C for pulsing, stainless steel U-$ZrH_{1.65}$ ... fuel is used as a design value to preclude the loss of clad integrity when the clad temperature is below 500°C. When clad temperatures can equal the fuel temperature, the fuel temperature limit is 950°C. There is also a steady-state operational fuel temperature design limit of 750°C based on consideration of irradiation- and fission-product-induced fuel growth and deformation....*

As this section demonstrates, even under extraordinarily conservative assumptions and approximations, the maximum fuel temperature reached in a loss of coolant accident is 290°C, well below any safety limit for TRIGA reactor fuel. Conservatism notwithstanding, the margin between computed temperature and design limits is sufficiently great to accommodate a design margin of at least a factor of two.

a. Initial Conditions, Assumptions, and Approximations

The following conditions establish an extremely conservative scenario for analysis of the loss of coolant accident.

- The reactor is assumed to have been operating for infinite time at power P_o = 1,250 kW at the time coolant is lost.
- Coolant loss is assumed to be instantaneous.
- Reactor scram is assumed to occur simultaneously with coolant loss.

- Decay heat is from fission product gamma and x rays, beta particles, and electrons. Effects of delayed neutrons are neglected.
- Thermal power is distributed among $N =$ [redacted] fuel elements, with a radial peak-to-average ratio of 2.0. In individual elements, thermal power is distributed axially according to a sinusoidal function.
- Cladding and gap resistance are assumed to be negligible, i.e., cladding temperature is assumed to be equal to the temperature at the outside surface of the fuel matrix.
- Cooling of the fuel occurs via natural convection to air at inlet temperature T_i = 300°K. Radiative cooling and conduction to the grid plates are neglected.
- Heat transfer in the fuel is one dimensional, i.e., axial conduction is neglected, and fuel is assumed to be uniform in thermophysical properties.
- Heat transfer in the fuel is treated on the basis of pseudo-steady-state behavior, i.e., at any one instant, heat transfer is described by steady-state conduction and convection equations.[1]

b. *Core Geometry*

The following data on core geometry are derived from the KSU TRIGA Mechanical Maintenance and Operating Manual (1962). The core contains [redacted] fuel positions in five circular rings (B - F), plus the central thimble (A ring). The upper grid plate is 0.495 m in diameter and 0.019 m thick. Holes to position the fuel are 0.03823 m diameter and the central thimble is very slightly larger in diameter, 0.0384 m.

Cooling water passes through the differential area between the triangular spacer block on the top of each fuel element and the round holes in the upper grid plate. The nominal diametral clearance between the tips of the spacer blocks and the grid plate is approximately 0.001 m.

The lower grid plate is 0.405 m diameter, with 36 holes, 0.0159 m diameter, for water flow. However, the bulk of the water flow is through the annular space provided between the top of the lower grid plate and the bottom of the reflector. The radial reflector is D_r = 0.457 m inside diameter and 0.559 m height.

The effective hydraulic diameter for flow through the core, with an experiment in place in the central thimble, is given by

$$D_h = \frac{4 * A_{flow}}{P_{wet}} = \frac{4 * (\frac{\pi * D_r^2}{4} - 91 * \pi * r^2)}{\pi * D_r + 91 * 2 * \pi * r_0} = 0.02127m \quad \text{(Equation 13.2.2.1)}$$

[1] See Todreas & Kazemi (1990) or El-Wakil (1971) for steady-state conduction equations.

If, in thermal-hydraulic calculations, one approximates conditions as flow through an annular section around any one fuel element, the outer radius of the annulus, say r_o, is given by

$$D_h = \frac{4\pi(r_o^2 - r_e^2)}{2\pi r_e}, \text{ or}$$
$$r_o = \sqrt{D_h r_e / 2 + r_e^2} = 0.02339 \text{ m}, \qquad \text{(Equation 13.2.2.2)}$$

The flow area A_c per fuel rod is $\pi(r_o^2 - r_e^2) = \pi r_e D_h / 2 = 0.0006238$ m^2.

The total length of a fuel rod is 0.7206 m (28.37 in.), of which the length of the fuel matrix, the heated length, is L_f = 0.3810 (15 in). The lengths of upper and lower axial reflectors, L_u and L_l, are each 0.0874 m (3.44 in). Beneath the lower reflector is a bottom end fixture of length L_l about 0.0824 m (3.245 in.). Above the upper reflector is a triangular spacer of length L_t about 0.0191 m (0.75 in.) and an upper end fitting of length L_o about 0.0634 m (2.495 in.). The zone between grid plates is $L_c = L_l + L_t + L_f + L_u = 0.6382$ m.

c. Decay Power

The time dependence of the thermal power in the core as a function of time after shutdown is based on calculations by the CINDER code [England et al. 1976] as reported by George, LaBauve, and England [1980, 1982]. Sample results are presented in Figure 13.1 and Table 13.5 as the function $R(t)$ defined as the ratio of the thermal power $P_d(t)$ from gamma ray and beta particle decay at time t after shutdown to the steady power P_o prior to shutdown, based on 200 MeV energy release per fission.

For the purpose of this analysis, the time dependence function for 1 to 10^6 s may be approximated as

$$R(t) = \frac{0.04856 + 0.1189x - 0.0103x^2 + 0.000228x^3}{1 + 2.5481x - 0.19632x^2 + 0.05417x^3}, \qquad \text{(Equation 13.2.2.3)}$$

in which x is the natural log of the time after shutdown, in seconds. Time dependence of the thermal source in the worst-case element is given by

$$P_d(t) = \frac{2P_o}{N} R(t), \qquad \text{(Equation 13.2.2.4)}$$

in which the worst case element generates twice the power as the core average, P_o is the total-core thermal power prior to shutdown (1,250 kW), and N [redacted] is the minimum number of fuel elements required for operation.

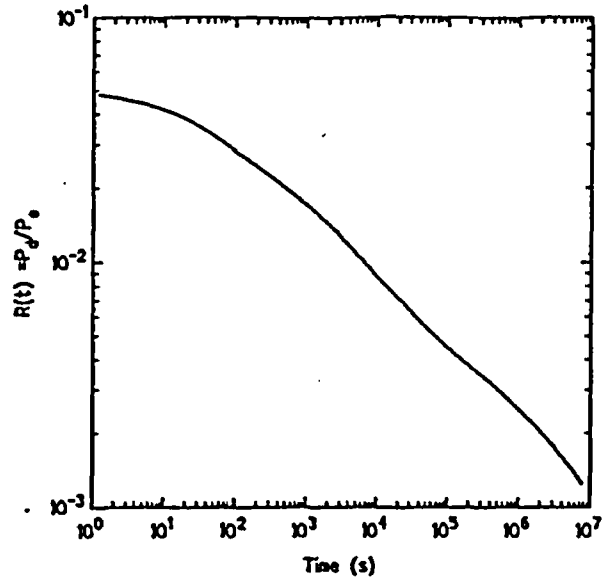

Figure 13.1: Decay Heat Function $R(t)$.

Table 13.5, Decay Heat Function for Thermal Fission of ^{235}U.

Time t (s)	$R(t) = P_d(t)/P_o$
0	0.0526
1 (10^0)	0.0486
10 (10^1)	0.0418
100 (10^2)	0.0282
1000 (10^3)	0.0172
10,000 (10^4)	0.0087
100,000 (10^{45})	0.0044
1,000,000 (10^6)	0.0025

d. Maximum Air Temperature

The fundamental relationships between buoyancy driven differential pressure and pressure losses from friction provide an independent verification for results of the previous calculations.

Buoyancy Driven Pressure Difference

The total mass flow rate w (kg/s) associated with the worst-case fuel element is determined by a balance between the buoyancy driven pressure difference vertically across the core and the frictional pressure loss within the core, which is discussed in the next section. The temperature rise across the core is

$$\Delta T_m(t) = T_o(t) - T_i = \frac{P_d(t)}{wc_{pm}^{air}} = \frac{2P_o R(t)}{Nwc_{pm}^{air}}, \qquad \text{(Equation 13.2.2.5)}$$

in which the heat capacity of the air evaluated at the inlet air temperature. At time zero, for example,

$$\Delta T_m(0) = T_o(0) - T_i \cong 0.6153 / w. \qquad \text{(Equation 13.2.2.6)}$$

Air inlet temperature T_i is assumed to remain constant at 27°C. Suppose ρ_i and ρ_o are respectively the densities of air at the inlet and outlet temperatures.[2] Suppose further that the effective chimney height is H. The chimney height is the distance between the center of the zone in which the air is heated and the center of the zone in which the air is cooled. Evaluation of the latter is difficult to determine because of uncertainties in mixing of the air after it leaves the upper grid plate. Here we follow the lead of the UT SAR (1991) and choose 10 hydraulic diameters as the effective distance. Thus, H is given by $L_f/2 + L_t + 10D_h = 0.422$ m. and the buoyancy pressure difference is given by

$$\Delta p_b = (\rho_i - \rho_0) * g * H \qquad \text{(Equation 13.2.2.7)}$$

in which g is the acceleration of gravity, 9.8 m s^{-2}. Since

$$\rho_i - \rho_0 \cong \frac{353 * (T_o - T_i)}{T_i^2}, \qquad \text{(Equation 13.2.2.8)}$$

and $T_i = 300\ K$, it follows from Eqs. (13.2.2-5) and (13.2.2-8) that

$$\Delta p_b(t) = 0.190 R(t) / w, \qquad \text{(Equation 13.2.2.9)}$$

Frictional Pressure Difference

In this calculation, only frictional losses within the core, computed on the basis of the equivalent annulus model, are accounted for. Based on air inlet density and an air mass flow rate per fuel rod of w, the frictional pressure difference is given by

$$\Delta p_f = \frac{L_c f w^2}{2\rho_i D_h A_c^2}. \qquad \text{(Equation 13.2.2.10)}$$

The laminar-flow (Moody) friction factor f for the equivalent annulus model, with $r_o / r_c = 1.193$ is given by Sparrow and Loeffler (1959) as

$$f = 100 / \mathrm{Re}, \qquad \text{(Equation 13.2.2.11)}$$

Re, the Reynolds number, is given by $D_h w / \mu_i A_c$, and μ_i is the dynamic viscosity of the air at the inlet temperature.[3] Equation (13.2.2-10) may be rewritten as

[2] Density at 1 atm, for air as an ideal gas, is given by ρ (kg/m^3) = 353.0/T(°K). Heat capacity, from 300 to 700 °K is 1030 J/kgK ± 3% (Incropera and DeWitt, 1990).

[3] Dynamic viscosity, over the range 250 - 1000 °K is given by $10^7 \mu$ (Ns/m^2) = -106.2941 + 16.81986[T(°K)]$^{1/2}$ or $\mu = 1.85 \times 10^{-5}$ Ns/m^2 at 300 °K. (Incropera and DeWitt, 1990).

$$\Delta p_f = \frac{0.1416 L_c \mu_i T_i w}{D_h^2 A_c} = 1780 w, \qquad \text{(Equation 13.2.2.12)}$$

Equating the frictional pressure drop with the buoyancy pressure driving force, using Equations (13.2.2-9) and (13.2.2-12),

$$w = 0.0103\sqrt{R(t)}, \qquad \text{(Equation 13.2.2.13)}$$

or

$$T_o(t) - T_i = \Delta T(t) = 1140\sqrt{R(t)}. \qquad \text{(Equation 13.2.2.14)}$$

Results

For R(t) at time zero of 0.0526, maximum air temperature rise above 300 K is 261 K.

e. Fuel and Cladding Temperature Distribution

With design power P_o = 1,250 kW, a factor of two radial peak to average power, and a fuel surface area in the heated zone equal to $A_f = 2\pi r_o L_f = 0.04469$ m^2, the worst-case average heat flux at post-accident time t in the heated zone is:

$$q''_{-} = 2 * 1.25e6 * R(t) / A_f N = 3.37e5 \text{ W/m}^2. \qquad \text{(13.2.2-15)}$$

With the conservative approximation that the axial variation of heat flux is sinusoidal, the local value of the heat flux (W/m^2) is given by:

$$q''(z) = q''_{max} \sin(\pi z / L_f), \qquad \text{(13.2.2-16)}$$

in which z is the distance along the fuel channel, measured from the inlet and $q''_{max} = (\pi/2) q''_{avg} = 4.235 \times 10^5 R(t)$ W/m^2. Similarly, the local value of the air temperature in the coolant channel is given by

$$T_{air}(z) = T_i + \frac{0.6153 R(t)}{2}\left[1 - \cos(\pi z / L_f)\right]. \qquad \text{(13.2.2-17)}$$

According to Dwyer and Berry (1970), the Nusselt number for laminar flow in a cooling channel is approximately Nu = 4.24. The corresponding heat transfer coefficient is

$$h = \frac{k_{air} \text{Nu}}{D_h}. \qquad \text{(13.2.2-18)}$$

By using as an approximation the air thermal conductivity[4] of 26.3 W/mK at 300°K, one computes h = 5240 W/m^{2}K, and the cladding surface temperature

[4] For the range 200 to 1000°K, data of Incropera and DeWitt (1990) is very well fit by the formula $k_{air} = -22.055 + 2.8057\sqrt{T(^\circ K)}$ in units of W/mK.

$$T_{clad}(z) = T_{air}(z) + q''(z)/h. \qquad (13.2.2\text{-}19)$$

By using the fuel thermal conductivity k_f = 18 W/mK, and neglecting the temperature drop across the cladding, one computes the fuel centerline temperature as

$$T_{fuel}(z) = T_{clad}(z) + \frac{q''(z) r_e}{2k_f}. \qquad (13.2.2\text{-}20)$$

Fuel and cladding temperatures are reported in Table 13.6 and illustrated in Figure 13.2 for the case of zero time post accident. This is based on three conservative assumptions: equilibrium fission product buildup at full power, instantaneous loss of coolant when the reactor scram occurs, and equilibrium temperature based on initial decay heat production.

Table 13.6, Post-Accident Fuel and Cladding Temperatures.

z/L_f	q'' (W/m^2)	T_{air} (°K)	T_{clad} (°K)	T_{fuel} (°K)
0.00	0	300	300	300
0.10	17209	306	309	318
0.20	32733	325	331	348
0.30	45053	354	362	385
0.40	52963	390	400	427
0.50	55688	431	441	470
0.60	52963	471	481	508
0.70	45053	508	516	539
0.80	32733	536	542	559
0.90	17209	555	558	567
1.00	0	561	561	561

The K-State reactor does not operate 24 hours per day, 7 days per week, so that the total inventory of fission products is significantly lower than the assumed value. During actual loss of coolant, overall heat transfer coefficient will be based on water rather than air. There is at least 16 feet of water over the core that has to drain before the core is uncovered. Experiments reported in GA-6596."Simulated Loss-of-Coolant Accident for TRIGA Reactors" (General Atomics, August 18, 1965) demonstrated that with a constant and continuous heat production, temperature rises to about 50% of the equilibrium temperature in approximately 30 minutes (1800 seconds). At 10^3 seconds, R(t) is 0.0172, 33% of the heat production following shutdown. Equilibration takes a significant amount of time, while heat production is decaying.

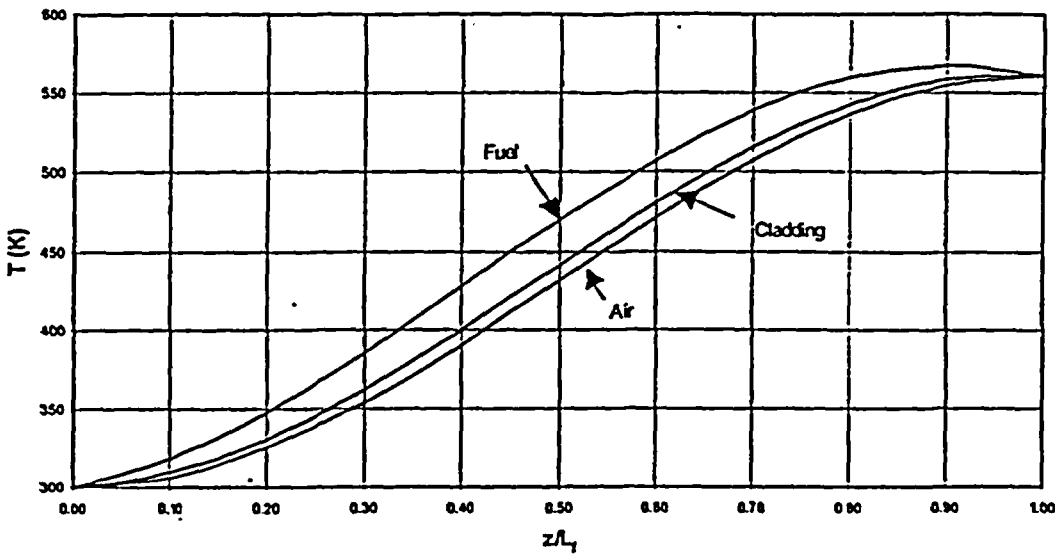

Figure 4.13, Axial Variation of fuel, cladding, and air temperature immediately following a loss of coolant accident, with equilibrium fission product heating.

f. Radiation Levels from the Uncovered Core

Although there is only a very remote possibility that the primary coolant and reactor shielding water will be totally lost, direct and scattered dose rates from an uncovered core following 1,250 kW operations have been calculated.

This section describes calculations of on-site and off-site radiological consequences of the loss-of-coolant accident. Extremely conservative assumptions are made in the calculations, namely, operation at 1,250 kW for one year followed by instant and simultaneous shutdown and loss of coolant. The reactor core is homogenized and the ORIGEN-2 [CCC-371] is used to define gamma-ray source strengths, by energy group. Radiation transport calculations are performed using the MCNP code (Briesmeister 1997), with doses evaluated at the 22-ft elevation of the reactor (one meter above the operating deck), in the reactor bay at the 0-foot elevation (one meter above the floor, 30-cm from the outer wall, and at one-meter above ground level at the site boundary and at points beyond the site boundary extending to 100 m radial distance from the core.

Modeling of the reactor core for radiation transport calculations is based on the following approximations. The TRIGA reactor core is approximated as a right circular cylinder 0.4572 m diameter (OD of F ring). The fuel region is 0.381 m (15 in.) high. On each end axially is a graphite zone 0.0874 m (3.44 in.) high and an aluminum grid plate 0.0191 m (0.75 in.) thick. In [redacted] fuel locations, there are [redacted] fuel elements, 3 standard control rods and 1 transient control rod, 1 void location, 1 central thimble (void), 1 source (assume void), and 1 pneumatic transfer site (assume void). The fuel region may is treated as a homogeneous zone, as are the axial graphite zones and the grid plates.

Fuel elements are 1.43-in. ID and 1.47-in OD, clad with type 304 stainless steel[5]. Fuel density is 5996 kg/m^3. Fuel composition is [redacted]% uranium, [redacted]%$ZrH_{1.65}$. The uranium is [redacted]^{235}U and [redacted]^{238}U. Steel density is 7900 kg/m^3. Standard control rods are 0.875-in. OD, the transient rod 1.25-in. OD. Both types of rods are clad with 30-mil thick aluminum (2700 kg/m^3 density). The control material may be approximated as pure graphite, with density 1700 kg/m^3.

In radiation transport calculations, the core is modeled conservatively as a central homogenous fuel zone (air density neglected) bounded on either end by a homogeneous axial reflector zone, and by a 0.75-in. thick aluminum grid plate, treated as a homogeneous solid. Densities of the homogenous zones are as follow:

Fuel	3602 kg/m^3
Reflector	1147 kg/m^3
Grid Plate	2700 kg/m^3

Composition of the three zones, by weight fraction, are given in Table 13.7.

Table 13.7, Compositions of Homogenized Core Zones.

Element	Mass Fraction	Element	Mass Fraction
Fuel Zone		*Axial Reflector Zone*	
C	0.0617	C	0.7920
Al	0.0010	Al	0.0033
H	0.0139	Mn	0.0041
Zr	0.7841	Cr	0.0368
Mn	0.0013	Ni	0.0164
Cr	0.0117	Fe	0.1474
Ni	0.0052		
Fe	0.0469	*Grid Plate*	
U	0.0741	Al	1.0000

The reactor bay is approximated as a right circular cylinder 36 ft (10.973 m) high and 36.68 ft (11.18 m) radius. The reactor vessel structure is approximated as a right circular cylinder, co-axial with the bay, 22 ft (6.706 m) high and 11 ft (3.3528 m) radius. The free volume is 144,000 ft^3 (4078 m^3). The site boundary, at its nearest approach to the reactor bay, is about 2 m beyond the bay boundary, that is, at a radius of 13.13 m from the center of the reactor.

Gamma-ray source strengths vs. times after shutdown are listed in Table 13.8 for an operating time of one year and a thermal power of 1,250 kW. The source strengths are gamma rays per second, by group, for the entire reactor core. In the MCNP calculations, the source is assumed to be uniformly distributed within the core.

The roof of the reactor bay is modeled as a concrete slab 10 cm thick and with density 2.35 g/cm^3. In fact, the roof is a composite structure, so reflection from the concrete slab conservatively models gamma-ray transport and dose rates at the site boundary.

[5] Composition, by weight, 2% Mn, 18% Cr, 8% Ni, balance Fe.

Table 13.9 reveals substantial dose rates above the void reactor tank with long-term 500-kW operation. One day after loss of coolant, the dose rate is 17 Sv/h (1700 rem/h). However, dose rates inside the reactor bay at the 0-ft. and 12-ft. elevations are only about 4 rem/h immediately after coolant loss, declining to about 1.5 rem/h after 1 hour and 100 mrem/h after 30 days. These dose rates show that personnel could occupy the reactor bay shortly after the loss of coolant to undertake mitigating actions without exceeding NRC occupational dose limits.

Dose rates at other receptor locations are shown in Table 13.9 as indicators of areas that should be checked following a loss of reactor pool water event. These dose rates are unrealistically conservative in view of the assumption of one-year operation at full power (not possible) and scattering from a thick concrete roof. Dose rates at the site boundary (facility fence) decline from about 3 rem/h immediately after the loss of coolant to 350 mrem/h after 1 day. Kansas State University has complete control over access to campus locations within the zones defined by receptor locations in the analysis.

Table 13.8,. Full Core Gamma-Ray Sources Strengths (Number Per Second) Following Operation for One Year at 1,250 kW Thermal Power.

	Time after shutdown				
E (MeV)	0	1 h	24 h	30 days	180 days
1.00E-02	8.72E+15	2.92E+15	1.05E+15	2.43E+14	6.20E+13
2.50E-02	2.09E+15	7.50E+14	3.04E+14	5.97E+13	1.32E+13
3.75E-02	1.74E+15	7.37E+14	3.97E+14	6.72E+13	1.45E+13
5.75E-02	1.81E+15	5.50E+14	1.77E+14	4.15E+13	1.20E+13
8.50E-02	1.50E+15	5.20E+14	2.33E+14	3.21E+13	8.39E+12
1.25E-01	1.50E+15	7.65E+14	4.81E+14	8.98E+13	1.31E+13
2.25E-01	3.11E+15	1.03E+15	4.44E+14	2.42E+13	6.83E+12
3.75E-01	1.94E+15	5.72E+14	2.20E+14	3.81E+13	3.41E+12
5.75E-01	3.25E+15	1.71E+15	7.54E+14	1.01E+14	1.08E+13
8.50E-01	4.16E+15	2.26E+15	8.94E+14	4.51E+14	1.15E+14
1.25E+00	2.22E+15	8.15E+14	7.83E+13	1.62E+12	6.01E+11
1.75E+00	9.30E+14	5.14E+14	2.23E+14	4.78E+13	7.72E+10
2.25E+00	5.00E+14	2.19E+14	6.69E+12	1.12E+12	3.72E+11
2.75E+00	1.99E+14	7.32E+13	8.13E+12	1.82E+12	1.55E+09
3.50E+00	1.16E+14	1.72E+13	7.12E+10	1.50E+10	9.37E+07
5.00E+00	6.23E+13	2.42E+11	6.96E+08	4.67E+00	4.63E+00
7.00E+00	5.05E+11	5.27E-01	5.27E-01	5.26E-01	5.22E-01
9.50E+00	9.49E+07	5.98E-02	5.98E-02	5.98E-02	5.93E-02
Total	3.39E+16	1.35E+16	5.27E+15	1.20E+15	2.61E+14
MeV/s	1.43E+16	6.28E+15	2.02E+15	5.77E+14	1.13E+14

Dose rates vs. post accident times are listed in Table 13.9 for a number of receiver locations. Locations are specified at radial distances from the center of the reactor bay. The22-foot level provides direct access to the reactor pool, the 12-foot level access to valves controlling water flow to the reactor pool. The 0-foot level provides access to valves and pumps, which allow water to be added to the reactor pool. The 13-meter distance marks a zone defined by the fence surrounding the reactor bay.

g. Conclusions

Although a loss of pool water is considered to be an extremely improbable event, calculations show the maximum fuel temperature that could be expected to result from such an event (after long-term operation at full power of 1,250 kW) is 294°C, well below any safety limit for TRIGA reactor fuel.

Maximum possible dose rates resulting from a complete loss of pool water permit mitigating actions. The area surrounding the reactor is under control of the Kansas State University, and exposures outside the reactor bay environment can be limited by controlling access appropriately. Kansas State University has complete authority to control access to campus locations.

Table 13.9, Gamma-Ray Ambient (Deep) Dose Rates (R/h) at Selected Locations for Times Following Loss of Coolant After Operation for One Year at 1,250 kW Thermal Power.

	Time post accident				
	0	1 h	24 h	30 d	180 d
On-site (elev.)					
22 ft. (center)	3.75E+06	1.38E+06	4.25E+05	1.03E+05	1.98E+04
12 ft. (boundary)	1.08E+03	4.00E+02	1.43E+02	3.25E+01	7.00E+00
0 ft. (boundary	9.75E+02	3.75E+02	1.23E+02	3.00E+01	6.25E+00
Off-site (radius from center of reactor bay)					
13 m	6.75E+02	2.75E+02	8.75E+01	2.15E+01	4.50E+00
15 m	5.00E+02	2.00E+02	6.75E+01	1.60E+01	3.25E+00
20 m	2.50E+02	1.00E+02	3.50E+01	8.75E+00	1.73E+00
30 m	8.25E+01	3.25E+01	1.10E+01	2.75E+00	5.50E-01
40 m	3.75E+01	1.40E+01	5.25E+00	1.18E+00	2.33E-01
50 m	1.93E+01	7.25E+00	2.43E+00	6.25E-01	1.23E-01
70 m	6.50E+00	2.75E+00	9.00E-01	2.18E-01	4.00E-02
100 m	2.35E+00	9.50E-01	2.75E-01	6.75E-02	1.33E-02

13.2.3 Insertion of Excess Reactivity

Rapid compensation of a reactivity insertion is the distinguishing design feature of the TRIGA reactor. Characteristics of a slow (ramp) reactivity insertion are less severe than a rapid transient since temperature feedback will occur rapidly enough to limit the maximum power achieved during the transient. Analyses of plausible accident scenarios reveal no challenges to safety limits for the TRIGA. The fuel-integrity safety limit, according to Simnad (1980), may be stated as follows:

> *Fuel-moderator temperature is the basic limit of TRIGA reactor operation. This limit stems from the out-gassing of hydrogen from the ZrH_x and the subsequent stress produced in the fuel element clad material. The strength of the clad as a function of temperature can set the upper limit on the fuel temperature. A fuel temperature safety limit of 1150°C for pulsing, stainless steel U-$ZrH_{1.65}$ ... fuel is used as a design value to preclude the loss of clad integrity when the clad temperature is below 500°C. When clad temperatures can equal the fuel temperature, the fuel temperature limit is 950°C. ....*

Two reactivity accident scenarios are presented. The first is the insertion of 2.1% reactivity at zero power by sudden removal of a control rod. The second is the sudden removal of the same reactivity with the core operating at the maximum power level permitted by the balance of the core excess reactivity (i.e., core excess less $3.00). Movements of control rods for the first case are controlled, in part, administratively, while movements for the second are prevented by control circuit design.

As the analysis shows, in neither scenario does the peak fuel temperature approach the temperature limit. The nearest approach is 869°C, incurred by a pulse insertion of 0.7% while the reactor is operating at a steady power of 94 kW, an action prevented both by administrative requirements and by interlocks.

a. Initial Conditions, Assumptions, and Approximations

The following conditions establish an extremely conservative scenario for analysis of insertion of excess reactivity.

- The reactor operates with a minimum of $N =$ [redacted] fuel rods.
- Reactor and coolant ambient (zero power) temperature is 27°C.
- Maximum reactivity insertion for pulsing or for the worth of experiments is set at $3.00, $\delta k_{max} = 2.1\%$ or $\rho_{max} = 0.021$.
- Reactor power equivalent to the core excess reactivity of $1.00, i.e., $\delta k = \delta k_{ex} - \delta k_{max} = 0.7\%$ ($\rho = 0.007$) is $P_o = 107$ kW and the maximum fuel temperature at that power is $T_o = 150$°C. Basis: Data for the Torrey Pines TRIGA, as included in the KSU TRIGA Operations Manual.
- A control rod interlock preventing pulsing operations from power levels greater than a maximum of 10 kW is not credited
- Conservative hot channel factors as calculated in 4.5.3 are used

b. Computational Model for Power Excursions

The following relationships are for the Fuchs-Nordheim model, modified by Scalletar, for power excursions, as described for the TRIGA reactor by West et al. (1967).

If the heat capacity of the fuel is given by , $c_{pf} = 340.1 + 0.6952T(°C)$ (J/kg°K), and there are N fuel elements, each of mass $m_f = 2.367$ kg, then the overall core heat capacity is given by

$$K(J/K^{\circ}) = m_f N c_{pf} = C_o + C_1 T(^{\circ}C) \qquad (13.2.3\text{-}1)$$

in which $C_o = 6.682 \times 10^4$ and $C_1 = 136.6$. If P_o (W) is the reactor power at the initiation of the pulse power excursion, and ρ_o is the magnitude of an initiating step change in reactivity, then the maximum power increase (W) is given by

$$P_{max} - P_o = \frac{(\rho-\beta)^2 C_o}{2\alpha l} + \frac{(\rho-\beta)^3 C_1}{6\alpha^2 l}. \qquad (13.2.3\text{-}2)$$

A maximum pulse of $3.00 would result in a power rise of approximately 1430 MW(t). If T_o is the average core temperature at the start of the excursion, the maximum temperature rise (°K) is given by

$$T_{max} - T_0 = \left[\frac{2*(\rho-\beta)}{\alpha}\right] * \left[-\frac{3}{8}*(\sigma-1) \pm \frac{3}{8}*\sqrt{(\sigma-1)^2 + \frac{16}{3}*\sigma}\right] \qquad (13.2.3\text{-}3)$$

in which

$$\sigma = \frac{\alpha C_o}{(\rho-\beta)C_1}, \qquad (13.2.3\text{-}4)$$

and the "+" sign applies when $\sigma > 1$. Although there are nonlinear terms in the model, calculation of temperature change as a function of temperature shows a nearly linear response. Therefore the major factor in determining core-average peak temperature is the amount of reactivity available to pulse. To remain within 1000°C at all locations, core average temperature cannot exceed 318°C (based on Table 13.2.1.4 peaking factors).

The maximum worth of the pulse rod is $3.00, therefore peak temperature following a pulse was calculated based on a maximum reactivity available from the pulse rod at reference core temperature (27°C). The core-average temperature change is 229°C, with a hot spot change of 716°C (based on Table 13.2.1.4 peaking factors). Therefore, core-average peak temperature for a $3.00 pulse from 27°C is 256°C, with a hot spot temperature of 746°C.

With $3.00 reserved for a maximum pulse, the reactor has remaining reactivity $1.00 greater than critical to support operation at power. Reactivity of $1.00 allows operation 94 kW; 94 kW operation results in an average fuel temperature of 48°C, and a hot-spot

fuel temperature of 150°C. A $3.00 pulse increases this hot spot temperature from 150°C to 869°C.

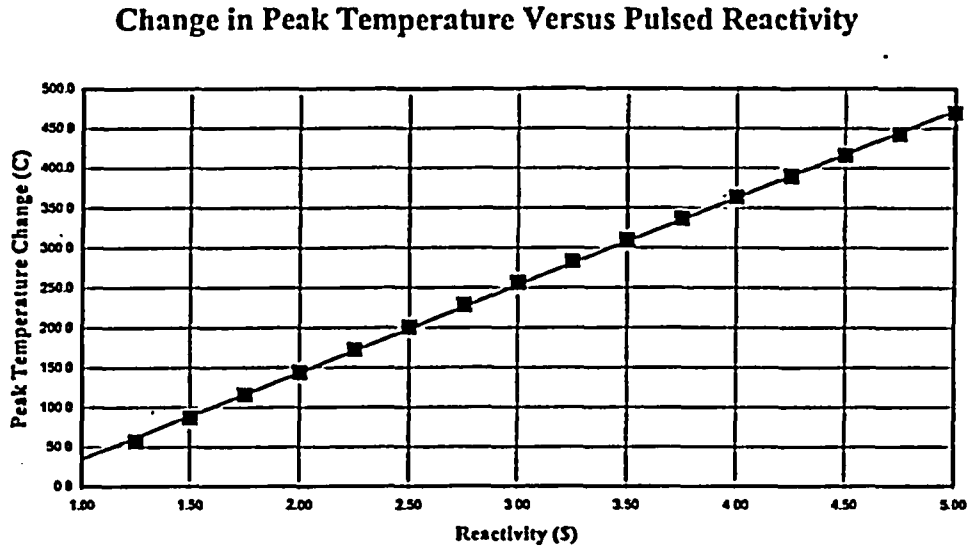

Figure 13.3, Change in Peak Temperature Versus Pulsed Reactivity Insertion

The postulated scenarios do not result in fuel damage, but physical aspects of system prevent these scenarios from occurring. It is not possible to achieve full power operation with the pulse rod fully inserted; since the pulse rod is partially withdrawn with air applied to the pulse solenoid, it physically cannot be pulsed. Although not required to ensure the safety of the reactor, an interlock prevents pulsing from power levels greater than a maximum of 10 kW.

c. Conclusions

Insertion of the maximum possible reactivity without initial temperature feedback (i.e., fuel temperature is too low to limit core available reactivity) results in a peak hot spot fuel temperature of 746°C, well below the safety limit.

Insertion of the maximum possible reactivity with initial temperature feedback (i.e., fuel temperature limits available) results in a peak hot spot fuel temperature of 869°C, well below the safety limit.

13.2.4 Single Element Failure in Air

Source quantities of radioactive noble gases and iodine are computed and tabulated for a maximum hypothetical accident involving cladding failure in a single TRIGA fuel element and the escape of the radionuclides into the environment. Two limiting cases of operation are considered. For short lived radionuclides, source terms are computed for element failure subsequent to eight hours full-power operation per day for five days. For long-lived radionuclides, source terms are computed for element failure subsequent to continuous operation

for 40 years at the average power experienced by the reactor over its first 33 years of operation. Also examined are residual sources still present in fuel, but generated in reactor operations prior to local receipt of the fuel in 1973. Potential consequences of radiological releases are examined. Even in the maximum hypothetical accident, no workers or members of the public are at risk of receiving radiation doses in excess of limits prescribed in federal regulations.

a. Assumptions and Approximations

Following are assumptions and approximations applied to calculations.

1. For long-lived radionuclides, calculations of radionuclide inventory in fuel are based on continuous operation prior to fuel failure for 40 years at the average thermal power experienced by the reactor during its first 33 years of operation, namely, 3.50 kW.

2. For short-lived radionuclides, calculations of radionuclide inventory in fuel are based on operation at the full thermal power of 500 kW for eight hours per day, for five successive days prior to fuel failure, an average of 12.5 kW-hr/day.

3. Radionuclide inventory in one "worst-case" fuel element is based on [redacted] elements in the core for the historical period and [redacted] elements for full power operation, which is the case for core II-16, [redacted] grams of ^{235}U per element [NUREG-2382], and a value of 2.0 as a very conservative value of the ratio of the maximum power in the core to the average power. Thus, for the historical period, the worst case element has operated at a thermal power of (3500/[redacted])×2 = [redacted] W, and for the one-week full-power operation, (500/[redacted])×2 = [redacted] kW.

4. The fraction of noble gases and iodine contained within the fuel that is actually released is 1.0×10^{-4}. This is a very conservative value prescribed in NUREG 2387 [Hawley and Kathren, 1982] and may be compared to the value of 1.5×10^{-5} measured at General Atomics [Simnad et al., 1976] and used in SARs for other reactor facilities [NUREG-1390, 1990].

5. The fractional release of particulates (radionuclides other than noble gases and iodine) is 1.0×10^{-6}, a very conservative estimate used by Hawley and Kathren [1982].

b. Radionuclide Inventory Buildup and Decay

Consider a mass of ^{235}U yielding thermal power P (kW) due to thermal-neutron induced fission. The fission rate is related to the thermal power by the factor $k = 3.12 \times 10^{13}$ fissions per second per kW.[6] Consider also a fission product radionuclide, which is produced with yield Y, and which decays with rate constant λ. It is easily shown that the equilibrium activity A_∞ (Bq) of the fission product, which exists when the rate of creation by fission is equal to the rate of loss by decay, is given by $A_\infty = kPY$. Here it should be noted that the power must be small enough or the uranium mass large enough that the

[6] Note that the product of k and yield Y may be stated as $3.12 \times 10^{13} \times Y$ Bq/kW or $843 \times Y$ Ci/kW.

depletion of the ^{235}U is negligible.[7] Starting at time $t = 0$, the buildup of activity is given by

$$A(t) = A_\infty * \left(1 - e^{-\lambda * t}\right) \qquad (13.2.4\text{-}1)$$

For times much greater than the half-life of the radionuclide, $A \approx A_\infty$, and for times much less than the half-life, $A(t) = A_\infty * \lambda * t$. If the fission process ceases at time t_1, the specific activity at later time t is given by

$$A(t) = A_\infty * \left(1 - e^{-\lambda * t}\right) * e^{-\lambda * (t - t_1)} \qquad (13.4.2\text{-}2)$$

Consider the fission product ^{131}I, which has a half-life of 8.04 days ($\lambda = 0.00359\ h^{-1}$) and a chain (cumulative) fission product yield of about 0.031. At a thermal power of 1 kW, the equilibrium activity is about $A_\infty = 9.67 \times 10^{11}$ Bq (26.1 Ci). After only four hours of operation, though, the activity is only about 0.37 Ci. For equilibrium operation at 3.5 kW, distributed over [redacted] fuel elements, the average activity per element would be $26.1 \times 3.5 \div 81 = 1.13$ Ci per fuel element. The worst case element would contain twice this activity. With a release fraction of 1.0×10^{-4}, the activity available for release would be about $1.13 \times 2 \times 1.0 \times 10^{-4} = 2.26 \times 10^{-4}$ Ci. This type of calculation is performed by the ORIGEN code [CCC-371] for hundreds of fission products and for arbitrary times and power levels of operation as well as arbitrary times of decay after conclusion of reactor operation. The code accounts for branched decay chains. It also may account for depletion of ^{235}U and ingrowth of ^{239}Pu, although those features were not invoked in the calculations reported here because of minimal depletion in TRIGA fuel elements.

c. Data From Origen Calculations

ORIGEN-2.1 calculation output files are included as Appendices A and B; App. A contains data for the buildup of long-lived radionuclides over the 40-year entire operating history of the KSU TRIGA reactor, modeled as 86.42 W continuous thermal power. App. B contains data for the buildup of relatively short-lived radionuclides during a worst-case scenario modeled as 8-hours/day operations at 12.05 kW thermal power for five consecutive days. Tabulated results for Appendices A and B are μCi activities, by nuclide, immediately after reactor shutdown, and at 1, 2, 3, 7, and 14 days after shutdown. In Appendix A, which deals with relatively long-lived radionuclides, data are provided only for those nuclides present at activities greater than 100 mCi in a single fuel element at 1 day after reactor shutdown. In Appendix B, which deals with relatively short-lived radionuclides, data are provided only for those nuclides present at activities greater than 100 mCi in a single fuel element immediately after reactor shutdown. In both Appendices A and B, the activities per element are multiplied by the release fractions previously cited, thus yielding maximum activities available for release in a maximum hypothetical accident.

[7] Negligible burnup is modeled in ORIGEN calculations by setting the fuel mass very large (1 tonne) and the thermal power very low (1 kW or less).

d. Reference Case Source Terms

Appendices A and B data for worst case TRIGA fuel element are compared; greater values for any one isotope are selected as reference case source terms for maximum hypothetical accident. Data are presented in Table 13.10 for halogens/noble gases, and Table 13.11 for particulate radionuclides.

e. Derived Quantities

The raw data of Tables 13.10 and 13.11 are activities potentially released from a single worst-case fuel element that has experienced a cladding failure. This activity may itself be compared to the annual limit of intake (ALI) to gauge the potential risk to an individual worker. By dividing the activity by the 144,000 ft^3 free volume of the reactor bay in the Nuclear Reactor Facility, one obtains an air concentration (specific activity) that may be compared to the derived air concentration (DAC) for occupational exposure as given 10CFR20 or in EPA federal guidance [Eckerman et al., 1988].

Table 13.10, Reference Case Halogen & Noble Gas Activities Potentially Released in Maximum Hypothetical Accident at KSU TRIGA Mk. II Nnuclear Reactor. [1]

		Available activity (μCi) at time in days after reactor shutdown						
Element	Nuclide	0	1	2	3	7	14	28
Br	83	12110	13	0	0	0	0	0
Br	84	25388	0	0	0	0	0	0
I	131	8490	8245	7695	7130	5125	2810	840
I	132	23280	20943	16930	13685	5838	1318	68
I	133	69950	33530	15073	6773	278	0	0
I	134	192228	0	0	0	0	0	0
I	135	98750	7980	645	53	0	0	0
Kr	85	45	45	45	45	45	45	45
Kr	87	64498	0	0	0	0	0	0
Kr	88	79048	225	0	0	0	0	0
Kr	83M	9953	48	0	0	0	0	0
Kr	85M	23368	580	15	0	0	0	0
Xe	133	20363	24105	24010	22390	14110	5673	895
Xe	135	58955	30518	6595	1195	0	0	0
Xe	138	158548	0	0	0	0	0	0
Xe	133M	35	33	28	20	8	0	0
Xe	135M	205	15	0	0	0	0	0

NOTE: Available activity (> 10 μCi) is from a single worst-case fuel element as a function of time after reactor operation. Data are derived from ORIGEN 2.1 calculations [CCC-371] as summarized in Appendices A and B. Data are raw computational results and the number of significant figures exceeds the precision of the calculation.

Table 13.11, Reference Case Particulate Activities Potentially Released in a Maximum Hypothetical Accident at the KSUTRIGA Mk. II Nuclear Reactor.

		Available activity (μCi) at time in days after reactor shutdown						
Element	Nuclide	0	1	2	3	7	14	28
BA	139	1605	0	0	0	0	0	0
BA	140	128	120	115	108	88	60	28
BA	141	1480	0	0	0	0	0	0
BA	142	1470	0	0	0	0	0	0
CE	141	48	53	53	50	45	40	30
CE	143	553	340	205	125	18	0	0
CS	138	1713	0	0	0	0	0	0
LA	140	68	88	98	103	95	68	33
LA	141	1140	18	0	0	0	0	0
LA	142	1455	0	0	0	0	0	0
LA	143	1493	0	0	0	0	0	0
MO	99	395	308	240	185	68	13	0
MO	101	1273	0	0	0	0	0	0
NB	97	598	248	93	35	0	0	0
NB	98	1463	0	0	0	0	0	0
ND	147	55	50	48	45	35	23	10
ND	149	263	0	0	0	0	0	0
ND	151	105	0	0	0	0	0	0
PM	151	40	23	13	8	0	0	0
PR	143	70	88	98	100	90	65	33
PR	145	638	40	3	0	0	0	0
PR	147	573	0	0	0	0	0	0
RB	88	800	3	0	0	0	0	0
RB	89	1218	0	0	0	0	0	0
RH	105	78	65	40	25	5	0	0
RH	107	40	0	0	0	0	0	0
RU	105	188	5	0	0	0	0	0
SE	81	53	0	0	0	0	0	0
SE	83	50	0	0	0	0	0	0
SN	128	83	0	0	0	0	0	0
SR	89	28	28	28	28	25	23	20
SR	91	795	138	25	5	0	0	0
SR	92	1325	3	0	0	0	0	0
TC	101	1273	0	0	0	0	0	0
TC	104	460	0	0	0	0	0	0
TE	129	95	3	0	0	0	0	0
TE	131	628	5	3	3	0	0	0
TE	132	250	203	165	133	58	13	0
TE	133	965	0	0	0	0	0	0
TE	134	1713	0	0	0	0	0	0
Y	92	848	38	0	0	0	0	0
Y	93	863	170	33	8	0	0	0
Y	94	1583	0	0	0	0	0	0
Y	95	1613	0	0	0	0	0	0
Y	91M	423	88	15	3	0	0	0
ZR	95	30	30	30	28	28	25	23
ZR	97	658	245	93	35	0	0	0

Available activity (> 10 μCi) is for a single worst-case fuel element as a function of time after reactor operation. Data are derived from ORIGEN 2.1 calculations [CCC-371] as summarized in Appendices A and B. The table includes only those nuclides with activities in excess of 10 μCi. Data are raw computational results and the number of significant figures exceeds the precision of the calculation.

f. Comparison with the DAC and the ALI

The ALI is the activity that, if ingested or inhaled, would lead to either (a) the maximum permissible committed effective dose equivalent incurred annually in the workplace, nominally 5 rem, or (b) the maximum permissible dose to any one organ or tissue, nominally 50 rem. The DAC is the air concentration that, if breathed by reference man for one work year (2000 h), would result in the intake of the ALI. ALI does not apply to noble-gas radionuclides.

Potential activity releases are compared to ALIs, and air concentrations in the reactor bay are compared to DACs in Tables 13.12 and 13.13. Only for radioiodine does the available activity exceed the ALI. However, there is no credible scenario for accidental inhalation or ingestion of the undiluted radioiodine released from a fuel element.

When one compares with DACs the potential airborne concentration of radionuclides in the reactor bay, only the ^{131}I, ^{133}I, and ^{135}I isotopes plus ^{87}Kr and ^{88}Kr are of potential consequence. However, annual dose limits could be attained only with a constant air concentration over a long period of time. The ^{131}I released in the failure of a single element, for example, would decay with a half-life of 8.04 days. Thus, even the undetected failure of a fuel element would not be expected to lead to violations of the occupational dose limits expressed in 10CFR20 or in other federal guidance.

g. Comparison with the effluent concentration

Effluent concentration, listed in the last columns of Tables 13.12 and 13.13, are defined in continuous exposure (8760 hours per year) rather than 2000 hours per year occupational exposure. Exposure to a constant airborne concentration equal to the effluent concentration for one full year results in the annual dose limit of 100 mrem to members of the public. As is apparent from Tables 13.12 and 13.13, the reactor bay average concentrations immediately after fuel element failure exceed the effluent concentrations for several radionuclides. Thus, only for these radionuclides is it necessary to consider radioactive decay and atmospheric dispersal after release in estimating potential risk to members of the public. For posting purposes, concentrations relative to DACs are additive. For dosimetry purposes, products of concentrations and times, relative to DAC-hours, are additive.

h. Potential downwind dose to a member of the public

In this dose assessment, it is assumed that the available activity in a failed fuel element is released instantaneously and immediately after reactor shutdown. It is further assumed that a member of the public is positioned directly downwind from the Nuclear Reactor Facility and remains in place during the entire passage of the airborne radioactivity. The very conservative approximations of Hawley and Kathren [1982] are adopted in the assessment, namely, that the atmospheric dispersion (χ/Q) factor is 0.01 s/m^3 (2.78×10^{-6} h/m^3) and the breathing rate V is 1.2 m^3/h. No credit is taken for partial containment, plateout, or other potential mitigating mechanisms, however realistic and probable.
Let the activity of nuclide i released be A (μCi) as given in Tables 13.12 and 13.13. If one neglects radioactive decay, the activity inhaled during passage of the airborne

activity is $A\ V(\times \chi/Q)$ [Faw and Shultis, 1993]. The product of the activity inhaled and the dose conversion factor $\Re$ (mrem/μCi) [Eckerman et al., 1988] yields D_I (mrem); the more critical of the organ dose or the effective dose equivalent to the total body. Results of such calculations are presented in Table 12.14. As is apparent from the table, individual organ doses as well as the total committed effective dose equivalent are well below any regulatory limits. Entries are shown only for doses of 0.001 mrem or greater.

Table 13.12, Comparison of Halogen and Noble Gas Available Activities Immediately After Reactor Shutdown with ALIs and Reactor Bay Concentrations with DACs and Effluent Concentrations.

Element	Nuclide	Half-life	Available activity (μCi)	Inhalation ALI (μCi)	DAC (μCi/cm³)	Reactor bay conc. (μCi/cm³)	Effluent conc. (μCi/cm³)	Ratio to DAC	Ratio to Eff Limit
Br	83	2.39 h	12100	6.E+04	3.E-5	3.00E-06	9E-08	0.1	33.3
Br	84	31.8 m	25375	6.E+04	2.E-5	6.25E-06	8E-08	0.3	78.1
I	131	8.04 d	8500	5.E+01	2.E-8	2.08E-06	2E-10	103.8	10375.0
I	132	2.30 h	23275	8.E+03	3.E-6	5.75E-06	2E-08	1.9	287.5
I	133	20.8 h	69950	3.E+02	1.E-7	1.73E-05	1E-09	172.5	17250.0
I	134	52.6 m	192225	5.E+04	2.E-5	4.75E-05	6E-08	2.4	791.7
I	135	6.61 h	98750	2.E+03	7.E-7	2.43E-05	6E-09	34.6	4041.7
Kr	83m	1.83 h	9950		1.E-2	2.45E-06	5E-05	0.0	0.0
Kr	85m	4.48 h	23375		2.E-5	5.75E-06	1E-07	0.3	57.5
Kr	85	10.7 y	50		1.E-4	1.25E-08	7E-07	0.0	0.0
Kr	87	76.3 m	64500		5.E-6	1.58E-05	2E-08	3.2	787.5
Kr	88	2.84 h	79050		2.E-6	1.95E-05	9E-09	9.8	2166.7
Xe	133m	2.19 d	0		1.E-4	1.00E-08	6E-07	0.0	0.0
Xe	133	5.25 d	20350		1.E-4	5.00E-06	5E-07	0.1	10.0
Xe	135m	15.3 m	25		9.E-6	6.25E-09	4E-08	0.0	0.2
Xe	135	9.09 h	58950		1.E-5	1.45E-05	7E-08	1.5	207.1

[a]Bay concentration exceeds DAC.
[b]Bay concentration exceeds effluent concentration.

Table 13.13, Comparison of Particulate Available Activities (> 100 μCi) with ALIs and Reactor Bay Concentrations with DACs and Effluent Concentrations.

Element	Nuclide	Half-life	Available activity (μCi)	Inhalation ALI (μCi)	DAC (μCi/cm³)	Reactor bay conc. (μCi/cm³)	Effluent conc. (μCi/cm³)	Ratio to DAC	Ratio to Eff Limit
Ba	139	82.7 m	1600	75000	0.00001	4E-07	2E-09	4.00E-02	2.00E+02
Ba	140	12.7 d	125	2500	6E-07	3E-08	2E-09	5.00E-02	1.50E+01
Ba	141		1475	175000	0.00003	3.5E-07	1E-07	1.17E-02	3.50E+00
Ce	141		50	1500	2E-07	1.23E-08	8E-10	6.13E-02	1.53E+01
Ce	143	33.0 h	550	5000	7E-07	1.35E-07	2E-09	1.93E-01	6.75E+01
Cs	138	32.2 m	1700	150000	0.00002	4.25E-07	8E-08	2.13E-02	5.31E+00
La	140		75	2500	5E-07	1.85E-08	2E-09	3.70E-02	9.25E+00
La	141	3.93 h	1150	22500	0.000004	2.75E-07	1E-08	6.88E-02	2.75E+01
La	142	92.5 m	1450	50000	0.000009	3.5E-07	3E-08	3.89E-02	1.17E+01
La	143		1500	225000	0.00004	3.75E-07	1E-07	9.38E-03	3.75E+00
Mo	99	66.0 h	400	2500	6E-07	9.75E-08	2E-09	1.63E-01	4.88E+01
Nb	98		1475	125000	0.00002	3.5E-07	7E-08	1.75E-02	5.00E+00
Nd	147	1.73 h	50	2000	4E-07	1.23E-08	1E-09	3.06E-02	1.23E+01
Pm	151		50	7500	0.000001	1.23E-08	4E-09	1.23E-02	3.06E+00
Pr	143		75	1750	3E-07	1.85E-08	9E-10	6.17E-02	2.06E+01
Pr	145	5.98 h	650	20000	0.000003	1.6E-07	1E-08	5.33E-02	1.60E+01
Rb	88	17.8 m	800	150000	0.00003	1.95E-07	9E-08	6.50E-03	2.17E+00
Rb	89		1225	250000	0.00006	3E-07	2E-07	5.00E-03	1.50E+00
Ru	105	4.44 h	200	25000	0.000005	5E-08	2E-08	1.00E-02	2.50E+00
Se	81	18.5 m	50	500000	0.00009	1.23E-08	3E-07	1.36E-04	4.08E-02
Sn	128	59.1 m	75	75000	0.00001	1.85E-08	4E-08	1.85E-03	4.63E-01
Sr	89		25	250	6E-08	6.25E-09	2E-10	1.04E-01	3.13E+01
Sr	91	9.5 h	800	10000	0.000001	1.95E-07	5E-09	1.95E-01	3.90E+01
Sr	92	2.71 h	1325	17500	0.000003	3.25E-07	9E-09	1.08E-01	3.61E+01
Te	129	69.6 m	100	150000	0.00003	2.45E-08	9E-08	8.17E-04	2.72E-01
Te	131	25.0 m	625	12500	0.000002	1.53E-07	1E-09	7.63E-02	1.53E+02
Te	132	78.2 h	250	500	9E-08	6.25E-08	9E-10	6.94E-01	6.94E+01
Te	133	12.5 m	975	50000	0.000009	2.4E-07	8E-08	2.67E-02	3.00E+00
Te	134	41.8 m	1725	50000	0.00001	4.25E-07	7E-08	4.25E-02	6.07E+00
Y	91m	49.7 m	425	500000	0.00007	1.05E-07	2E-07	1.50E-03	5.25E-01
Sr	91	9.5 h	800	10000	0.000001	1.95E-07	5E-09	1.95E-01	3.90E+01
Sr	92	2.71 h	1325	17500	0.000003	3.25E-07	9E-09	1.08E-01	3.61E+01
Te	129	69.6 m	100	150000	0.00003	2.45E-08	9E-08	8.17E-04	2.72E-01
Te	131	25.0 m	625	12500	0.000002	1.53E-07	1E-09	7.63E-02	1.53E+02
Te	132	78.2 h	250	500	9E-08	6.25E-08	9E-10	6.94E-01	6.94E+01
Te	133	12.5 m	975	50000	0.000009	2.4E-07	8E-08	2.67E-02	3.00E+00

Table 13.13, Comparison of Particulate Available Activities (> 100 μCi) with ALIs and Reactor Bay Concentrations with DACs and Effluent Concentrations.

Element	Nuclide	Half-life	Available activity (μCi)	Inhalation ALI (μCi)	DAC (μCi/cm³)	Reactor bay conc. (μCi/cm³)	Effluent conc. (μCi/cm³)	Ratio to DAC	Ratio to Eff Limit
Te	134	41.8 m	1725	50000	0.00001	4.25E-07	7E-08	4.25E-02	6.07E+00
Y	91m	49.7 m	425	500000	0.00007	1.05E-07	2E-07	1.50E-03	5.25E-01
Y	92	3.54 h	850	20000	0.000003	2.08E-07	1E-08	6.92E-02	2.08E+01
Y	93	10.1 h	850	5000	0.000001	2.08E-07	3E-09	2.08E-01	6.92E+01
Zr	95		25	250	5E-08	6.25E-09	4E-10	1.25E-01	1.56E+01
Zr	97	16.9 h	650	2500	5E-07	1.6E-07	2E-09	3.20E-01	8.00E+01

i. Residual Activity from Fuel Utilization Prior to Receipt

All but a few instrumented Mark-II fuel elements in the original 1962 core loading were replaced by Mark-III elements on July 10, 1973. The replacement elements had seen considerable use prior to their installation at Kansas State University. The two most heavily used elements, with serial numbers 4078 and 4079, had experienced, respectively, consumption of [redacted] and [redacted] g of ^{235}U. Even after about 25 years of subsequent use, considerable ^{137}Cs, ^{90}Sr, and ^{85}Kr remain from fission during the pre-1973 use. However, the ^{85}Kr atmospheric concentration inside the reactor bay immediately after release would be orders of magnitude lower than the DAC. Therefore only ^{37}Cs and ^{90}Sr offer a potential for occupational or public risk. In the absence of knowledge about the pattern of early fuel utilization, it is assumed that all the generation of fission products took place in 1973 and that fission product decay took place over the period of 28 years from 1973 until 2001.

If Y is the fission yield, λ is the decay constant (s^{-1}), and N_a is Avogadro's number, the activity A (Bq) of any one radionuclide immediately after fissioning of mass m (g) of ^{235}U is

$$A = \frac{N_a}{235} m Y \lambda. \qquad (13.2.4\text{-}3)$$

Activity calculations using this formula and consequences, as computed in 13.14 are reported in Table 13.15.

Table 13.15. Worst Case Source Terms and Consequence Calculations for a Single TRIGA Fuel Element Experiencing 11.27 g of ^{235}U Consumption 28 Years Prior to Element Failure.

FACTOR	RADIONUCLIDE ^{90}Sr	^{137}Cs
Half life (y)	29.12	30.00
Decay constant λ (s^{-1})	7.54×10^{-10}	7.32×10^{-10}
Fission yield *Y*	0.0577	0.0615
Release fraction	1.00×10^{-06}	1.00×10^{-06}
Initial Bq/g contained in element	$1.12\times 10^{+11}$	$1.15\times 10^{+11}$
Initial μCi available for release	34.0	35.2
μCi available for release in 28 y	17.4	18.4
ALI (μCi)	4	200
Reactor bay concentration (μCi/cm^3)	4.3×10^{-09}	4.5×10^{-09}
DAC (μCi/cm^3)	$2.\times 10^{-09}$	$6.\times 10^{-08}$
Tissue at risk	Bone surface	Total body
Dose conversion factor (mrem/μCi)	2690	32
Maximum downwind dose (mrem)	0.16	0.0020

Whereas the ^{90}Sr activity available for release would exceed the occupational ALI and, if dispersed within the reactor bay, would have a concentration in excess of the DAC, credible mechanisms for ingestion or inhalation of the full available activity or even its full dispersion are not apparent. Thus, neither the ^{90}Sr nor the ^{137}Cs would pose a significant occupational threat. Even if the total available activity were somehow dispersed to the free atmosphere, no person downwind of the accidental release would receive doses even approaching regulatory limits.

j. Conclusions

Fission product inventories in TRIGA fuel elements were calculated with the ORIGEN code, using very conservative approximations. Then, potential radionuclide releases from worst-case fuel elements were computed, again using very conservative approximations. Even if it were assumed that releases took place immediately after reactor operation, and that radionuclides were immediately dispersed inside the reactor bay workplace, few radionuclide concentrations would be in excess of occupational derived air concentrations, and then only for a matter of hours or days. Only for certain nuclides of iodine would the potential release be in excess of the annual limit of intake. However, there is no credible scenario for accidental inhalation or ingestion of the undiluted radioiodine that might be released from a damaged fuel element.

For the residual ^{90}Sr and ^{137}Cs remaining in fuel elements from consumption of ^{235}U prior to receipt of the fuel at Kansas State University, only the former would pose any conceivable occupational threat. However, the total ^{90}Sr activity available for release is

estimated to be at most about 4 times the ALI and there is no credible scenario for its consumption by a worker.

As far as potential consequences to the general public are concerned, only for the few radionuclides listed in Table 13.14, are maximum concentrations inside the reactor facility in excess of effluent concentrations listed in 10CFR20 and potential doses 0.001 mrem or greater. However, even in the extremely unlikely event that radionuclides released from a damaged fuel element were immediately released to the outside atmosphere, very conservative calculations reveal that radionuclides inhaled by persons downwind from the release would lead to organ doses or effective doses very far below regulatory limits. As is shown in Table 13.15, the same is true for residual ^{90}Sr and ^{137}Cs remaining in fuel elements from early operations.

13.3 Bibliography

ANSI/ANS-5.1-1994, "American National Standard for Decay Heat Power in Light Water Reactors," American Nuclear Society, 1994.

ReportLA-12625-M, Version 4B, "MCNP-- A General Monte Carlo N-Particle Transport Code," Los Alamos National Laboratory, Los Alamos, NM (1997). Briesmeister, J.F. (ed),

CCC-371, "ORIGEN 2.1 Isotope Generation and Depletion Code: Matrix Exponential Method," Radiation Shielding Information Center, Oak Ridge National Laboratory, Oak Ridge, Tennessee, 1991.

Kansas State University TRIGA MkII Reactor Hazards Summary Report, License R-88, Docket 50-188 , (1961) Clack, R.W., J.R. Fagan, W.R. Kimel, and S.Z. Mikhail,.

"Laminar-Flow Heat Transfer for In-Line Flow Through Unbaffled Rod Bundles," Nucl. Sci. Engg. 42, 81-88 (1970), Dwyer, O.E. and H.C. Berry.

"Nuclear Heat Transport," International Textbook Company, Scranton, 1971, El-Wakil, M.M.,.

Federal Guidance Report No. 11, Report EPA-5201/1-88-020, U.S. Environmental Protection Agency, *"Limiting Values of Radionuclide Intake and Air Concentration and Dose Conversion Factors for Inhalation, Submersion, and Ingestion,"* Washington, DC, (1988), Eckerman, K.F., A.B. Wolbarst, and A.C.B. Richardson.

Report LA-5885-MS "CINDER-7: An Interim Report for Users,,, England, T.R., et al., Los Alamos Scientific Laboratory, Los Alamos, NM, 1976.

"Radiological Assessment," Prentice Hall, Englewood Cliffs, N.J., 1993, Faw, R.E., and J.K. Shultis.

Report LA-9362, "Application of Adjusted Data in Calculating Fission Produce Decay Energies and Spectra," Los Alamos Scientific Laboratory, 1982.George, D.C., R.J. LaBauve, and T.R. England.

NUREG/CR-2387 (PNL-4028), "Credible Accident Analyses for TRIGA and TRIGA-Fueled Reactors," Report Pacific Northwest Laboratory, Richland Washington, 1982., Hawley, S.C., and R.L. Kathren,

"Fundamentals of Heat and Mass Transfer," 3d ed., Wiley, New York, 1990, Incropera, F.P. and D.P. DeWitt,

GA-3399,KSU TRIGA Reactor Mechanical Maintenance and Operating Manual, General Atomics Report, 1962.

"Fission Product Analytical Source Functions," Nuclear Technology 56, 332-339 (1982).LaBauve, R.J., T.R. England, and D.C. George, See also Reports LA-9090-MS (1981) and LA-UR-80-3305 (1980), Los Alamos Scientific Laboratory, Los Alamos, NM.

Metals Handbook, 8th ed., Vol. 1, American Society for Metals, Metals Park, Ohio, 1961.

NUREG-1282, "Safety Evaluation Report on High-Uranium Content, Low-Enriched Uranium-Zirconium Hydride Fuels for TRIGA Reactors," Office of Nuclear Reactor Regulation, U.S. Nuclear Regulatory Commission, 1987.

NUREG-1390, "Safety Evaluation Report Relating to the Renewal of the Operating License for the TRIGA Training and Research Reactor at the University of Arizona," Report NUREG-1390, Office of Nuclear Reactor Regulation, U.S. Nuclear Regulatory Commission, 1990.

NUREG-1537, "Guidelines for Preparing and Reviewing Applications for the Licensing of Non-Power Reactors, Format and Content," Report NUREG-1537 Part 1, Office of Nuclear Reactor Regulation, U.S. Nuclear Regulatory Commission, 1996.

"The U-Zr-Hx Alloy: Its Properties and Use in TRIGA Fuel," Report E-117-833, Simnad, M.T, General Atomics Corp., 1980.

"Fuel Elements for Pulsed TRIGA Research Reactors," Nuclear Technology 28, 31-56 (1976) Simnad, M.T., F.C. Faushee, and G.B. West

"Longitudinal Laminar Flow Between Cylinders Arranged in a Regular Array," AIChE Journal 5, 325 (1959), Sparrow, E.M., and A.L. Loeffler, and H.A. Hubbard.

Nuclear Systems I: Thermal Hydraulic Fundamentals, Todreas, N.E. and M.S. Kazimi, Hemisphere, New York, 1990.

Safety Analysis Report, TRIGA Reactor Facility, Nuclear Engineering Teaching Laboratory, University of Texas at Austin, Revision 1.01, Docket 50-602, May, 1991.

"Kinetic Behavior of TRIGA Reactors," Report GA-7882, West, G.B., W.L. Whittemore, J.R. Shoptaugh, Jr., J.B. Dee, and C.O. Coffer, , General Atomics Corp., 1967.

APPENDICES TO CHAPTER 13

A Origen 2.1 input file for ^{235}U fission at 1 W thermal power for 40 years.

B Origen 2.1 input file for ^{235}U fission at 1 W thermal power 8 hours per day for 5 days.

C Origen 2.1 output file extracts for ^{235}U fission at 1 W thermal power for 40 years.

D Origen 2.1 output file extracts for ^{235}U fission at 1 W thermal power 8 hours per day for 5 Days.

E Maximum activity available for release from a single TRIGA fuel element as a function of time after shutdown for a ^{235}U-fueled thermal reactor operating at 3.5 kW thermal power for 40 years, based on one element of 81 at 86.42 W.

F Maximum activity available for release from a single TRIGA fuel element as a function of time after shutdown for a ^{235}U-fueled thermal reactor operating at 500 kW kW thermal power for 8 hours per day for 5 days, based on one element of 83 at 12.05 kW

CHAPTER 13 APPENDIX A

```
      ORIGEN Input file for 1 tonne U-235 at 1 watt for 40 years
-1
-1
-1
  RDA     ORIGEN2, VERSION 2.1 (8-1-91)  TRIGA REACTOR REFERENCE PROBLEM
  RDA     UPDATED BY: Richard E. Faw, Kansas State University
  BAS     ONE TONNE OF U-235
  RDA     Continuous operation for 40 years at 1 watt
  RDA     WARNING:  VECTORS ARE OFTEN CHANGED WITH RESPECT TO THEIR CONTENT.
  RDA               THESE CHANGES WILL BE NOTED ON RDA CARDS.
  CUT     -1
  RDA     LIBRARY PRINT (1=PRINT,0=DON'T PRINT)
  LIP     0 0 0
  RDA     DECAY LIBRARY CHOICES (0=PRINT; 1 2 3 DECAY LIBRARIES; 601 ...
  RDA     CROSS SECTIONS; ETC, SEE P. 47)
  LIB     0  1 2 3  201  202  203   9   3   0  1   38
  PHO     101 102 103 10   <<< PHOTON LIBRARIES, P. 47
  TIT     INITIAL COMPOSITIONS OF UNIT AMOUNTS OF FUEL AND STRUCT MAT'LS
  RDA     READ FUEL COMPOSITION INCLUDING IMPURITIES (1 G)
  INP     -1   1  -1  -1  1  1
  TIT     IRRADIATION OF ONE TONNE U-235
  MOV     -1   1   0   1.0
  HED      1                                                  CHARGE
  BUP
  IRP      5 .000001   1   2   5 2  1 W/Tonne FOR 5 YEARS
  IRP     10 .000001   2   1   5 0  1 W/Tonne FOR 5 YEARS
  IRP     15 .000001   1   2   5 0  1 W/Tonne FOR 5 YEARS
  IRP     20 .000001   2   1   5 0  1 W/Tonne FOR 5 YEARS
  IRP     25 .000001   1   2   5 0  1 W/Tonne FOR 5 YEARS
  IRP     30 .000001   2   1   5 0  1 W/Tonne FOR 5 YEARS
  IRP     35 .000001   1   2   5 0  1 W/Tonne FOR 5 YEARS
  IRP     40 .000001   2   1   5 0  1 W/Tonne FOR 5 YEARS
  BUP
  OPTL      24*8           ACTIVATION PRODUCT OUTPUT OPTS P. 56
  OPTA      24*8           ACTINIDE OUTPUT OPTIONS P. 59
  OPTF       6*8 5   17*8  FISSION PRODUCT OUTPUT OPTIONS P. 59
  RDA     DECAY TO 28 DAYS
  DEC      1      1   2   4   2
  DEC      2      2   3   4   0
  DEC      3      3   4   4   0
  DEC      7      4   5   4   0
  DEC     14      5   6   4   0
  DEC     28      6   7   4   0
  OUT      -7     1     -1    0
  OUT       7     1     -1    0
  END
  2   922340    0.0  922350 1.E06 922380  0.      0    0.0   PURE U-235
  0
```

CHAPTER 13 APPENDIX B

ORIGEN Input File for 1 tonne U-235 at 1 watt
8 hours per day for 5 days

```
-1
-1
-1
  RDA     ORIGEN2, VERSION 2.1 (8-1-91)  TRIGA REACTOR REFERENCE PROBLEM
  RDA     UPDATED BY: Richard E. Faw, Kansas State University
  BAS     One tonne U-235
  RDA     -1 = Fuel composition
  CUT     -1
  RDA     LIBRARY PRINT (1=PRINT,0=DON'T PRINT)
  LIP     0 0 0
  RDA     DECAY LIBRARY CHOICES (0=PRINT; 1 2 3 DECAY LIBRARIES; 601 ...
  RDA     CROSS SECTIONS; ETC, SEE P. 47)
  LIB     0  1 2 3  201  202  203   9   3  0  1   38
  PHO     101 102 103 10   <<< PHOTON LIBRARIES, P. 47
  TIT     INITIAL COMPOSITIONS OF UNIT AMOUNTS OF FUEL AND STRUCT MAT'LS
  RDA     READ FUEL COMPOSITION INCLUDING IMPURITIES
  INP     -1   1  -1  -1  1  1
  TIT     One tonne U-235 8 h/d for 5 days at 1 kWt
  MOV     -1   1   0   1.0
  HED      1                                                  CHARGE
  BUP
  IRP      8.0   0.001    1   2   3 2  OPERATE FOR 8 HR AT 1 kW
  DEC     24.0            2   3   3 0  COOL FOR 16 HOURS
  IRP     32.0   0.001    3   4   3 0  OPERATE FOR 8 HR
  DEC     48.0            4   5   3 0  COOL FOR 16 HOURS
  IRP     56.0   0.001    5   6   3 0  OPERATE FOR 8 HR
  DEC     72.0            6   7   3 0  COOL FOR 16 HOURS
  IRP     80.0   0.001    7   8   3 0  OPERATE FOR 8 HR
  DEC     96.0            8   9   3 0  COOL FOR 16 HOURS
  IRP    104.0   0.001    9  10   3 0  OPERATE FOR 8 HR
  OPTL     24*8            ACTIVATION PRODUCT OUTPUT OPTS P. 56
  OPTA     24*8            ACTINIDE OUTPUT OPTIONS P. 59
  OPTF      6*8 5   17*8   FISSION PRODUCT OUTPUT OPTIONS P. 59
  RDA     MOVE COMPOSITION VECTOR FROM 10 TO 1
  MOV      10     1   0  1.0
  RDA     DECAY TO 0.1 UNITS (2=MINUTES) FROM COMP VEC 1 TO VEC 3
  DEC      1     1  2   4   2
  DEC      2     2  3   4   0
  DEC      3     3  4   4   0
  DEC      7     4  5   4   0
  DEC      14    5  6   4   0
  DEC      28    6  7   4   0
  OUT      -7     1     -1    0
  OUT       7     1     -1    0
  END
  2   922340    0.0  922350  1.E6 922380    0.00  0    0.0   1 g U-235
  0
```

CHAPTER 13 APPENDIX C

ORIGEN Output File Extracts for 1 tonne U-235 at 1 watt for 40 Years
NUCLIDE TABLE: RADIOACTIVITY, CURIES

		Time post discharge						
		0	1.0 D	2.0 D	3.0 D	7.0 D	14.0 D	28.0 D
AG	111	1.65E-04	1.51E-04	1.37E-04	1.25E-04	8.62E-05	4.50E-05	1.22E-05
BA	140	5.23E-02	4.96E-02	4.70E-02	4.45E-02	3.58E-02	2.45E-02	1.15E-02
BA	137	2.93E-02	2.93E-02	2.93E-02	2.93E-02	2.93E-02	2.93E-02	2.92E-02
CE	141	4.93E-02	4.85E-02	4.75E-02	4.65E-02	4.27E-02	3.68E-02	2.73E-02
CE	143	4.98E-02	3.03E-02	1.83E-02	1.11E-02	1.47E-03	4.32E-05	3.72E-08
CE	144	4.56E-02	4.55E-02	4.54E-02	4.53E-02	4.48E-02	4.41E-02	4.26E-02
CS	137	3.10E-02	3.10E-02	3.09E-02	3.09E-02	3.09E-02	3.09E-02	3.09E-02
EU	155	2.75E-04	2.75E-04	2.75E-04	2.75E-04	2.75E-04	2.74E-04	2.72E-04
EU	156	1.13E-04	1.10E-04	1.06E-04	1.01E-04	8.43E-05	6.13E-05	3.23E-05
I	131	2.37E-02	2.20E-02	2.03E-02	1.87E-02	1.33E-02	7.28E-03	2.18E-03
I	132	3.56E-02	2.95E-02	2.39E-02	1.93E-02	8.23E-03	1.86E-03	9.45E-05
I	133	5.68E-02	2.62E-02	1.18E-02	5.29E-03	2.16E-04	8.00E-07	1.10E-11
I	135	5.31E-02	4.29E-03	3.46E-04	2.80E-05	1.19E-09	2.66E-17	1.34E-32
KR	85	2.10E-03	2.10E-03	2.10E-03	2.10E-03	2.10E-03	2.10E-03	2.09E-03
KR	85M	1.07E-02	2.64E-04	6.44E-06	1.57E-07	5.58E-14	2.88E-25	0.00E+00
LA	140	5.24E-02	5.19E-02	5.06E-02	4.89E-02	4.08E-02	2.82E-02	1.32E-02
LA	141	4.93E-02	7.77E-04	1.13E-05	1.64E-07	7.27E-15	9.89E-28	0.00E+00
MO	99	5.06E-02	3.94E-02	3.06E-02	2.38E-02	8.68E-03	1.49E-03	4.36E-05
NB	95	5.38E-02	5.38E-02	5.38E-02	5.37E-02	5.35E-02	5.28E-02	5.04E-02
NB	97	4.93E-02	1.85E-02	6.90E-03	2.58E-03	5.03E-05	5.14E-08	5.70E-14
NB	95M	3.78E-04	3.77E-04	3.76E-04	3.74E-04	3.64E-04	3.41E-04	2.95E-04
NB	97M	4.66E-02	1.74E-02	6.51E-03	2.43E-03	4.74E-05	4.84E-08	5.01E-14
ND	147	1.90E-02	1.79E-02	1.68E-02	1.58E-02	1.23E-02	7.91E-03	3.29E-03
PM	147	1.91E-02	1.91E-02	1.91E-02	1.91E-02	1.91E-02	1.90E-02	1.89E-02
PM	149	9.11E-03	6.89E-03	5.04E-03	3.68E-03	1.05E-03	1.17E-04	1.46E-06
PM	151	3.52E-03	1.97E-03	1.10E-03	6.11E-04	5.86E-05	9.70E-07	2.65E-10
PR	143	4.98E-02	4.93E-02	4.80E-02	4.64E-02	3.86E-02	2.71E-02	1.33E-02
PR	144	4.56E-02	4.55E-02	4.54E-02	4.53E-02	4.48E-02	4.41E-02	4.26E-02
PR	145	3.29E-02	2.06E-03	1.27E-04	7.89E-06	1.16E-10	4.06E-19	5.14E-36
PR	144	5.48E-04	5.46E-04	5.45E-04	5.43E-04	5.38E-04	5.29E-04	5.11E-04
RH	105	8.53E-03	6.09E-03	3.83E-03	2.39E-03	3.64E-04	1.35E-05	1.86E-08
RH	106	3.27E-03	3.26E-03	3.26E-03	3.25E-03	3.23E-03	3.18E-03	3.10E-03
RH	103	2.37E-02	2.33E-02	2.29E-02	2.25E-02	2.09E-02	1.85E-02	1.45E-02
RU	103	2.63E-02	2.58E-02	2.54E-02	2.49E-02	2.32E-02	2.05E-02	1.60E-02
RU	105	8.53E-03	2.08E-04	4.90E-06	1.16E-07	3.57E-14	1.44E-25	0.00E+00
RU	106	3.27E-03	3.26E-03	3.26E-03	3.25E-03	3.23E-03	3.18E-03	3.10E-03
SB	125	2.49E-04	2.49E-04	2.49E-04	2.49E-04	2.48E-04	2.47E-04	2.45E-04
SB	127	1.10E-03	9.28E-04	7.75E-04	6.47E-04	3.15E-04	8.93E-05	7.18E-06
SB	129	5.33E-03	1.15E-04	2.45E-06	5.20E-08	1.06E-14	2.08E-26	0.00E+00
SM	151	9.34E-04	9.34E-04	9.34E-04	9.34E-04	9.34E-04	9.33E-04	9.33E-04
SM	153	1.36E-03	9.55E-04	6.69E-04	4.68E-04	1.13E-04	9.30E-06	6.34E-08
SN	125	1.13E-04	1.05E-04	9.75E-05	9.07E-05	6.80E-05	4.11E-05	1.50E-05
SR	89	4.05E-02	3.99E-02	3.94E-02	3.89E-02	3.68E-02	3.34E-02	2.76E-02
SR	90	2.97E-02	2.97E-02	2.97E-02	2.97E-02	2.97E-02	2.97E-02	2.97E-02
SR	91	4.94E-02	8.59E-03	1.49E-03	2.59E-04	2.35E-07	1.12E-12	2.51E-23
SR	92	5.04E-02	1.09E-04	2.35E-07	5.07E-10	1.10E-20	0.00E+00	0.00E+00
TC	99M	4.43E-02	3.76E-02	2.95E-02	2.29E-02	8.36E-03	1.43E-03	4.20E-05
TE	127	1.09E-03	1.02E-03	8.88E-04	7.68E-04	4.49E-04	2.27E-04	1.37E-04
TE	129	5.25E-03	6.43E-04	4.99E-04	4.86E-04	4.48E-04	3.88E-04	2.90E-04
TE	131	2.13E-02	3.95E-04	2.27E-04	1.30E-04	1.42E-05	2.92E-07	1.24E-10
TE	132	3.54E-02	2.86E-02	2.32E-02	1.87E-02	7.99E-03	1.80E-03	9.17E-05
TE	127	1.53E-04	1.53E-04	1.52E-04	1.52E-04	1.50E-04	1.44E-04	1.33E-04
TE	129	7.91E-04	7.78E-04	7.63E-04	7.47E-04	6.88E-04	5.95E-04	4.46E-04
TE	131	3.04E-03	1.75E-03	1.01E-03	5.79E-04	6.30E-05	1.30E-06	5.52E-10
XE	133	5.68E-02	5.47E-02	5.03E-02	4.52E-02	2.74E-02	1.09E-02	1.72E-03
XE	135	5.52E-02	2.02E-02	4.15E-03	7.39E-04	5.35E-07	1.47E-12	1.09E-23
XE	131	2.63E-04	2.62E-04	2.61E-04	2.58E-04	2.41E-04	1.97E-04	1.11E-04
XE	133	1.65E-03	1.51E-03	1.24E-03	9.65E-04	2.96E-04	3.27E-05	3.90E-07
XE	135	9.52E-03	6.87E-04	5.55E-05	4.48E-06	1.91E-10	4.27E-18	2.14E-33
Y	90	2.97E-02	2.97E-02	2.97E-02	2.97E-02	2.97E-02	2.97E-02	2.97E-02
Y	91	4.94E-02	4.91E-02	4.86E-02	4.80E-02	4.58E-02	4.21E-02	3.57E-02
Y	92	5.05E-02	1.60E-03	1.70E-05	1.60E-07	1.10E-15	5.65E-30	0.00E+00
Y	93	5.44E-02	1.06E-02	2.04E-03	3.93E-04	5.41E-07	5.32E-12	5.15E-22
Y	91M	2.86E-02	5.46E-03	9.47E-04	1.64E-04	1.49E-07	7.09E-13	1.60E-23
ZR	95	5.38E-02	5.32E-02	5.26E-02	5.21E-02	4.99E-02	4.62E-02	3.97E-02
ZR	97	4.92E-02	1.84E-02	6.87E-03	2.57E-03	5.00E-05	5.11E-08	5.29E-14

CHAPTER 13 APPENDIX D

ORIGEN Output File Extracts for 1 tonne U-235 at 1 W for 8 h/d, 5 Days
NUCLIDE TABLE: RADIOACTIVITY, CURIES

		Time post discharge						
		0	1.0 D	2.0 D	3.0 D	7.0 D	14.0 D	28.0 D
AS	78	1.24E-01	2.17E-05	5.66E-10	1.16E-14	1.11E-33	0.00E+00	0.00E+00
BA	139	5.33E+01	3.47E-04	1.99E-09	1.14E-14	1.28E-35	0.00E+00	0.00E+00
BA	140	4.22E+00	4.00E+00	3.79E+00	3.59E+00	2.89E+00	1.98E+00	9.27E-01
BA	141	4.91E+01	0.00E+00	0.00E+00	0.00E+00	0.00E+00	0.00E+00	0.00E+00
BA	142	4.88E+01	0.00E+00	0.00E+00	0.00E+00	0.00E+00	0.00E+00	0.00E+00
BR	83	4.02E+00	4.13E-03	3.92E-06	3.72E-09	3.01E-21	0.00E+00	0.00E+00
BR	84	8.43E+00	2.19E-13	5.13E-27	0.00E+00	0.00E+00	0.00E+00	0.00E+00
CE	141	1.57E+00	1.74E+00	1.71E+00	1.67E+00	1.54E+00	1.32E+00	9.81E-01
CE	143	1.84E+01	1.13E+01	6.83E+00	4.13E+00	5.49E-01	1.61E-02	1.39E-05
CE	144	1.85E-01	1.84E-01	1.84E-01	1.83E-01	1.82E-01	1.79E-01	1.73E-01
CS	138	5.68E+01	3.40E-12	1.17E-25	0.00E+00	0.00E+00	0.00E+00	0.00E+00
I	131	2.82E+00	2.74E+00	2.55E+00	2.37E+00	1.70E+00	9.33E-01	2.79E-01
I	132	7.73E+00	6.95E+00	5.62E+00	4.54E+00	1.94E+00	4.37E-01	2.22E-02
I	133	2.32E+01	1.11E+01	5.00E+00	2.25E+00	9.17E-02	3.40E-04	4.66E-09
I	134	6.38E+01	1.62E-06	9.36E-15	5.37E-23	0.00E+00	0.00E+00	0.00E+00
I	135	3.28E+01	2.65E+00	2.14E-01	1.73E-02	7.35E-07	1.65E-14	8.26E-30
KR	87	2.14E+01	4.51E-05	9.39E-11	1.96E-16	0.00E+00	0.00E+00	0.00E+00
KR	88	2.62E+01	7.49E-02	2.14E-04	6.09E-07	4.03E-17	6.19E-35	0.00E+00
KR	83M	3.30E+00	1.59E-02	1.65E-05	1.58E-08	1.29E-20	0.00E+00	0.00E+00
KR	85M	7.76E+00	1.93E-01	4.70E-03	1.15E-04	4.07E-11	2.10E-22	0.00E+00
LA	140	2.25E+00	2.88E+00	3.22E+00	3.38E+00	3.19E+00	2.27E+00	1.07E+00
LA	141	3.79E+01	6.11E-01	8.86E-03	1.29E-04	5.72E-12	7.77E-25	0.00E+00
LA	142	4.83E+01	1.15E-03	2.43E-08	5.12E-13	1.01E-31	0.00E+00	0.00E+00
LA	143	4.96E+01	0.00E+00	0.00E+00	0.00E+00	0.00E+00	0.00E+00	0.00E+00
MO	99	1.31E+01	1.02E+01	7.93E+00	6.17E+00	2.25E+00	3.85E-01	1.13E-02
MO	101	4.23E+01	0.00E+00	0.00E+00	0.00E+00	0.00E+00	0.00E+00	0.00E+00
NB	97	1.98E+01	8.19E+00	3.06E+00	1.14E+00	2.23E-02	2.28E-05	2.53E-11
NB	98	4.86E+01	0.00E+00	0.00E+00	0.00E+00	0.00E+00	0.00E+00	0.00E+00
ND	147	1.79E+00	1.69E+00	1.59E+00	1.49E+00	1.16E+00	7.50E-01	3.12E-01
ND	149	8.74E+00	5.96E-04	3.98E-08	2.65E-12	5.23E-29	0.00E+00	0.00E+00
ND	151	3.50E+00	0.00E+00	0.00E+00	0.00E+00	0.00E+00	0.00E+00	0.00E+00
PD	109	1.19E-01	3.50E-02	1.02E-02	2.95E-03	2.11E-05	3.69E-09	1.13E-16
PM	151	1.36E+00	7.72E-01	4.30E-01	2.39E-01	2.30E-02	3.80E-04	1.04E-07
PR	143	2.31E+00	2.92E+00	3.22E+00	3.33E+00	3.03E+00	2.16E+00	1.06E+00
PR	144	1.86E-01	1.84E-01	1.84E-01	1.83E-01	1.82E-01	1.79E-01	1.73E-01
PR	145	2.12E+01	1.33E+00	8.25E-02	5.11E-03	7.52E-08	2.63E-16	3.22E-33
PR	147	1.90E+01	0.00E+00	0.00E+00	0.00E+00	0.00E+00	0.00E+00	0.00E+00
RB	88	2.65E+01	8.37E-02	2.39E-04	6.80E-07	4.50E-17	7.40E-35	0.00E+00
RH	105	2.57E+00	2.17E+00	1.37E+00	8.55E-01	1.30E-01	4.84E-03	6.68E-06
RH	107	1.37E+00	1.84E-20	0.00E+00	0.00E+00	0.00E+00	0.00E+00	0.00E+00
RU	103	7.45E-01	7.33E-01	7.20E-01	7.08E-01	6.59E-01	5.83E-01	4.55E-01
RU	105	6.23E+00	1.54E-01	3.62E-03	8.54E-05	2.64E-11	1.07E-22	0.00E+00
SB	127	2.19E-01	1.96E-01	1.63E-01	1.36E-01	6.64E-02	1.88E-02	1.51E-03
SE	81	1.76E+00	2.49E-09	6.77E-17	1.84E-24	0.00E+00	0.00E+00	0.00E+00
SE	83	1.64E+00	8.98E-20	0.00E+00	0.00E+00	0.00E+00	0.00E+00	0.00E+00
SM	153	4.27E-01	3.01E-01	2.11E-01	1.48E-01	3.55E-02	2.93E-03	2.00E-05
SM	155	2.76E-01	8.53E-21	0.00E+00	0.00E+00	0.00E+00	0.00E+00	0.00E+00
SN	127	6.52E-01	2.37E-04	8.59E-08	3.12E-11	5.40E-25	0.00E+00	0.00E+00
SN	128	2.78E+00	1.25E-07	5.62E-15	2.53E-22	0.00E+00	0.00E+00	0.00E+00
SR	89	9.30E-01	9.27E-01	9.15E-01	9.02E-01	8.54E-01	7.76E-01	6.40E-01
SR	91	2.64E+01	4.60E+00	7.99E-01	1.39E-01	1.26E-04	5.98E-10	1.35E-20
SR	92	4.40E+01	9.50E-02	2.05E-04	4.42E-07	9.59E-18	1.62E-36	0.00E+00
TC	101	4.23E+01	0.00E+00	0.00E+00	0.00E+00	0.00E+00	0.00E+00	0.00E+00
TC	104	1.53E+01	0.00E+00	0.00E+00	0.00E+00	0.00E+00	0.00E+00	0.00E+00
TE	127	1.61E-01	1.77E-01	1.55E-01	1.31E-01	6.49E-02	1.94E-02	2.81E-03
TE	129	3.11E+00	1.18E-01	1.87E-02	1.62E-02	1.49E-02	1.29E-02	9.65E-03
TE	131	2.09E+01	1.51E-01	8.68E-02	4.99E-02	5.43E-03	1.12E-04	4.76E-08
TE	132	8.32E+00	6.74E+00	5.45E+00	4.41E+00	1.88E+00	4.24E-01	2.16E-02
TE	133	3.20E+01	6.42E-08	9.61E-16	1.44E-23	0.00E+00	0.00E+00	0.00E+00
TE	134	5.69E+01	2.42E-09	1.03E-19	4.40E-30	0.00E+00	0.00E+00	0.00E+00
XE	133	6.76E+00	8.00E+00	7.97E+00	7.43E+00	4.68E+00	1.88E+00	2.97E-01
XE	135	1.96E+01	1.01E+01	2.19E+00	3.97E-01	2.91E-04	7.99E-10	5.94E-21
XE	138	5.26E+01	0.00E+00	0.00E+00	0.00E+00	0.00E+00	0.00E+00	0.00E+00
Y	91	7.71E-01	9.16E-01	9.32E-01	9.25E-01	8.84E-01	8.13E-01	6.89E-01
Y	92	2.81E+01	1.25E+00	1.35E-02	1.28E-04	8.81E-13	4.51E-27	0.00E+00
Y	93	2.86E+01	5.64E+00	1.09E+00	2.09E-01	2.88E-04	2.83E-09	2.74E-19
Y	94	5.26E+01	0.00E+00	0.00E+00	0.00E+00	0.00E+00	0.00E+00	0.00E+00
Y	95	5.35E+01	0.00E+00	0.00E+00	0.00E+00	0.00E+00	0.00E+00	0.00E+00

Y	91M	1.41E+01	2.93E+00	5.08E-01	8.81E-02	8.00E-05	3.80E-10	8.56E-21
ZR	95	9.72E-01	9.68E-01	9.58E-01	9.47E-01	9.07E-01	8.41E-01	7.23E-01
ZR	97	2.18E+01	8.15E+00	3.05E+00	1.14E+00	2.22E-02	2.27E-05	2.34E-11

CHAPTER 13 APPENDIX E

Maximum Activity Available for Release
One TRIGA Element at 86.42 W for 40 Years
(Release fractions: 1E-04 for halogens and noble gases, 1E-06 for particulates)

		Potential Activity Release (μCi) Time post discharge (days)							Inhalation ALI	DAC	Initial Bay Concentration
		0	1	2	3	7	14	28	μCi	μCi/cm³	μCi/cm³
AG	111	0.0	0.0	0.0	0.0	0.0	0.0	0.0	9.E+02	4.E-07	3.5E-12
BA	140	4.5	4.3	4.1	3.8	3.1	2.1	1.0	1.E+03	6.E-07	1.1E-09
BA	137	2.5	2.5	2.5	2.5	2.5	2.5	2.5	na	na	6.2E-10
CE	141	4.3	4.2	4.1	4.0	3.7	3.2	2.4	6.E+02	2.E-07	1.0E-09
CE	143	4.3	2.6	1.6	1.0	0.1	0.0	0.0	2.E+03	7.E-07	1.1E-09
CE	144	3.9	3.9	3.9	3.9	3.9	3.8	3.7	1.E+01	6.E-09	9.7E-10
CS	137	2.7	2.7	2.7	2.7	2.7	2.7	2.7	2.E+02	6.E-08	6.6E-10
EU	155	0.0	0.0	0.0	0.0	0.0	0.0	0.0	9.E+01	4.E-08	5.8E-12
EU	156	0.0	0.0	0.0	0.0	0.0	0.0	0.0	5.E+02	2.E-07	2.4E-12
I	131	204.6	190.1	175.3	161.4	114.9	62.9	18.8	5.E+01	2.E-08	5.0E-08
I	132	307.3	255.3	206.4	166.8	71.2	16.0	0.8	8.E+03	3.E-06	7.5E-08
I	133	490.5	226.5	101.8	45.7	1.9	0.0	0.0	3.E+02	1.E-07	1.2E-07
I	135	458.6	37.0	3.0	0.2	0.0	0.0	0.0	2.E+03	7.E-07	1.1E-07
KR	85	18.1	18.1	18.1	18.1	18.1	18.1	18.1		1.E-04	4.5E-09
KR	85M	92.2	2.3	0.1	0.0	0.0	0.0	0.0		2.E-05	2.3E-08
LA	140	4.5	4.5	4.4	4.2	3.5	2.4	1.1	1.E+03	5.E-07	1.1E-09
LA	141	4.3	0.1	0.0	0.0	0.0	0.0	0.0	9.E+03	4.E-06	1.0E-09
MO	99	4.4	3.4	2.6	2.1	0.7	0.1	0.0	1.E+03	6.E-07	1.1E-09
NB	95	4.6	4.6	4.6	4.6	4.6	4.6	4.4	1.E+03	5.E-07	1.1E-09
NB	97	4.3	1.6	0.6	0.2	0.0	0.0	0.0	7.E+04	3.E-05	1.0E-09
NB	95M	0.0	0.0	0.0	0.0	0.0	0.0	0.0	2.E+03	9.E-07	8.0E-12
NB	97M	4.0	1.5	0.6	0.2	0.0	0.0	0.0	na	na	9.9E-10
ND	147	1.6	1.5	1.4	1.4	1.1	0.7	0.3	8.E+02	4.E-07	4.0E-10
PM	147	1.6	1.6	1.6	1.6	1.6	1.6	1.6	1.E+02	5.E-08	4.0E-10
PM	149	0.8	0.6	0.4	0.3	0.1	0.0	0.0	2.E+03	8.E-07	1.9E-10
PM	151	0.3	0.2	0.1	0.1	0.0	0.0	0.0	3.E+03	1.E-06	7.5E-11
PR	143	4.3	4.3	4.2	4.0	3.3	2.3	1.1	7.E+02	3.E-07	1.1E-09
PR	144	3.9	3.9	3.9	3.9	3.9	3.8	3.7	1.E+05	5.E-05	9.7E-10
PR	145	2.8	0.2	0.0	0.0	0.0	0.0	0.0	8.E+03	3.E-06	7.0E-10
PR	144	0.0	0.0	0.0	0.0	0.0	0.0	0.0	na	na	1.2E-11
RH	105	0.7	0.5	0.3	0.2	0.0	0.0	0.0	6.E+03	2.E-06	1.8E-10
RH	106	0.3	0.3	0.3	0.3	0.3	0.3	0.3	na	na	6.9E-11
RH	103	2.0	2.0	2.0	1.9	1.8	1.6	1.2	1.E+06	5.E-04	5.0E-10
RU	103	2.3	2.2	2.2	2.2	2.0	1.8	1.4	6.E+02	3.E-07	5.6E-10
RU	105	0.7	0.0	0.0	0.0	0.0	0.0	0.0	1.E+04	5.E-06	1.8E-10
RU	106	0.3	0.3	0.3	0.3	0.3	0.3	0.3	1.E+01	5.E-09	6.9E-11
SB	125	0.0	0.0	0.0	0.0	0.0	0.0	0.0	5.E+02	2.E-07	5.3E-12
SB	127	0.1	0.1	0.1	0.1	0.0	0.0	0.0	9.E+02	4.E-07	2.3E-11
SB	129	0.5	0.0	0.0	0.0	0.0	0.0	0.0	9.E+03	4.E-06	1.1E-10
SM	151	0.1	0.1	0.1	0.1	0.1	0.1	0.1	1.E+02	4.E-08	2.0E-11
SM	153	0.1	0.1	0.1	0.0	0.0	0.0	0.0	3.E+03	1.E-06	2.9E-11
SN	125	0.0	0.0	0.0	0.0	0.0	0.0	0.0	4.E+02	1.E-07	2.4E-12
SR	89	3.5	3.5	3.4	3.4	3.2	2.9	2.4	1.E+02	6.E-08	8.6E-10
SR	90	2.6	2.6	2.6	2.6	2.6	2.6	2.6	4.E+00	2.E-09	6.3E-10
SR	91	4.3	0.7	0.1	0.0	0.0	0.0	0.0	4.E+03	1.E-06	1.0E-09
SR	92	4.4	0.0	0.0	0.0	0.0	0.0	0.0	7.E+03	3.E-06	1.1E-09
TC	99M	3.8	3.3	2.5	2.0	0.7	0.1	0.0	2.E+05	6.E-05	9.4E-10
TE	127	0.1	0.1	0.1	0.1	0.0	0.0	0.0	2.E+04	7.E-06	2.3E-11
TE	129	0.5	0.1	0.0	0.0	0.0	0.0	0.0	6.E+04	3.E-05	1.1E-10
TE	131	1.8	0.0	0.0	0.0	0.0	0.0	0.0	5.E+03	2.E-06	4.5E-10
TE	132	3.1	2.5	2.0	1.6	0.7	0.2	0.0	2.E+02	9.E-08	7.5E-10
TE	127	0.0	0.0	0.0	0.0	0.0	0.0	0.0	3.E+02	1.E-07	3.2E-12
TE	129	0.1	0.1	0.1	0.1	0.1	0.1	0.0	2.E+02	1.E-07	1.7E-11
TE	131	0.3	0.2	0.1	0.1	0.0	0.0	0.0	4.E+02	2.E-07	6.4E-11
XE	133	490.7	473.1	434.5	390.3	236.8	94.5	14.9		1.E-04	1.2E-07
XE	135	477.0	174.2	35.8	6.4	0.0	0.0	0.0		1.E-05	1.2E-07
XE	131	2.3	2.3	2.3	2.2	2.1	1.7	1.0		4.E-04	5.6E-10
XE	133	14.3	13.1	10.7	8.3	2.6	0.3	0.0		1.E-04	3.5E-09
XE	135	82.3	5.9	0.5	0.0	0.0	0.0	0.0		9.E-06	2.0E-08
Y	90	2.6	2.6	2.6	2.6	2.6	2.6	2.6	1.E+02	5.E-08	6.3E-10
Y	91	4.3	4.2	4.2	4.1	4.0	3.6	3.1	8.E+03	3.E-06	1.0E-09
Y	92	4.4	0.1	0.0	0.0	0.0	0.0	0.0	2.E+03	1.E-06	1.1E-09
Y	93	4.7	0.9	0.2	0.0	0.0	0.0	0.0	2.E+03	1.E-06	1.2E-09
Y	91M	2.5	0.5	0.1	0.0	0.0	0.0	0.0	2.E+05	7.E-05	6.1E-10
ZR	95	4.6	4.6	4.5	4.5	4.3	4.0	3.4	1.E+02	5.E-08	1.1E-09
ZR	97	4.3	1.6	0.6	0.2	0.0	0.0	0.0	1.E+03	5.E-07	1.0E-09

CHAPTER 13 APPENDIX F

Maximum Activity Available for Release
One TRIGA Element at 31.125 kW, 8 h/d, 5 Days
(Release fractions: 1E-04 for halogens and noble gases, 1E-06 for particulates)

	Potential Activity Release (uCi) Time post discharge							ALI	DAC	Effluent Hwy Concentration	
	0	1	2	3	4	7	28	uCi	uCi/ml	uCi/ml	Ratio
AS 78	3.75	0	0	0	0	0	0	2.E+04	9.E-06	9.25E-10	NA
BA 139	1604.3	0	0	0	0	0	0	3.E+04	1.E-05	4.00E-07	NA
BA 140	127.25	120.5	114.3	108.3	87.25	59.5	28	1.E+03	6.E-07	3.00E-08	NA
BA 141	1480.3	0	0	0	0	0	0	7.E+04	3.E-05	3.75E-07	NA
BA 142	1470.5	0	0	0	0	0	0	1.E+05	6.E-05	3.50E-07	NA
BR 83	12110	12.5	0	0	0	0	0	6.E+04	3.E-05	3.00E-06	NA
BR 84	25386	0	0	0	0	0	0	6.E+04	2.E-05	6.25E-06	NA
CE 141	47.25	52.5	51.5	50.25	46.25	39.75	29.5	6.E+02	2.E-07	1.15E-08	NA
CE 143	553.5	340.75	205.8	124.3	16.5	0.5	0	2.E+03	7.E-07	1.35E-07	NA
CE 144	5.5	5.5	5.5	5.5	5.5	5.5	5.25	1.E+01	6.E-09	1.38E-09	NA
CS 138	1711.8	0	0	0	0	0	0	6.E+04	2.E-05	4.25E-07	NA
I 131	8489.3	8245.3	7694	7131	5124	2810	840.5	5.E+01	2.E-08	2.08E-06	103.8
I 132	23281	20943	16930	13686	5838	1317	67	8.E+03	3.E-06	5.75E-06	1.9
I 133	69950	33529	15072	6772	276.3	1	0	3.E+02	1.E-07	1.73E-05	172.5
I 134	192228	0	0	0	0	0	0	5.E+04	2.E-05	4.75E-05	2.4
I 135	98750	7980	644.3	52	0	0	0	2.E+03	7.E-07	2.43E-05	34.6
KR 87	64498	0.25	0	0	0	0	0	na	5.E-06	1.58E-05	3.2
KR 88	79048	225.75	0.75	0	0	0	0	na	2.E-06	1.95E-05	9.8
KR 83M	9953.3	47.75	0	0	0	0	0	na	1.E-02	2.45E-06	NA
KR 85M	23368	580.25	14.25	0.25	0	0	0	na	2.E-05	5.75E-06	NA
LA 140	67.75	86.75	97	101.8	96	68.5	32.25	1.E+03	5.E-07	1.68E-08	NA
LA 141	1140.3	18.5	0.25	0	0	0	0	9.E+03	4.E-06	2.75E-07	NA
LA 142	1454.5	0	0	0	0	0	0	2.E+04	9.E-06	3.50E-07	NA
LA 143	1493.3	0	0	0	0	0	0	9.E+04	4.E-05	3.75E-07	NA
MO 99	395.5	307.5	239	185.8	67.75	11.5	0.25	1.E+03	6.E-07	9.75E-08	NA
MO 101	1272.8	0	0	0	0	0	0	1.E+05	6.E-05	3.00E-07	NA
NB 97	596.75	246.75	92.25	34.5	0.75	0	0	7.E+04	3.E-05	1.48E-07	NA
NB 98	1463.5	0	0	0	0	0	0	5.E+04	2.E-05	3.50E-07	NA
ND 147	53.75	51	48	45	35	22.5	9.5	8.E+02	4.E-07	1.33E-08	NA
ND 149	263.25	0	0	0	0	0	0	2.E+04	1.E-05	6.50E-08	NA
ND 151	105.5	0	0	0	0	0	0	2.E+05	8.E-05	2.50E-08	NA
PD 109	3.5	1	0.25	0	0	0	0	5.E+03	2.E-06	8.75E-10	NA
PM 151	41	23.25	13	7.25	0.75	0	0	3.E+03	1.E-06	1.00E-08	NA
PR 143	69.5	88	97	100.3	91.25	65	31.75	7.E+02	3.E-07	1.70E-08	NA
PR 144	5.5	5.5	5.5	5.5	5.5	5.5	5.25	1.E+05	5.E-05	1.38E-09	NA
PR 145	638	40.25	2.5	0.25	0	0	0	8.E+03	3.E-06	1.58E-07	NA
PR 147	572	0	0	0	0	0	0	2.E+05	8.E-05	1.40E-07	NA
RB 88	799	2.5	0	0	0	0	0	6.E+04	3.E-05	1.95E-07	NA
RH 105	77.5	65.25	41.25	25.75	4	0.25	0	6.E+03	2.E-06	1.90E-08	NA
RH 107	41	0	0	0	0	0	0	2.E+05	1.E-04	1.00E-08	NA
RU 103	22.5	22	21.75	21.25	19.75	17.5	13.75	6.E+02	3.E-07	5.50E-09	NA
RU 105	187.5	4.75	0	0	0	0	0	1.E+04	5.E-06	4.50E-08	NA
SB 127	6.5	6	5	4	2	0.5	0	9.E+02	4.E-07	1.63E-09	NA
SE 81	53	0	0	0	0	0	0	2.E+05	1.E-04	1.30E-08	NA
SE 83	49.5	0	0	0	0	0	0	1.E+05	5.E-05	1.23E-08	NA
SM 153	12.75	9	6.25	4.5	1	0	0	3.E+03	1.E-06	3.25E-09	NA
SM 155	8.25	0	0	0	0	0	0	2.E+05	9.E-05	2.05E-09	NA
SN 127	19.75	0	0	0	0	0	0	2.E+04	8.E-06	4.75E-09	NA
SN 128	83.75	0	0	0	0	0	0	3.E+04	1.E-05	2.05E-08	NA
SR 89	28	28	27.5	27.25	25.75	23.25	19.25	1.E+02	6.E-08	6.75E-09	NA
SR 91	796.25	138.75	24	4.25	0	0	0	4.E+03	1.E-06	1.95E-07	NA
SR 92	1325.8	2.75	0	0	0	0	0	7.E+03	3.E-06	3.25E-07	NA

		Potential Facility Release (Ci)						ALDA	PAG	Initial Bq/L Concentration	
		Tuck pod ductwork									
TE	132	250.75	203	164.3	132.8	56.75	12.75	0.75	2.E+02	9.E-08	6.25E-08	NA
TE	133	964.25	0	0	0	0	0	0	2.E+04	9.E-06	2.38E-07	NA
TE	134	1712.5	0	0	0	0	0	0	2.E+04	1.E-05	4.25E-07	NA
XE	133	20362	24106	24010	22389	14111	5673	894.75	na	1.E-04	5.00E-06	NA
XE	135	58955	30517	6594	1195	1	0	0	na	1.E-05	1.45E-05	1.5
XE	138	158548	0	0	0	0	0	0	na	4.E-06	4.00E-05	10.0
Y	91	23.25	27.5	28	28	26.5	24.5	20.75	1.E+02	5.E-08	5.75E-09	NA
Y	92	846.75	37.75	0.5	0	0	0	0	8.E+03	3.E-06	2.08E-07	NA
Y	93	861.25	169.75	32.75	6.25	0	0	0	2.E+03	1.E-06	2.10E-07	NA
Y	94	1583.8	0	0	0	0	0	0	8.E+04	3.E-05	4.00E-07	NA
Y	95	1613	0	0	0	0	0	0	1.E+05	6.E-05	4.00E-07	NA
Y	91M	423.5	88	15.25	2.75	0	0	0	2.E+05	7.E-05	1.05E-07	NA
ZR	95	29.25	29.25	28.75	28.5	27.25	25.25	21.75	1.E+02	5.E-08	7.25E-09	NA
ZR	97	657	245.5	91.75	34.25	0.75	0	0	1.E+03	5.E-07	1.60E-07	NA